

博士論文

**Exacerbation of hepatic injury during rodent malaria**

**by myeloid-related protein 14**

(myeloid-related protein 14 によるローデントマラリア肝障害の悪化)

溝渕 悠代

# Contents

Abbreviation

General Introduction

Chapter 1: Exacerbation of hepatic injury during rodent malaria by administrating recombinant MRP14

Introduction

Materials and methods

Results

Discussion

Chapter 2: Unimproved hepatic injury in MRP14-KO BALB/c mice during rodent malaria

Introduction

Materials and methods

Results

Discussion

Chapter 3: Enhanced TLR4 signaling in BMCs of MRP14-KO BALB/c mice

Introduction

Materials and methods

Results

Discussion

General discussion

Acknowledgement

References

Figure legends

Figures and Tables

Summary (in Japanese)

## Abbreviations

MRP	myeloid-related protein
Pb	<i>Plasmodium berghei</i>
AST	aspartate aminotransferase
ALT	alanine aminotransferase
pRBC	parasitized red blood cell
nRBC	naive red blood cell
BMC	bone marrow cell
NO	nitric oxide
iNOS	inducible isoform of NO synthase
Arg-1	arginase-1
TLR	toll-like receptor
DAMPs	damage-associated endogenous molecular patterns
PAMPs	pathogen-associated molecular patterns
SPC	splenocyte
LPS	lipopolysaccharide
PEC	peritoneal exudate cell
KO	knockout
WT	wild-type

## **General introduction**

Malaria is caused by protozoan parasites of the genus *Plasmodium*. *Plasmodium* parasites are transmitted by the bites of infected *Anopheles* mosquitoes, which inject sporozoites into the host's dermis. They are carried with the blood stream to the liver and mature in the hepatocytes (exoerythrocytic stage). Matured merozoites are released into the hepatic sinusoids and then invade the red blood cells, starting the erythrocytic stage, which comprises ring forms, trophozoites, and, subsequently, schizonts that contain a new generation of merozoites (1). According to World Malaria Report 2016 released by World Health Organization 91 countries and territories are considered endemic, and there were 212 million cases and 429,000 deaths in 2015. Symptoms of severe malaria include fever, anemia, splenomegaly, jaundice and hepatic injury. Considering that malaria patients develop those clinical symptoms in the erythrocytic stage, host immunity is supposed to play a role in the pathogenesis.

Severe liver dysfunction occurs occasionally in severe malaria in association with multi-organ failure and poor prognosis (2). In adult non-immune patients in South-East Asia and India, jaundice and liver dysfunction occur in up to 50% of cases in severe malaria, almost always as part of multi-organ disease (3). Elevations of liver cytoplasm enzymes are common, including raised aspartate aminotransferase (AST), alanine aminotransferase (ALT) and alkaline phosphatase (4, 5). Histopathological examination of liver biopsies of severe malaria patients showed that dilated sinusoids, parasitized red blood cell (pRBC) sequestration within hepatic sinusoids and adhesion of pRBCs to sinusoidal endothelial cells, and the retention of malaria pigment, accompanied with hepatocyte swelling and necrosis, host macrophage infiltration and

focal centrilobular hepatic necrosis (2, 3, 6, 7). It is reported that the degree of jaundice, hepatomegaly and liver enzyme abnormalities correlates with the overall parasite load in the body, and the sequestration of pRBCs in the liver was quantitatively associated with liver weight, serum bilirubin and AST levels (8). Rodent malaria model using BALB/c mice and lethal *P. berghei* (Pb) ANKA strain shows clinical manifestations as parasitemia, anemia, splenomegaly and hepatic injury, which are also observed in human severe malaria patients as described above. Also, in histopathological analysis of the liver of the mouse model, vasodilatation, remarkable macrophage infiltration, and necrosis of hepatocytes are observed (9–12). However, the mechanism of hepatic injury during malaria is still unknown.

Myeloid-related protein (MRP) 14 has been characterized as an inflammation-related protein (13–15). MRP14, which is also known as S100A9, belongs to the S100 calcium-binding protein family and can form the heterodimer with MRP8, which is also known as S100A8 (16–18). These proteins are expressed by neutrophils and monocytes (16) and are also known as markers of inflammatory macrophages (19). The studies with C57BL/6 mice have revealed that MRP14 play a pivotal role in the pathogenesis of various inflammatory disorders. In inflammatory diseases such as rheumatoid arthritis, psoriatic arthritis, and coronary syndromes, the accumulation of cells expressing MRP14 is observed at inflammatory sites (20–22). In addition, the protein is secreted by the inflammatory cells when activated (23). Actually, MRP14 in serum is elevated in various diseases including rheumatoid arthritis (21), coronary syndromes(24), and psoriatic arthritis (25). Moreover, some studies suggest the function of MRP14, not only as biomarkers but also inflammation mediators (13, 26). Those results in

C57BL/6 mice suggest that extracellular MRP14 is involved in the inflammation accompanied with the accumulation of MRP14<sup>+</sup> macrophages. For malaria, there is a report that elevated serum MRP14 levels in falciparum malaria patients correlated with an elevated parasite load (27). In my graduation thesis, it is revealed that serum MRP14 is elevated during rodent malaria accompanied with the accumulation of MRP14<sup>+</sup> macrophages in the liver of BALB/c mice.

Taken together, it was hypothesized that extracellular MRP14 is involved in hepatic injury during rodent malaria in BALB/c mice as reported in other inflammatory models with C57BL/6 mice. In chapter 1, it is demonstrated that extracellular MRP14 exacerbates hepatic injury during rodent malaria by MRP14 administration to Pb-infected mice. In chapter 2, since it was hypothesized that MRP14 deletion improves hepatic injury during rodent malaria as reported in several inflammatory disorder models with C57BL/6 mice, MRP14-knockout (KO) BALB/c mice were established. However, it was shown that hepatic injury during rodent malaria was not improved in MRP14-KO BALB/c mice. Those results suggest that MRP14 deficiency induces not only the simple deletion of extracellular MRP14 function to promote inflammation but also affects intracellular MRP14 function, which leads to other changes in immunological characters in myeloid cells of BALB/c mice. Thus in chapter 3, immunological characters of BALB/c-background MRP14-KO mice were analyzed using LPS-induced shock model as reported on the KO mice with C57BL/6 background. Although it is reported that MRP14-KO C57BL/6 mice were less severely affected and survived significantly longer (28), it was revealed that MRP14 deficiency could not improve the survival rate of LPS-induced shock in BALB/c mice. Besides, the study elucidated the higher TNF- $\alpha$  production from BMCs of MRP14-KO

BALB/c mice than wild-type (WT) controls, which is contrast to the reported results of the suppression of TNF- $\alpha$  production in BMCs of MRP14-KO C57BL/6 mice. Those results suggest that the deletion of intracellular MRP14 induces hyperresponsiveness of TLR4 signaling in BMCs in BALB/c mice unlike C57BL/6 mice. It is considered that hepatic injury is not improved in MRP14-KO BALB/c mice because the higher cellular capacity of BMCs keeps comparable inflammatory cytokine levels in MRP14-KO BALB/c mice. In the present study, it is revealed that extracellular MRP14 promotes inflammation in pathology of hepatic injury during rodent malaria. Besides, it is elucidated that MRP14 has multiple functions not only to promote inflammation but also to maintain TLR4 signaling in myeloid cells of BALB/c mice.

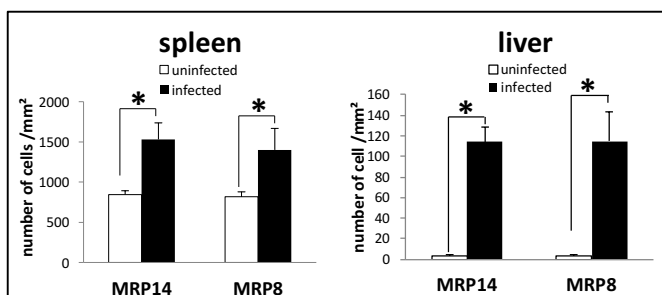
**Chapter 1. Exacerbation of hepatic injury during rodent malaria by  
administrating recombinant MRP14**

## Introduction

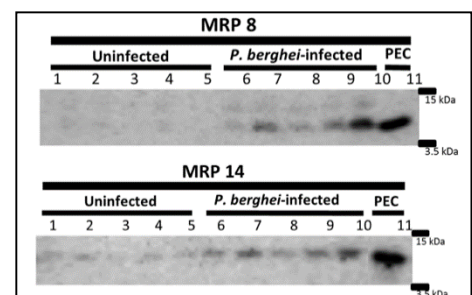
Hepatic injury can be established by using BALB/c mice and *P. berghei* ANKA strain. Mice infected with this plasmodial parasite develop such clinical manifestations as parasitemia, anemia, splenomegaly and hepatic injury, which also observed in human malaria patients. Previous murine studies have shown that IL-12 and IFN- $\gamma$  have a pivotal role in liver injury caused by *P. berghei*. Yoshimoto *et al.* revealed that the lethal *P. berghei* NK65 infection induces IL-12 production and the IL-12 is involved in the pathogenesis of liver injury via IFN- $\gamma$  production rather than the protection (10). Also, in the study by Adachi *et al.*, it was demonstrated that the liver injury induced by *P. berghei* NK65 infection of mice induces activation of the toll-like receptor (TLR)-MyD88 signaling pathway which results in IL-12 production and activation of the perforin-dependent cytotoxic activities of MHC-unrestricted hepatic lymphocytes (11). These studies suggested that the liver injury induced by *P. berghei* is caused by the local production of cytokines that activates inflammatory cells which reside in the liver. However, the pathogenesis of hepatic injury during *Plasmodium* species infection has not been completely elucidated.

MRP14 is expressed by inflammatory macrophages and secreted upon activation (16, 23, 29) and has been characterized as an inflammation-related protein (13–15). With C57BL/6 mice, increased serum MRP14 accompanied with the accumulation of MRP14<sup>+</sup> macrophages at inflammatory sites has been reported in various diseases including rheumatoid arthritis, psoriatic arthritis, and coronary syndromes (20–22, 24, 25). Not only as biomarkers, some studies suggested that MRP14 worked also as an inflammation mediator (13, 26). In malaria, there is

only one report on increased MRP14 in patient sera (27) whereas the mechanism behind the elevated serum MRP14 levels was unclear. In my graduation thesis, in order to elucidate whether MRP14<sup>+</sup> macrophages increased during malaria, I investigated macrophages expressing MRP14 in the organs of BALB/c mice infected with *P. berghei* ANKA (30). Immunohistochemical staining of the spleen and liver revealed the accumulation of mononuclear cells expressing MRP14 after Pb-infection (see the left panel of the figure). Since the locations of those cells were similar to those of CD11b<sup>+</sup> cells, it is suggested that the accumulated MRP14<sup>+</sup> cells are macrophages. Besides, immunohistochemical analysis showed that the locations of MRP14<sup>+</sup> macrophages were similar to those of MRP8<sup>+</sup> macrophages, which indicates that MRP14<sup>+</sup> macrophages also express MRP8. In addition, the MRP14 level in the plasma was also elevated during Pb-infection compared with uninfected controls (see the right panel of the figure). My graduation thesis first revealed the increase of MRP14 in plasma accompanied with the accumulation of MRP14<sup>+</sup> macrophages in the spleen and liver of BALB/c mice during experimental rodent malaria as seen in the other inflammatory disease models of C57BL/6 mice (30), suggesting that increased MRP14<sup>+</sup> macrophages secrete MRP14 during rodent malaria. In addition, studies on the function of extracellular MRP14 will be intriguing as a cytokine of



Increased MRP14<sup>+</sup> cells and MRP8<sup>+</sup> cells in the spleen and liver during Pb-infection



Increased MRP14 and MRP8 in plasma during Pb-infection

inflammation mediators (13, 26). However, the role of MRP14 in hepatic injury during rodent malaria has been unclear.

Taken together, it is hypothesized that the accumulation of MRP14<sup>+</sup> cells in the tissue is associated with an increase in MRP14 in serum during malaria and that the extracellular MRP14 are involved in hepatic injury. In chapter 1, in order to verify whether extracellular MRP14 is involved in the pathology of hepatic injury during malaria, *P. berghei*-infected BALB/c mice were intravenously administrated MRP14.

## **Material and methods**

**Animals.** Male BALB/c mice and BALB/c-*nu/nu* (*nu/nu*) mice were purchased from Japan Clea, Tokyo, Japan. All mice were maintained under specific pathogen-free conditions. The mice were used for experiments at the age of 8-9 weeks. *P. berghei* ANKA was used to infect mice. The animal experiments were reviewed and approved by an institutional animal research committee at the Graduate School of Agricultural and Life Sciences, The University of Tokyo (Approval No. P15-91).

**Experimental infection and hematological analysis.** Experimental infection was performed as previously described (30). Briefly, to prepare Pb-pRBCs, blood was collected from a BALB/c mouse infected with *P. berghei* and was mixed well with Citrate-phosphate-dextrose as anticoagulant. The RBCs were washed two times with Hanks' Balanced Salt Solution (Life Technologies, Carlsbad, CA) by centrifugation at 400 *xg* for 5 min. Mice were infected intraperitoneally with  $10^6$  Pb-pRBCs and sacrificed at day 7 of post-infection. For administration of MRP14, mice were injected with recombinant MRP14 (50  $\mu$ g/mouse) or PBS intravenously every day for 7 days. Blood samples were collected every day by cutting the tip of tail to monitor parasitemia by counting 1,000 RBCs on Giemsa-stained thin blood smears for each mouse by microscopic examination. To analyze the inflammatory responses to Pb-infection *in vivo*, the liver, spleen and serum were collected from mice at day 7 of post-infection. Whole blood was collected by cardiac puncture of mice and centrifuged for 10 min at 5,000 *xg* to collect serum.

For hematological analysis, blood was collected using the heparinized capillary tubes

(TERUMO, Tokyo, Japan) and hematocrit was determined by centrifuging the tubes at 15,000 xg for 10 min. For quantitative analyses of leukocytes, peripheral leukocytes were counted with Türk's solution (Merck Millipore, Darmstadt, Germany).

**Production of recombinant MRP14 and MRP8.** An open reading frame of murine MRP14 or MRP8 was amplified by PCR, and each amplified product was inserted into the *NdeI/HindIII* site of the vector pET-28a (+) (Merck Millipore). The pET-28a vectors cloned for MRP14 and MRP8 were transformed into *Escherichia coli* Rosetta2 (DE3) pLysS competent cells (Merck Millipore). The transformed *E. coli* was cultured in SOB medium and expression of the recombinant protein was induced by cultivation with 0.5 mM isopropyl- $\beta$ -D-thiogalactoside (IPTG) for 3 hr. For MRP8, inclusion body was formed after lysing cells by sonication and centrifuging at 10,000 xg. The inclusion body was washed with 1% CHAPS and then resolubilized in 8M urea. MRP14 and MRP8 were then purified as 6xHis-tagged proteins using Ni-NTA agarose (Qiagen Inc., Valencia, CA) by binding protein to the agarose, washing the agarose with sodium deoxycolate. MRP14 was eluted with 200 mM imidazole and MRP8 was eluted with Tris buffer (pH 4.0) in 8M urea. The eluted MRP14 was dialyzed with PBS (pH 7.4) and the eluted MRP8 was dialyzed with 50mM Tris (pH 10). Concentration of the purified protein was measured by BCA protein assay (Bio-Rad Laboratories, Inc., Berkeley, CA). An endotoxin level of the protein was measured by LAL endotoxin assay (GenScript USA Inc., Piscataway, NJ) and shown to be below 100 EU/mg of protein.

**Determination of cytokines and hepatic enzymes.** AST and ALT were measured by Japan Society of Clinical Chemistry standard method using automatic analyzer, Hitachi 7189 (Hitachi, Tokyo, Japan). MRP14 or MRP8 concentration in serum and TNF- $\alpha$  and IFN- $\gamma$  in culture supernatants were measured by using commercial sandwich ELISA kit (R&D systems, Minneapolis, MN for MRP14 and MRP8; eBioscience, San Diego, CA for TNF- $\alpha$  and IFN- $\gamma$ ).

**Nitric Oxide (NO) measurement.** NO production was assessed by measuring the accumulation of nitrites in the cell culture medium using the colorimetric Griess reaction. Culture medium was mixed with Griess reagent (1% sulfanilamide, 0.1% N-1-naphthyl-ethylendiamide and 2.5% phosphoric acid) in 1:1 ratio. After incubation for 10 min, the optical density (OD) was read at 550 nm on an absorbance detector. Standard curve was generated using NaNO<sub>2</sub> to determine the quality of NO<sub>2</sub><sup>-</sup>.

**HE-staining and immunohistochemical analyses.** HE-staining and immunohistochemical staining was performed as previously described (30). Briefly, for immunohistochemical staining, paraffin-embedded tissues, sectioned at 4  $\mu$ m thickness, were dewaxed and boiled in Tris-EDTA buffer (10 mM Tris Base, 1mM EDTA-2Na, 0.05% Tween 20, pH 9.0) for 20 minutes. After blocking, anti-MRP8 (Santa Cruz Biotechnology, Santa Cruz, CA), anti-MRP14 (Santa Cruz Biotechnology), anti-CD3 antibody (Santa Cruz Biotechnology) or anti-CD45R (BD Biosciences, San Jose, CA) was applied to the serial sections of tissues. After washing with PBS, sections were incubated with biotinylated anti-goat IgG (Nichirei Bioscience, Tokyo, Japan) or

biotinylated anti-rat IgG (Nichirei Bioscience), followed by incubation with alkaline phosphatase-conjugated streptavidin (Nichirei Bioscience). Finally, enzymatic color development was performed by using 4-[(4-amino-m-tolyl) (4-imino-3-methylcyclohexa-2,5-dien-1-ylidene)methyl]-o-toluidine monohydrochloride (new fuchsin, Nichirei Bioscience).

For quantitative analyses of infiltrating MRP<sup>+</sup> cells in the tissues, the number of MRP14<sup>+</sup> or MRP8<sup>+</sup> cells in the immunohistochemically stained tissues was counted in 5 random microscopic fields at 400x magnification. For the spleen, the cells in the red pulp were counted.

**Cell stimulation assay.** The murine macrophage cell line RAW264.7 cells were purchased from American Type Culture Collection, Manassas, VA. RAW264.7 cells were grown in DMEM culture medium (Sigma-Aldrich, St Louis, MO) supplemented with 10% fetal bovine serum (Thermo Fisher Scientific, Waltham, MA), 100 U/ml penicillin and 100 µg/ml streptomycin (P/S; Life Technologies), at 37°C in 5% CO<sub>2</sub>. RAW264.7 cells (2 x 10<sup>5</sup> cells /ml) were applied and incubated in 96-well plates. 24 hr later, cells were treated with MRP14 (5 µg/ml), MRP8 (5 µg/ml) or lipopolysaccharide (LPS) (5 ng/ml, from *E. coli* 055:B5, Sigma-Aldrich) with or without IFN-γ (20 ng/ml, PeproTech, Rocky Hill, NJ). After incubation for 3-48 hr, RNA was extracted with TRIzol (Thermo Fisher Scientific.). Polymyxin B (50 µg/ml) (Sigma-Aldrich) was used as a LPS inhibitor. Paquinimod (250 µg/ml) was used as a MRP14 inhibitor, and was gently provided from Active Biotech, Lund, Sweden. EGFP is a recombinant protein with polyhistidine-tag and was used as negative control.

Single suspension of splenocytes (SPCs) were collected by passing the tissue through

a 70  $\mu\text{m}$  cell strainer (BD Biosciences). Erythrocytes were lysed with Red Blood Cell Lysing buffer Hybri-MAX™ (Sigma-Aldrich) for 2 min at room temperature, and remaining cells were washed three times with PBS. SPCs ( $5 \times 10^6$  cells/ml) were cultured in RPMI 1640 medium (Sigma-Aldrich) supplemented with 10% FBS, 100 U/ml penicillin and 100  $\mu\text{g/ml}$  streptomycin (Life Technologies), at 37°C in 5% CO<sub>2</sub>. SPCs were treated with Pb-pRBCs ( $1 \times 10^8$  cells/ml), naïve RBC (nRBC) ( $1 \times 10^8$  cells/ml) or concanavalin A (conA: 3  $\mu\text{g/ml}$ , Sigma-Aldrich). After incubation for 24 hr, supernatants were collected for determination of cytokine concentrations.

For TLR screening assay, TLR stimulation was tested by assessing NF- $\kappa$ B activation in HEK293 cells, which express one of the murine TLRs (TLR2, 3, 4, 5, 7, 8 and 9) (InvivoGen, San Diego, CA). The secreted embryonic alkaline phosphatase (SEAP) reporter is under the control of promoter inducible by the NF- $\kappa$ B. This reporter gene allows the monitoring of signaling through the TLRs, based on the activation of NF- $\kappa$ B. In a 96-well plate containing  $2.5 \times 10^5$  cells/ml, MRP14 (5  $\mu\text{g/ml}$ ) was added. After incubation for 24 hr, the OD of SEAP was read at 650 nm on an absorbance detector.

**Quantitative RT-PCR.** RNA was extracted and cDNA was synthesized by reverse transcription. Tissues were homogenized with 1 ml TRIzol and  $\phi$ 1.0 stainless steel beads in the 2 ml tube using Micro Smash MS100R (TOMY, Tokyo, Japan) at 4°C. After transferred to the Eppendorf tube, 0.2  $\mu\text{l}$  chloroform was added and centrifuged at 12,000  $\times g$  for 15 min at 4°C. The supernatant was mixed with 0.5 ml 2-propanol and centrifuged at 12,000  $\times g$  for 15 min at 4°C. After washing with ethanol, RNA was dissolved in UltraPure distilled water (Thermo Fisher Scientific). The

concentration of total RNA was measured by DU 730 Life Science UV/vis spectrophotometer (Beckman Coulter, Brea, CA), and 400 ng of total RNA was used as the template for the synthesis of 20  $\mu$ l cDNA. The mixture including 1.25  $\mu$ M oligo (dT)<sub>16</sub>, and 0.5 mM dNTPs (Thermo Fisher Scientific) with template RNA in the tube was incubated for 5 min at 65°C. After adding 5x first strand buffer and 10 mM DTT (Thermo Fisher Scientific), 200 U M-MLV (Thermo Fisher Scientific) was added and the tube was incubated for 50 min at 37°C and 15 min at 70°C. cDNA was synthesized and analyzed for expression of cytokines (primers are listed in Supplemental Table 1.). Real-time polymerase chain reaction (PCR) assay was carried out using 2  $\mu$ l of cDNA as the template and 10 $\mu$ l of SYBR Select Master Mix (Thermo Fisher Scientific) on the ABI Prism 7000 Sequence Detection System (Thermo Fisher Scientific). Data was analyzed by  $2^{-\Delta\Delta Ct}$  methods and normalized by GAPDH. The thermal cycling conditions for the PCR were 94°C for 10 min, followed by 40 cycles of 94°C for 15 sec and 60°C for 1 min.

**Statistical analysis.** Statistical analysis was performed using GraphPad Prism 7.0 software package (GraphPad Software Inc., San Diego, CA). Results are presented as mean + standard deviation (SD). The differences between the groups of mice were analyzed by two-way ANOVA followed by Sidak multiple comparisons test. Student's *t* test was used to compare the differences in the results from two independent groups. *P* value less than 0.05 were considered significantly different.

## Results

**Enhanced serum MRP14 level dependent on hepatic injury during rodent malaria.** *P. berghei* ANKA causes fatal infection in BALB/cA mice; infection with  $10^6$  pRBCs kills mice in 8 days with an associated 60-80% parasitemia level. In this study, therefore, pRBC rate was monitored every day, and mice were sacrificed at day 7 post-infection to collect blood and tissues. In order to elucidate whether T cells are involved in hepatic injury during malaria, T cell-deficient *nu/nu* mice were infected with Pb-pRBCs. There was no significant difference in pRBC rate and hematocrit between *nu/nu* mice and WT mice. On day 7 post-infection, the mean  $\pm$  SD of pRBC rate was  $31.4 \pm 8.1\%$  in *nu/nu* mice and  $27.8 \pm 4.9\%$  in WT mice (Figure 1a), and the mean  $\pm$  SD of hematocrit was  $34.0 \pm 4.3\%$  in *nu/nu* mice and  $32.8 \pm 3.0\%$  in WT mice (Figure 1b). On the other hand, WT mice lost significantly more body weight than *nu/nu* mice during infection. On day 7 post-infection, the mean  $\pm$  SD of body weight change was  $1.4 \pm 1.6\%$  in *nu/nu* mice and  $-7.3 \pm 3.2\%$  in WT mice (Figure 1c). The concentrations of serum AST and ALT were not increased in *nu/nu* mice during Pb-infection. (Figure 1d). In *nu/nu* mice, there was no difference in serum concentration of AST (naïve:  $93.8 \pm 27.1$  IU/L, Pb-infected:  $179.4 \pm 21.2$  IU/L) and ALT (naïve:  $33.8 \pm 3.3$  IU/L, Pb-infected:  $45.6 \pm 04.3$  IU/L) between naïve and Pb-infected mice, whereas the serum concentrations of AST and ALT were significantly higher after Pb-infection in WT mice (naïve:  $134.4 \pm 27.7$  IU/L, Pb-infected:  $593.2 \pm 150.3$  IU/L for AST; naïve:  $36.6 \pm 2.6$  IU/L, Pb-infected:  $128.4 \pm 28.4$  IU/L for ALT). The mRNA expression of iNOS and IFN- $\gamma$  in the liver was significantly higher in WT mice than in *nu/nu* mice after Pb-injection (Figure 1e). In *nu/nu* mice, the expression of iNOS and IFN- $\gamma$  in the liver was low and not

different between naïve mice and Pb-infected mice. SPC assay showed that Pb-pRBCs induced IFN- $\gamma$  production by SPCs (Figure 1f). While IFN- $\gamma$  produced by naïve SPCs stimulated with Pb-pRBCs or nRBCs was below the detection limit, SPCs from Pb-infected mice produced higher IFN- $\gamma$  when stimulated with Pb-pRBCs than when stimulated with nRBCs.

The concentrations of serum MRP8 and MRP14 showed similar tendency to that of serum AST and ALT. The increase levels of serum MRP8 and MRP14 were significantly lower in *nu/nu* mice than WT mice (Figure 2a). In *nu/nu* mice, there was no difference in serum concentration of MRP8 (naïve:  $135.4 \pm 72.5$  ng/ml, Pb-infected:  $151.3 \pm 72.3$  ng/ml) and MRP14 (naïve:  $2.1 \pm 0.4$   $\mu$ g/ml, Pb-infected:  $2.1 \pm 0.7$   $\mu$ g/ml) between naïve mice and Pb-infected mice (Figure 2a), while serum concentration of MRP8 and MRP14 was significantly higher after Pb-infection in WT mice (naïve:  $30.9 \pm 15.4$  ng/ml, Pb-infected:  $315.2 \pm 93.5$  ng/ml for MRP8; naïve:  $0.06 \pm 0.04$   $\mu$ g/ml, Pb-infected:  $3.8 \pm 0.6$   $\mu$ g/ml for MRP14). In immunohistochemical analysis, the accumulation of MRP8<sup>+</sup> cells and MRP14<sup>+</sup> cells in the liver and spleen was observed in both of *nu/nu* mice and WT mice after infection (Figure 2b). The accumulation level of MRP8<sup>+</sup> cells and MRP14<sup>+</sup> cells was similar, and representative images are shown in Figure 2b. It was shown that not only MRP14<sup>+</sup> and MRP8<sup>+</sup> cells but also CD3<sup>+</sup> cells and CD45R<sup>+</sup> cells were accumulated in the liver and spleen after Pb-infection (Figure 2c). Besides, immunohistochemistry of the serial sections with anti-MRP14, anti-CD3 and anti-CD45R antibodies showed that MRP14<sup>+</sup> cells were co-localized with CD3<sup>+</sup> cells and CD45R<sup>+</sup> cells.

**Macrophage activation induced by MRP14.** RAW264.7 cells were stimulated by MRP14 and

the concentration of secreted TNF- $\alpha$  in the supernatant was measured by ELISA. TNF- $\alpha$  was induced after stimulation with MRP14 as much as with MRP8. Moreover, the increase of TNF- $\alpha$  concentration was proportional to the increase of MRP14 concentration (Figure 3a). The increase of TNF- $\alpha$  induced by MRP14 and MRP8 was not blocked by addition of polymyxin B (Figure 3b). In contrast, polymyxin B efficiently blocked TNF- $\alpha$  induction by LPS. The increase of TNF- $\alpha$  induced by MRP14 was blocked by addition of paquinimod (Figure 3c). The concentration of TNF- $\alpha$  remained low after stimulation with EGFP, which is a recombinant protein with polyhistidine-tag. In order to reveal activation of TLR signal pathway by MRP14, HEK293 cells transfected with a TLR gene were stimulated by MRP14 and SEAP induced by NF- $\kappa$ B activation through TLR was measured. HEK293 cells expressing TLR4 showed significantly strong induction of SEAP after stimulation with MRP14 (Figure 3d). In addition, HEK293 cells expressing TLR2 also showed a strong induction of SEAP after stimulation with rMRP14. In contrast, HEK 293 cells transfected TLR3, 5, 7, 8 or 9 showed the low level of SEAP (Figure 3d). HEK293/Null cells showed no response to MRP14. RT-PCR analysis showed that MRP14 and MRP8 induced the mRNA expression of IL-1 $\beta$ , TNF- $\alpha$ , IL-6, CCL2 and iNOS in RAW264.7 cells (Figure 3e). The expression of IL-1 $\beta$ , TNF- $\alpha$ , IL-6 and CCL2 was promoted at 3-6 hr after stimulation, and the expression of iNOS was promoted at 24 hr after stimulation. In order to analyze cellular activity induced by stimulation with MRP8 or MRP14 in the presence of and IFN- $\gamma$ , NO produced by RAW264.7 cells stimulated with MRP8/MRP14 plus IFN- $\gamma$  was measured (Figure 3f). The concentration of NO in culture medium was below the detection limit when RAW264.7 cells were stimulated with only MRP14, MRP8 or LPS. In contrast, NO

production was induced by RAW264.7 cells stimulated with both of MRP8 and MRP14 in the presence of IFN- $\gamma$ . Besides, NO production was higher when RAW264.7 cells were stimulated with IFN- $\gamma$  coupled with MRP8 or MRP14 than when stimulated with IFN- $\gamma$  only.

**Weight loss exacerbated by MRP14.** In order to verify whether extracellular MRP14 is involved in the pathology of hepatic injury during malaria, recombinant MRP14 (50  $\mu$ g/mouse) was intravenously administrated every day to Pb-infected mice. There was no significant difference in pRBC rate and hematocrit between MRP14-injected mice and PBS-injected mice. On day 7 post-infection, the mean  $\pm$  SD of pRBC rate was  $37.8 \pm 2.0\%$  in MRP14-injected mice and  $33.2 \pm 5.0\%$  in PBS-injected mice (Figure 4a), and the mean  $\pm$  SD of hematocrit was  $31.2 \pm 2.2\%$  in MRP14-injected mice and  $32.8 \pm 3.0\%$  in PBS-injected mice (Figure 4b). MRP14-injected mice lost significantly more body weight than PBS-injected mice during Pb-infection. On day 7 post-infection, the mean  $\pm$  SD of body weight change was  $-12.9 \pm 1.8\%$  in MRP14-injected mice and  $-7.3 \pm 3.2\%$  in PBS-injected mice (Figure 4c). Splenomegaly, a typical symptom of malaria, was observed in both of mouse groups. There was no significant difference in the spleen weight between MRP14-injected mice ( $0.39 \pm 0.04$  g) and PBS-injected mice ( $0.40 \pm 0.05$  g) at day 7 of post-infection (Figure 4d). Serum concentration of MRP14 increased significantly at day 7 after Pb-infection in MRP14-injected mice ( $8.9 \pm 1.0$   $\mu$ g/ml) than PBS-injected controls ( $5.0 \pm 1.8$   $\mu$ g/ml), whereas the concentration of serum MRP8 was not different between MRP14-injected mice ( $436 \pm 123$  ng/ml) and PBS-injected mice ( $320 \pm 164$  ng/ml) (Figure 4e).

**Exacerbation of hepatic injury by MRP14 during rodent malaria.** Histopathological analysis of the and liver showed that hepatic injury was exacerbated by MRP14 during Pb-infection. In both of MRP14-injected and PBS-injected liver, vasodilatation, remarkable cellular infiltration, and degeneration of hepatocytes were observed after Pb-infection. In the liver of MRP14-injected mice, a lot of focal necrosis area was observed, whereas few focal necrosis areas were observed in PBS-injected mice after Pb-infection (Figure 5a). Serum concentration of AST and ALT increased significantly higher in MRP14-injected mice than in PBS-injected controls at day 7 after Pb-injection (Figure 5b and c). On day 7 post-infection, the concentration of serum AST was  $1,467 \pm 110$  IU/L in MRP14-injected mice and  $833 \pm 89$  IU/L in PBS-injected mice, and the concentration of serum ALT was  $338 \pm 66$  IU/L in MRP14-injected mice and  $151 \pm 40$  IU/L in PBS-injected mice. In the absence of Pb-infection, no significant difference was observed in serum AST (MRP14-injected,  $119 \pm 27$  IU/L; PBS-injected,  $134 \pm 28$  IU/L) and ALT (MRP14-injected,  $25 \pm 6$  IU/L; PBS-injected,  $29 \pm 10$  IU/L) between MRP14-injected mice and PBS-injected mice.

**The accumulation of MRP8<sup>+</sup> and MRP14<sup>+</sup> cells promoted by MRP14 during rodent malaria.** Immunohistochemical analysis showed that MRP8<sup>+</sup> and MRP14<sup>+</sup> cells were accumulated in the liver and spleen at day 7 after Pb-infection, and the accumulation of MRP8<sup>+</sup> and MRP14<sup>+</sup> cells was amplified by MRP14-injection (Figure 6a). The quantitative analysis demonstrated that the number of the MRP8<sup>+</sup> and MRP14<sup>+</sup> cells was significantly higher in

MRP14-injected mice (MRP8<sup>+</sup> cells: spleen, 4,269 ± 484 cells/mm<sup>2</sup>; liver, 507 ± 57 cells/mm<sup>2</sup>) (MRP14<sup>+</sup> cells: spleen, 4,065 ± 576 cells/mm<sup>2</sup>; liver, 491 ± 21 cells/mm<sup>2</sup>) than PBS-injected control mice (MRP8<sup>+</sup> cells: spleen, 2,190 ± 264 cells/mm<sup>2</sup>; liver, 207 ± 11 cells/mm<sup>2</sup>) (MRP14<sup>+</sup> cells: spleen, 2,137 ± 287 cells/mm<sup>2</sup>; liver, 208 ± 7.1 cells/mm<sup>2</sup>) after Pb-infection (Figure 6b and c). The peripheral leukocytes increased after infection in both mice groups, the number of peripheral leukocytes significantly higher in MRP14-injected mice (22,180 ± 3,468 cells/μl) than in PBS-injected mice (12,540 ± 2,484 cells/μl) on day 7 post-infection (Figure 6d). In the liver of MRP14-injected mice, it was observed that the more MRP8<sup>+</sup> and MRP14<sup>+</sup> cells were accumulated in focal necrosis area than in other area (Figure 6e).

**The accumulation of MRP8<sup>+</sup> and MRP14<sup>+</sup> cells promoted by MRP14.** Immunohistochemical analysis showed that the accumulation of MRP8<sup>+</sup> and MRP14<sup>+</sup> cells was induced by MRP14 itself even in the absence of Pb-infection (Figure 7a). The quantitative analysis demonstrated that the number of the MRP8<sup>+</sup> and MRP14<sup>+</sup> cells was significantly higher in MRP14-injected mice (MRP8<sup>+</sup> cells: spleen, 2,860 ± 326 cells/mm<sup>2</sup>; liver, 44 ± 10 cells/mm<sup>2</sup>) (MRP14<sup>+</sup> cells: spleen, 2,707 ± 448 cells/mm<sup>2</sup>; liver, 51 ± 10 cells/mm<sup>2</sup>) than PBS-injected control mice (MRP8<sup>+</sup> cells: spleen, 1,346 ± 101 cells/mm<sup>2</sup>; liver, 7.6 ± 1.5 cells/mm<sup>2</sup>) (MRP14<sup>+</sup> cells: spleen, 1,376 ± 52 cells/mm<sup>2</sup>; liver, 7.0 ± 0.7 cells/mm<sup>2</sup>) (Figure 7b and c). The number of peripheral leukocytes also significantly higher in MRP14-injected mice (11,560 ± 2,241 cells/μl) than in PBS-injected mice (7,080 ± 803 cells/μl) (Figure 7d). The splenomegaly was induced by MRP14, and the spleen weight was significantly heavier in MRP14-injected mice (0.112 ± 0.01 g) than in PBS-

injected controls ( $0.09 \pm 0.004$  g) (Figure 7e).

**The expression of pro-inflammatory molecules promoted by MRP14 in the liver during rodent malaria.** Quantitative RT-PCR analysis showed that the expression of pro-inflammatory molecules in the liver was promoted by MRP14 in the absence of Pb-infection (Figure 8). The expression of iNOS, IL-1 $\beta$ , IL-12 p40, TNF- $\alpha$ , IL-10, TGF- $\beta$ , NOX2, CCR2 and CCL2 was significantly up-regulated in the liver by MRP14. On the other hand, even though the accumulation of MRP8<sup>+</sup> and MRP14<sup>+</sup> cells was observed in both of the spleen and liver, the expression pattern of pro-inflammatory molecules in the spleen was different from that in the liver. In the spleen, the expression of arginase-1 (Arg-1), NOX2 and CCR2 was significantly up-regulated by MRP14, and the other pro-inflammatory molecules up-regulated in the liver were not changed by MRP14-injection. On day 7 post-infection, the expression of iNOS, IL-1 $\beta$ , IL-6, IL-12 p40, TNF- $\alpha$ , IL-10, TGF- $\beta$ , NOX2, CCR2, CCL2, IFN- $\gamma$  and IL-4 was significantly up-regulated, and the expression of Arg-1 and FIZZ-1 was down-regulated in the liver of Pb-infected mice (Figure 9). In contrast, in the spleen of Pb-infected mice, the expression of IL-1 $\beta$ , IL-12 p40, TNF- $\alpha$ , FIZZ-1, TGF- $\beta$  and NOX2 was significantly down-regulated, and the expression of iNOS, Arg-1 and CCL2 was significantly up-regulated (Figure 10). In both of liver and spleen, the expression of iNOS was more up-regulated in MRP14-injected mice than PBS-injected mice after Pb-infection. The expression pattern of inflammatory molecules in the liver and spleen was summarized in Figure 11.

## Discussion

Previous reports showed that T cells and IFN- $\gamma$  play a critical role in the protective immunity against non-lethal murine malarial strain, *P. chabaudi* or *P. berghei* XAT (31–33). On the other hand, other reports demonstrated that T cells and IFN- $\gamma$  are potentially involved in the pathogenesis during lethal rodent malarial strain, *P. berghei* NK65 or *P. berghei* ANKA (10, 34, 35). In order to elucidate whether T cells are involved in the pathogenesis of hepatic injury during infection with *P. berghei* ANKA, T cell-deficient *nu/nu* mice were infected with Pb-pRBCs. It is revealed that hepatic injury during Pb-infection was induced through T cell-dependent mechanism regardless of parasite number. Cell stimulation assay indicates that Pb-pRBC antigen-specific T cells play a pivotal role in IFN- $\gamma$  and iNOS production (Figure 1f and e). Besides, there was a positive correlation between serum concentration of hepatic enzymes and MRP14 (Figure 1d and 2a). This relation between hepatic injury and serum MRP14 level indicates that extracellular MRP14 has some functions involved in the pathogenesis of hepatic injury during rodent malaria. Considering that MRP14<sup>+</sup> cells were co-localized with T cells in the liver during Pb-infection (Figure 2c), it is suggested that MRP14 assists the function of T cells to induce NO through IFN- $\gamma$  in the liver during rodent malaria. Actually, MRP14 promoted NO production from RAW264.7 cells stimulated with IFN- $\gamma$  whereas MRP14 itself could not induce NO production without IFN- $\gamma$  stimulation (Figure 3f), which suggests that MRP14 potentiates IFN- $\gamma$ -induced NO production. Because high levels of NO, generated primarily by iNOS, have cytotoxic and pro-inflammatory effects leading to severe hepatic injury (36, 37), MRP14 seems to promote hepatic injury by increasing NO production during rodent malaria.

Interestingly, MRP14<sup>+</sup> cells were accumulated in the liver during Pb-infection in both of *nu/nu* and WT mice, suggesting a T cell-independent mechanism for accumulating MRP14<sup>+</sup> cells during Pb-infection.

Cell stimulation assay demonstrated that MRP14 is an agonist of TLR2 and TLR4 (Figure 3). TLRs are a class of transmembrane proteins that play important roles in the inflammatory responses. When activated by agonists, TLRs signal cascade leads to the activation of the transcription factor NF- $\kappa$ B and induces cytokine expression and secretion (38, 39). Actually, MRP14 induced pro-inflammatory molecules such as IL-1 $\beta$ , TNF- $\alpha$ , IL-6, CCL2 and iNOS from macrophages (Figure 3), whose expression was induced by downstream signaling of TLR. There is a report that MRP14 induces the secretion of TNF $\alpha$ , IL-1 $\beta$  and IL-6 dependent on TLR4 (40), and it is also reported that these inflammatory cytokines can be associated with the pathology during infection with *P. berghei* (41). Taken together, MRP14 can be involved in the pathology of hepatic injury during malaria through activation of TLR2 and TLR4 signaling. It is reported that MRP8 also acts as an endogenous activator of TLR4 and promotes inflammatory processes in infection and autoimmunity by amplifying TNF- $\alpha$  release in response to LPS (28, 42). Besides, TLRs recognize not only damage-associated endogenous molecular patterns (DAMPs) but also pathogen-associated molecular patterns (PAMPs) (43), and promotes inflammatory responses against pathogens. In malaria, it is known that hemozoin as malaria pigment activates innate immune response through TLR9 (44). TLR-TLR cross-talk induce the synergistic effect. It was reported that the stimulation with MALP2 and LPS (TLR2 and TLR4 ligands, respectively) results in the production of TNF- $\alpha$  at levels much greater than that

observed for each of the ligands alone (45). Besides, TLR4 and TLR9 were shown to synergize in the production of TNF- $\alpha$  in macrophages in a manner associated with enhanced MAPK signaling (46). To take those facts into account, the activation of TLR2 and TLR4 by MRPs as DAMPs can amplify immune response with TLR9 activation by hemozoin as PAMPs in malaria. Moreover, considering that TLRs are expressed in various cells such as macrophages and dendritic cells, the increase of MRP14 in plasma may be involved in the systemic inflammation through TLRs in malaria.

In order to verify whether extracellular MRP14 is involved in the pathology of hepatic injury during malaria, Pb-infected mice were intravenously injected with MRP14. Because MRP14 can form heterodimer with MRP8 (16), it is anticipated that the concentration of MRP14 measured by sandwich ELISA can be lower than the actual MRP14 concentration. Accordingly, the dose of MRP14 administration was set based on the western blot analyses for MRP14 in serum of Pb-infected mice in my graduation thesis. The MRP14 dose was consistent with the dose in other studies about MRP14 administration (28, 47–49). Even though the number of parasites was comparable between MRP14-injected mice and PBS-injected control mice, extracellular MRP14 exacerbated hepatic injury along with enhanced serum AST and ALT during rodent malaria (Figure 5). Actually, in human cases, it is reported that there was a significant correlation between plasma MRP8/MRP14 levels and liver damage as illustrated by elevated ALT levels of patients infected with *Salmonella typhi* (50), which suggests that extracellular MRP14 is involved in hepatic injury. Immunohistochemical analysis first demonstrated that extracellular MRP14 promotes the accumulation of MRP8<sup>+</sup> and MRP14<sup>+</sup> cells

in the liver during Pb-infection (Figure 6). The accumulation of MRP8<sup>+</sup> and MRP14<sup>+</sup> cells especially in focal necrosis area suggests that MRP14 can be involved in the inflammation and necrosis of hepatic cells (Figure 6e). Because the number of peripheral leukocytes also increased in MRP14-injected mice (Figure 6d and 7d), these accumulated MRP8<sup>+</sup> and MRP14<sup>+</sup> cells in the tissue seem to be recruited from bone marrow. Because the number of the accumulated MRP8<sup>+</sup> and MRP14<sup>+</sup> cells was not changed after perfusion, it is considered that the MRP8<sup>+</sup> and MRP14<sup>+</sup> cells were adherent to endothelial cells in the sinusoid of liver. Also, even in the absence of Pb-infection, administration of MRP14 could induce the accumulation of MRP8<sup>+</sup> and MRP14<sup>+</sup> cells in the tissue of naïve mice (Figure 7), which indicates that MRP8<sup>+</sup> and MRP14<sup>+</sup> cells can be accumulated by MRP14 alone. Quantitative RT-PCR analysis revealed that extracellular MRP14 induces the up-regulation of pro-inflammatory molecules such as iNOS, IL-1 $\beta$ , IL-12 p40, TNF- $\alpha$  and NOX2 in the liver of naïve mice (Figure 8), which is consistent with the result *in vitro* (Figure 3). iNOS, which induces high concentrations of NO, and is transcriptionally regulated and induced by inflammatory cytokines, i.e., IL-1 $\beta$ , TNF- $\alpha$  or IFN- $\gamma$  (51, 52). Because those cytokines and iNOS were elevated after Pb-infection (Figure 9 and 11), it is indicated that the pro-inflammatory cytokines and NO induced by MRP14 are involved in the inflammatory response, which leads to hepatic injury during rodent malaria. NOX2, which is expressed in macrophages, is also important to generate superoxide, which reacts with NO and leads to cytotoxic peroxynitrite (53). In the contrast to the results on uninfected mice, there was not significant difference in these inflammatory cytokines between MRP14-injected mice and PBS-injected controls during Pb-infection, which indicates that other factors induced by MRP14 is

related to iNOS induction. In the absence of Pb-infection, extracellular MRP14 alone could not induce hepatic injury illustrated by elevated AST and ALT levels (Figure 7). Although MRP14 induced iNOS (Figure 3e and 8), NO was not induced by MRP14 alone (Figure 3f), which indicates that iNOS level induced by MRP14 alone is not enough to induce NO. Since MRP14 administration did not influence the expression of IFN- $\gamma$  in naïve mice (Figure 8), and increase rate of iNOS expression induced in Pb-infected mice was much higher than that induced by MRP14 alone (Figure 8 and 9), IFN- $\gamma$  produced by Pb-antigen specific T cells have a potent role in iNOS induction and hepatic injury. Also, extracellular MRP14 induced the up-regulation of chemotactic factors, CCR2 and CCL2, which suggests that these molecules are associated with the cellular recruitment to the tissue during rodent malaria. Actually, it is reported that MRP can induce migration of neutrophils and monocytes (54–57). It is also reported that monocytes migrated by CCR2 and CCL2 aggravate hepatic injury (58, 59). Taken together, these data indicate that elevated MRP14 during malaria is one of the key molecules for pathology of hepatic injury, and it is concluded that extracellular MRP14 promotes the accumulation of MRP8<sup>+</sup> and MRP14<sup>+</sup> cells in the liver and the local production of pro-inflammatory molecules, which leads to hepatic injury during rodent malaria.

Interestingly, even though the accumulation of MRP8<sup>+</sup> and MRP14<sup>+</sup> cells was observed in both of the spleen and liver during rodent malaria, the expression pattern of pro-inflammatory molecules induced by MRP14 in the spleen was different from that in the liver (Figure 8-11). In contrast to enhanced iNOS expression in the liver, the up-regulation of Arg-1 was prominent in the spleen during Pb-infection (Figure 10), and the administration of MRP14

also induced the up-regulation of Arg-1 in the spleen of naïve mice (Figure 8). Also, it is reported that cytokine pattern was different between spleen and liver in other inflammatory models (60, 61). This different cytokine patterns suggest that the cellular activation and inflammatory responses are different between organs, which may be explained by the different cellular population. For example, even though their origins were common, tissue-resident macrophages differentiate to tissue-specific or niche-specific macrophages in each organ and have unique phenotypes which reflect the tissue-specific environment and endogenous factors (62–64). Depending on the microenvironment, inflammatory macrophages also can be polarized distinct subsets, M1 or M2 macrophages (65). Classically activated M1 macrophages are differentiated by IFN- $\gamma$  and LPS. M1 macrophages secrete IL-12, TNF- $\alpha$ , IL-1 $\beta$  and IL-6 and express iNOS. In contrast, M2 macrophages are induced by IL-4, IL-13, IL-10 and TGF- $\beta$ . Arg-1 is up-regulated in M2 macrophages and they secrete IL-10 and TGF- $\beta$  (66). Hence, the results of up-regulation of iNOS in the liver and Arg-1 in the spleen suggests that the activation of M1 macrophages is dominant in the liver, whereas the activation of M2 macrophages is dominant in the spleen during rodent malaria. Therefore, it is suggested that M1 macrophages activated by MRP14 promote the production of type 1 cytokines, which leads to hepatic injury during rodent malaria. Besides, the expression of TLRs also different between M1 and M2 macrophages. M1 macrophages express most TLRs, and their expression was higher than M2 macrophages (67). Considering that MRP14 is an activator of TLR2 and TLR4 (Figure 3d), M1 macrophages are more likely to be influenced by MRP14 than M2 macrophages. It is demonstrated that MRP14-induced inflammatory responses were different between organs, which leads a better

understanding the tissue-specific pathogenesis during rodent malaria. Besides, since it is reported that the expression pattern of chemotactic factors is also different between M1 and M2 macrophages (65), MRP14 can influence macrophage phenotypes, which may lead to different heterogeneity of accumulated macrophages between spleen and liver.

Taken together, in chapter 1, it is concluded that extracellular MRP14 promotes inflammatory reactions through the accumulation of MRP8<sup>+</sup> and MRP14<sup>+</sup> cells and the up-regulation of pro-inflammatory cytokines and NO, which exacerbates hepatic injury during rodent malaria.

**Chapter 2. Unimproved hepatic injury in MRP14-KO BALB/c mice during rodent malaria**

## Introduction

In chapter 1, it was elucidated that extracellular MRP14 exacerbates hepatic injury during rodent malaria. Since extracellular MRP14 promotes the accumulation of MRP8<sup>+</sup> and MRP14<sup>+</sup> cells and the up-regulation of pro-inflammatory cytokines, it was hypothesized that MRP14 deficiency impairs those inflammatory reactions and improves liver damage during Pb-infection.

Blood level of MRP14 was high in *P. berghei*-infected mice (2-5 µg/ml, Figure 1), and *in vivo* neutralization using commercial antibodies or inhibitor were not applicable. It is reported that a strain of MRP14-KO C57BL/6 mice has been established and, these mice also lack detectable levels of MRP8 protein in the peripheral tissues (68, 69). Hobbs *et al.* reported that MRP8 protein was not present in the myeloid cells of their MRP14-KO C57BL/6 mice (69). Manitz *et al.* reported that MRP8 was present in bone marrow cells (BMCs) but not detectable in the peripheral blood cells, SPCs or peritoneal exudate cells (PECs) of their KO C57BL/6 mice (68). These results suggest that MRP8 as well as MRP14 is not detectable in peripheral tissue of the MRP14-KO C57BL/6 mice. Besides, previous study demonstrated that MRP8-KO C57BL/6 mice die in utero (70). Studies with the MRP14-KO C57BL/6 mice have demonstrated that MRP14 play a critical role in the pathogenesis of various inflammatory disorders such as vasculitis, pneumonia, arthritis and cancer (71–75). In those reports, inflammation, pathology and survival rate were improved in the MRP14-KO C57BL/6 mice, indicating that MRP14 aggravates inflammation in various diseases. However, the study on malaria model using MRP14-KO mice has not been reported yet. Besides, a strain of BALB/c background MRP14-

KO mice has not been established yet, neither.

Taken together, it was hypothesized that MRP14 deficiency improves hepatic injury during rodent malaria in BALB/c mice as seen in the other inflammatory disease models of C57BL/6 mice. In this chapter, in order to verify this hypothesis described above, BALB/c-background MRP14-KO mice were first established in this study, and compared their phenotypes with WT mice during rodent malaria.

## Material and methods

**Animals.** BALB/c mice were purchased from Japan Clea, and were maintained under specific pathogen-free conditions. MRP14-KO BALB/c mice were bred in the animal facility at the Graduate School of Agricultural and Life Sciences, The University of Tokyo (Approval No. 764-2630 and P14-943). The male mice were used for experiments at the age of 8-9 weeks. The animal experiments were reviewed and approved by an institutional animal research committee and an institutional committee on genetically modified organisms at the Graduate School of Agricultural and Life Sciences, The University of Tokyo (Approval No. P15-91 and No. 830-2630). MRP14-KO BALB/c mouse was generated by offset-nicking method of CRISPR/Cas system according to previous report in collaboration with Dr. Wataru Fujii, Laboratory of Applied Genetics, Graduate school of Agricultural and Life Sciences, The University of Tokyo (76). Briefly, exon 2 of MRP14 locus, which includes EF-hand region, was deleted by using the four gRNAs which designed at the following loci; 5'-GGCCACTGTTAGGCAAGATAAGGAGGGG, 5'-GAGACTAGGTCAGGGAAGCTTGG, 5'-GGCAGAGCCCTACTGCCCCCGG, and 5'-GCAGTAGGGCTCTGCCATTAGAGG. (Figure 12). PCR genotyping was performed to confirm the deletion in the target gene, using the primers as follows: MRP14 forward, 5'-GTCAA AATTCTGTTTTGTGTATATGTGGAG-3'; MRP14 reverse, 5'-AATTCCTTGTGTTCTTAAAGTTATGTGTC-3'). PCR products were purified by 1.5% agarose gel electrophoresis and were subsequently sequenced. The mice were made specific pathogen-free at Central Institute for Experimental Animals, Kawasaki, Japan.

**Experimental infection and hematological analysis.** Experimental infection and hematological analysis were performed as described in chapter 1. Briefly, Mice were infected intraperitoneally with  $10^6$  Pb-pRBCs and sacrificed at day 7 of post-infection. Paquinimod was injected intraperitoneally every day from 3 days before Pb-infection to the 7<sup>th</sup> day after Pb-infection (25 mg/kg/day). To analyze the inflammatory responses to Pb-infection, the liver, spleen and serum were collected from mice at day 7 of post-infection. For hematological analysis, the measurement of hematocrit and the count of peripheral leukocytes were done at day 7 of post-infection.

**Morphological analyses of cells.** For cell population analyses, peripheral leukocytes in the Giemsa-stained smear were observed under a microscope and morphologically categorized as previously described (30). Briefly, monocyte was defined as a large cell which has round nucleus and large cytoplasm; lymphocyte was defined as a small cell which has round nucleus and small cytoplasm; neutrophil was distinguished by segmented nucleus as eosinophil and basophil were very few and negligible for neutrophil enumeration. The ratio of each cell type was also expressed as percentage.

**HE-staining and immunohistochemical analyses.** HE staining and immunohistochemical staining was performed as described in chapter 1. For quantitative analyses of infiltrating cells in the tissues, the numbers of macrophages, lymphocytes, and neutrophils in the HE-stained liver sections were counted, based on morphology as described above, in 5 random microscopic fields

at 1,000x magnification. The number of MRP8<sup>+</sup> cells in the immunohistochemically stained tissues was counted in 5 random microscopic fields at 400x magnification. For the spleen, the cells in the red pulp were counted.

**Determination of cytokines and hepatic enzymes.** Hepatic enzymes (AST and ALT), MRP14 or MRP8 concentration in serum were measured as described in chapter 1.

**Quantitative RT-PCR.** Quantitative RT-PCR analysis with the tissues were performed as described in chapter 1.

**Statistical analysis.** Statistical analysis was performed using GraphPad Prism 7.0 software package. Results are presented as mean + SD. The differences between MRP14-KO mice and WT mice were analyzed by two-way ANOVA followed by Sidak multiple comparisons test. Student's *t* test was used to compare the differences in the results from two independent groups. *P* value less than 0.05 were considered significantly different.

## Results

**No effect of MRP14 deficiency on weight loss.** In order to verify whether MRP14 deficiency is involved in the pathology during malaria, MRP14-KO mice were infected with Pb-pRBCs. There was no significant difference in pRBC rate or hematocrit between MRP14-KO mice and WT mice. On day 7 post-infection, the mean  $\pm$  SD of pRBC rate was  $28.4 \pm 3.0\%$  in MRP14-KO mice and  $27.8 \pm 5.0\%$  in WT mice (Figure 13a), and the mean  $\pm$  SD of hematocrit was  $37 \pm 4.3\%$  in MRP14-KO mice and  $35 \pm 4.6\%$  in WT mice (Figure 13b). There was no significant difference in body weight change between MRP14-KO mice and WT mice after Pb-infection. On day 7 post-infection, the mean  $\pm$  SD of body weight change was  $-4.8 \pm 5.3\%$  in MRP14-KO mice and  $-10.2 \pm 2.1\%$  in WT mice (Figure 13c). Splenomegaly, a typical symptom of malaria, was observed in both of mice groups. There was no significant difference in the spleen weight between MRP14-KO mice ( $0.40 \pm 0.04$  g) and WT mice ( $0.38 \pm 0.05$  g) at day 7 of infection (Figure 13d). The number of peripheral leukocytes significantly lower in MRP14-KO mice ( $7,440 \pm 939$  cells/ $\mu$ l) than in WT mice ( $15,400 \pm 3,346$  cells/ $\mu$ l) on day 7 post-infection (Figure 13e), and there was no significant difference in the percentage of the neutrophils (MRP14-KO:  $36.6 \pm 4.4\%$ , WT:  $32.7 \pm 4.5\%$ ), lymphocytes (MRP14-KO:  $53.2 \pm 4.7\%$ , WT:  $58.5 \pm 5.6\%$ ) or monocytes (MRP14-KO:  $10.2 \pm 1.9\%$ , WT:  $8.8 \pm 1.8\%$ ) in peripheral blood from MRP14-KO mice and WT mice (Figure 13f).

**Hepatic injury independent of MRP14 during rodent malaria.** In histopathological analysis of the liver, no pathological difference was observed between MRP14-KO mice and WT mice

after Pb-infection (Figure 14a). In Pb-infected liver of mice, vasodilatation and remarkable cellular infiltration were observed in both groups. Also, serum concentration of AST and ALT increased significantly at day 7 after Pb-infection in both of MRP14-KO mice and WT mice (Figure 14b). No significant difference was observed in serum AST (MRP14-KO,  $894 \pm 734$  IU/L; WT,  $1,077 \pm 405$  IU/L) and ALT (MRP14-KO,  $306 \pm 257$  IU/L; WT,  $252 \pm 147$  IU/L) between MRP14-KO mice and WT mice after Pb-injection.

#### **The accumulation of MRP8<sup>+</sup> cells independent of MRP14 in the liver during rodent malaria.**

Immunohistochemical analysis showed that MRP8<sup>+</sup> cells were similarly accumulated in the liver and spleen at day 7 after Pb-infection in both of MRP14-KO mice and WT mice (Figure 15a). The quantitative analysis demonstrated that the number of the MRP8<sup>+</sup> cells in the liver was comparable between MRP14-KO mice ( $252 \pm 78$  cells/mm<sup>2</sup>) and WT mice ( $328 \pm 48$  cells/mm<sup>2</sup>). On the other hand, the number of the MRP8<sup>+</sup> cells in the spleen was significantly lower in MRP14 KO mice ( $1,873 \pm 174$  cells/mm<sup>2</sup>) than WT mice ( $2,814 \pm 172$  cells/mm<sup>2</sup>) (Figure 15b). The quantitative analysis of accumulated cells in the liver and spleen showed that there was no significant difference in the number of monocytes/macrophages, neutrophils or lymphocytes between MRP14-KO mice and WT controls at day 7 after Pb-infection (Figure 15c). Serum concentration of MRP8 increased significantly at day 7 after Pb-injection in MRP14-KO mice (naïve:  $17.5 \pm 3.1$  ng/ml, Pb-infected:  $371.1 \pm 137$  ng/ml), and the concentration of serum MRP8 was not different between MRP14-KO mice ( $371.1 \pm 137$  µg/ml) and WT mice ( $315.2 \pm 93.5$  µg/ml) after Pb-infection (Figure 15d). Serum MRP14 was not detected in MRP14-KO mice.

**Enhanced pro-inflammatory molecules independent of MRP14 in the liver during rodent malaria.** Quantitative RT-PCR analysis showed that the expression of pro-inflammatory molecules in the liver and spleen was comparable between MRP14-KO mice and WT mice (Figure 16 and 17). In the liver on day 7 post-infection, the expression of iNOS, IL-1 $\beta$ , IL-6, IL-12 p40, TNF- $\alpha$ , IL-10, TGF- $\beta$ , CCR2, CCL2, IFN- $\gamma$  and IL-4 was significantly up-regulated, and the expression of Arg-1 was down-regulated in both of MRP14-KO mice and WT mice (Figure 16). On the other hand, in the spleen of Pb-infected mice, the expression of IL-1 $\beta$ , IL-12 p40, TNF- $\alpha$ , FIZZ-1, TGF- $\beta$  and CCR2 was significantly down-regulated, and the expression of iNOS, IL-6, Arg-1, IL-10 and CCL2 was significantly up-regulated in both of mice groups (Figure 17). In Pb-infected liver and spleen, the expression level of iNOS, IL-1 $\beta$ , IL-6, IL-12 p40, Arg-1, FIZZ-1, IL-10, TGF- $\beta$ , CCR2, CCL2, IFN- $\gamma$  and IL-4 was not significantly different between MRP14-KO mice and WT mice, though TNF- $\alpha$  was slightly up-regulated in MRP14-KO mice.

**The administration of paquinimod failed to suppress MRP14 *in vivo*.** The rate of pRBC in peripheral blood was significantly lower in paquinimod-injected mice than control mice at day 7 after Pb-infection. There was no significant difference in hematocrit between paquinimod-injected mice and control mice (Figure 18a and 18b). There was no significant difference in body weight change, spleen weight and peripheral leukocytes number between paquinimod-injected mice and control mice after Pb-infection (Figure 18c-e). The concentration of serum MRP14 was not different between paquinimod-injected mice and control mice after Pb-infection (Figure 18f).

Immunohistochemical analysis showed that MRP8<sup>+</sup> and MRP14<sup>+</sup> cells were accumulated in the liver and spleen at day 7 after Pb-infection in both of paquinimod-injected mice and WT mice (Figure 18g). The quantitative analysis demonstrated that the number of the MRP8<sup>+</sup> and MRP14<sup>+</sup> cells in the liver was comparable between paquinimod-injected mice and control mice. On the other hand, the number of the MRP8<sup>+</sup> and MRP14<sup>+</sup> cells in the spleen was significantly lower in paquinimod-injected mice than control mice (Figure 18g). No significant difference was observed in serum AST and ALT between paquinimod-injected mice and control mice after Pb-injection (Figure 18h).

## Discussion

As showed in chapter 1, MRP14 administration exacerbates hepatic injury during rodent malaria. Blood level of MRP14 was high in *P. berghei*-infected mice (2-5 µg/ml, Figure 1), and *in vivo* neutralization using commercial antibodies or inhibitor could not be directly applicable. Actually, I tried neutralization of MRP14 *in vivo* using paquinimod, which is recently identified as a MRP14 inhibitor (77). However, intraperitoneal administration of paquinimod failed to suppress MRP14 level *in vivo* (Figure 18), even though it inhibits MRP14 induced TNF- $\alpha$  secretion from macrophages *in vitro* (Figure 3). Those results indicate that paquinimod, even whose dose is as high as possible, was not enough to block MRP14 *in vivo*. Also, previous study demonstrated that MRP8-KO mice die at the embryonic stage (70). Therefore, MRP14-KO BALB/c mice were established and the function of MRP14 was analyzed using the KO mice in this study. In this chapter, in order to verify whether MRP14 deficiency improves hepatic injury during rodent malaria, MRP14-KO BALB/c mice were infected with *P. berghei*.

MRP14 deficiency did not influence on the body weight loss, the parasite number or spleen weight as seen in MRP14-injected mice (Figure 13a-d). Surprisingly, MRP14-KO mice also showed hepatic injury during Pb-infection, and their serum AST and ALT levels were comparable to WT controls (Figure 14), indicating that hepatic injury was not improved in MRP14-KO BALB/c mice during rodent malaria. Besides, there was no significant difference in pro-inflammatory cytokines levels in the liver between MRP14-KO mice and WT mice, i.e., iNOS, IL-1 $\beta$ , IL-12, IFN- $\gamma$ , CCR2 and CCL2 (Figure 16). The results indicate that MRP14 deficiency did not affect the induction of those pro-inflammatory molecules in MRP14-KO

BALB/c mice, and by which the hepatic injury in MRP14-KO BALB/c mice can be explained. Unlike previous reports on C57BL/6 mice, MRP8 was detectable in MRP14-KO BALB/c mice in this study (described detail in chapter 3). Serum MRP8 level in MRP14-KO BALB/c mice was comparable to that in WT (Figure 15d). Also, quantitative analysis revealed the number of MRP8<sup>+</sup> macrophages in the liver was comparable between MRP14-KO BALB/c mice and WT mice after Pb-infection (Figure 15b). Those results indicate that phenotype of MRP14-KO BALB/c mice is different from MRP14-KO C57BL/6 mice. The hypothesis, “MRP14 deletion improves inflammation since extracellular MRP14 as well as MRP8 is suppressed in MRP14-KO mice.”, has been established by studies with MRP14-KO C57BL/6 mice. However, the present study suggests that this hypothesis cannot be applied to MRP14-KO BALB/c mice. It is indicated that intracellular MRP14 may be related to the maintenance of MRP8 in myeloid cells.

The number of peripheral leukocytes in MRP14-KO mice was significantly lower than that in WT mice (Figure 13e), indicating that MRP14 is related to BMC proliferation or emigration. The result was not consistent with the comparable number of MRP8<sup>+</sup> macrophages in the liver (Figure 15b). It was indicated that even if the immigrating number of MRP8<sup>+</sup> cells was different between MRP14-KO and WT mice, the number of MRP8<sup>+</sup> cells trapped in liver was comparable between the two groups. Considering that the accumulated MRP8<sup>+</sup> cells were adherent to the sinusoid in the liver, the comparable expression level of adherent molecules may be related to the phenomenon. Quantitative analysis revealed the number of MRP8<sup>+</sup> macrophages in the liver was comparable between MRP14-KO mice and WT mice after Pb-infection (Figure 15b), while the number of MRP8<sup>+</sup> macrophages in the spleen was slightly lower

in MRP14 KO mice than WT mice (Figure 15b). The results suggest that MRP8<sup>+</sup> macrophages are likely to be trapped in the liver more than in spleen in MRP14-KO mice during rodent malaria. During Pb-infection, M1 macrophages and type 1 cytokines were dominant in the liver whereas M2 macrophages and type 2 cytokines were dominant in the spleen (chapter 1). Considering that MRP14 is related to type 1 cytokine production, it is anticipated that MRP14 deletion more promotes the activation of M2 macrophages in the spleen during Pb-infection. Actually, TGF- $\beta$  in the spleen was up-regulated in MRP14-KO mice (Figure 17). Since M1 macrophages activate type 1 cytokine cascade by positive feedback (78), it is suggested that M1 dominance in the liver recruits and stays more MRP8<sup>+</sup> macrophages than M2 dominance in the spleen during rodent malaria. The total number of accumulated macrophages in the spleen was comparable between MRP14 KO mice and WT mice (Figure 15c), which indicates that other macrophages which do not express MRP8 are accumulated in the spleen in compensation for MRP8<sup>+</sup> macrophages, which may contribute to the comparable cytokine expression in the spleen of MRP14-KO mice and WT mice.

In addition, some studies reported that MRP14 is dispensable for liver inflammation in several models (50, 79, 80). In a murine *Salmonella* infection model, though elevated serum MRP14 and the accumulation of MRP8<sup>+</sup> and MRP14<sup>+</sup> cells in the liver were observed, MRP14 deficiency did not influence bacterial growth, liver damage and mortality (50). Also, in the carbon tetrachloride-induced liver inflammation model, liver inflammation, fibrosis and recruitment of inflammatory cells were not affected upon MRP14 deletion (80). Those reports are consistent with my results in Pb-infection model.

In conclusion, in chapter 2, it was revealed that MRP14 deletion does not improve hepatic injury during rodent malaria even though MRP14 administration exacerbates the hepatic injury. Although the concept that MRP14 deficiency improves inflammation has been established in MRP14-KO C57BL/6 mice, the concept cannot be simply applied to BALB/c mice. Since the phenotype of MRP14-KO BALB/c mice is different from that of MRP14-KO C57BL/6 mice, it is indicated that MRP14 deficiency induces not only the simple deletion of extracellular MRP14 function to promote inflammation but also affects intracellular MRP14 function, which leads to other changes in immunological characters in myeloid cells of BALB/c mice. Therefore, it is indicated that MRP14-KO BALB/c mice were not the optimal model to prove inversely the extracellular MRP14 function as an inflammation enhancer. The detailed analyses of immunological characters of MRP14-KO BALB/c mice can help understanding of the pathogenesis of the hepatic injury during rodent malaria in MRP14-KO BALB/c mice.

### **Chapter 3. Enhanced TLR4 signaling in BMCs of MRP14-KO BALB/c mice**

## **Introduction**

Even though it was revealed that extracellular MRP14 exacerbates hepatic injury during rodent malaria in chapter 1, improvement of liver inflammation during Pb-infection could not be observed in MRP14-KO BALB/c mice in chapter 2. Those results suggest that intracellular MRP14 deletion affects the immunological characters of myeloid cells in MRP14-KO BALB/c mice. Besides, although MRP14-KO mice have contributed to understanding of the roles of MRP14 as well as MRP8 in inflammatory responses, only mice with C57BL/6 background have been available so far (68, 69), which limits more broad understanding of immunological functions of MRP14 and MRP8. In this chapter, immunological characteristics of established MRP14-KO BALB/c mice were evaluated by using an endotoxin shock model as reported on the KO mice with C57BL/6 background (28).

MRP14 and MRP8 have been characterized as inflammation-related proteins (13–15). MRP14 and MRP8 belong to the S100 calcium-binding protein family and can form the heterodimer MRP8/14 (16–18). These proteins are the most abundant cytoplasmic proteins of neutrophils and monocytes (16, 29), and are secreted by the inflammatory cells when activated (23). MRP14 and MRP8 are known as DAMPs, which are endogenous molecules or alarmins released after cell activation or necrotic cells. When released, the endogenous molecules recruit and activate cells through pattern-recognition receptors such as TLRs or receptor for advanced glycation endproducts (RAGE) (81). It is also reported that MRP14 and MRP8 acts as endogenous activators of TLR4 and promotes inflammatory processes in infection and autoimmunity (28, 40, 42, 82). Actually, MRP8 and MRP14 in serum are elevated in various

diseases (21, 24, 25). In some inflammatory diseases such as rheumatoid arthritis, psoriatic arthritis, and coronary syndromes, the accumulation of cells expressing MRP14 or MRP8 is observed at inflammatory sites (20–22, 71). Studies with MRP14-KO mice have demonstrated that MRP14 and MRP8 play a critical role in the pathogenesis of those inflammatory disorders (71–75).

Endotoxin-induced shock model with LPS is well-characterized, in which many inflammatory mediators activated by NF- $\kappa$ B such as IL-1 $\beta$ , TNF- $\alpha$ , IL-6 and NO are involved in the pathogenesis (83, 84). A previous study demonstrated that MRP8 and MRP14 contribute to the pathogenesis of lethal endotoxic shock by amplifying the release of TNF- $\alpha$  (28). MRP14-KO mice exhibited a significantly higher survival rate compared to their WT controls in LPS-induced shock, which was associated with reduced LPS-induced TNF- $\alpha$  secretion by BMCs lacking MRP14 (28). However, MRP14-KO mice generated and studied so far were those with a C57BL/6 background (68, 69), despite it is well-known that there are differences in inflammatory reactions, pathology and susceptibility to various diseases among mouse strains (85–87). In chapter 3, immunological characters of BALB/c-background MRP14-KO mice were analyzed and their phenotypes were compared with that of previously reported C57BL/6-background MRP14-KO mice to address the biological functions of MRP14 in LPS-induced shock.

## **Material and methods**

**Animals.** BALB/c mice and C57BL/6 mice were purchased from Japan Clea, and were maintained under specific pathogen-free conditions. MRP14-KO BALB/c mice were bred in the animal facility at the Graduate School of Agricultural and Life Sciences, The University of Tokyo. The male mice were used for experiments at the age of 8-9 weeks. The animal experiments were reviewed and approved by an institutional animal research committee and an institutional committee on genetically modified organisms at the Graduate School of Agricultural and Life Sciences, The University of Tokyo (Approval No. 830-2630). MRP14-KO BALB/c mouse was generated as described in chapter 2. The mice were made specific pathogen-free at Central Institute for Experimental Animals.

**LPS-induced shock model.** To analyze the influence of MRP14 to LPS-induced shock, LPS (30 mg per kg body weight, Sigma-Aldrich) was injected intravenously into MRP14-KO and WT mice, and their survival was monitored every 30 min. To analyze the inflammatory responses to LPS *in vivo*, the liver, spleen, BMC and serum were collected from another set of mice at 8 hr after LPS injection. Whole blood was collected by cardiac puncture of mice and centrifuged for 10 min at 5,000 xg to collect serum.

**Harvest of cells from mice.** PECs were collected as previously described (88) with minor modification. Briefly, 1 ml of 10% thioglycollate broth (Nissui Pharmaceutical, Tokyo, Japan) was inoculated into mice intraperitoneally, and PECs were collected after 12 hr by washing the

peritoneal cavity with PBS. To prepare PEC lysate as a source of native MRPs, the PECs from WT mice were resuspended in PBS and sonicated. The sample was centrifuged at 10,000  $\times g$  for 10 min at 4°C, and the supernatant was collected. BMCs were flushed from femurs with PBS. Whole spleen was cut into small pieces in ice-cold RPMI 1640 medium (Sigma-Aldrich), and single suspension of SPCs were collected as described in chapter 1. For quantitative analyses of leukocytes, peripheral leukocytes were counted with Türk's solution (Merck Millipore).

**Morphological analyses of cells.** For cell population analyses, peripheral leukocytes, BMCs and PECs in the Giemsa-stained smear, were observed under a microscope and morphologically categorized as previously described (30). Briefly, monocyte was defined as a large cell which has round nucleus and large cytoplasm; lymphocyte was defined as a small cell which has round nucleus and small cytoplasm; neutrophil was distinguished by segmented nucleus as eosinophil and basophil were very few and negligible for neutrophil enumeration. BMCs were categorized by their nuclear characters; polymorphonuclear cells, mononuclear cells with small cytoplasm or horseshoe-shaped nuclear cells with large cytoplasm. The ratio of each cell type was also expressed as percentage.

**SDS-PAGE and Western blotting.** To analyze protein components of PECs and BMCs, PEC lysates (1  $\mu g$  total protein per lane) or BMCs ( $5 \times 10^4$  cells per lane) were separated by electrophoresis on a 15% polyacrylamide gel, followed by Oriole™ Fluorescent Gel Stain (Bio-Rad) for PEC lysates or Coomassie Brilliant Blue staining for BMCs. Western blot analyses for

MRP8 and MRP14 were performed as previously described (30) with minor modifications. Briefly, BMCs, SPCs or PECs were diluted with SDS sample buffer and boiled for 5 min, and BMCs ( $5 \times 10^3$  cells per lane), SPCs ( $5 \times 10^4$  cells per lane) or PECs ( $5 \times 10^3$  cells per lane) were separated by electrophoresis on a 15% polyacrylamide gel followed by transfer to polyvinylidene difluoride membrane (GE Healthcare UK Ltd, Buckinghamshire, UK). After blocking the membrane with 4% skim milk, the membrane was probed with goat anti-MRP8 or anti-MRP14 antibody (Santa Cruz Biotechnology) at room temperature for 1hr, followed by HRP-conjugated anti-goat IgG antibody (SouthernBiotech, Birmingham, AL). The bound antibodies were visualized using Amersham ECL western blotting detection reagent (GE Healthcare). Chemiluminescent signals were detected using image analyzer LAS-3000mini (FUJIFILM, Tokyo, Japan) according to the manufacture's instruction.

**HE-staining and immunohistochemical analyses.** HE staining and immunohistochemical staining was performed as described in chapter 1. Quantitative analyses of infiltrating cells in the tissues was performed as described in chapter 2.

**Immunofluorescent assay.** For detection of MRP8, BMCs were fixed and permeabilized with Cytofix/Cytoperm<sup>TM</sup> Fixation/Permeabilization kit (BD Biosciences). After blocking with 1% fetal bovine serum (FBS), BMCs ( $1 \times 10^7$  cells) were incubated anti-MRP8 antibody for 30 min at 4°C. After three washes with PBS, the cells were incubated with Alexa Fluor 546-conjugated donkey anti-goat IgG (Thermo Fisher Scientific) for 30 min at 4°C. For detection of Gr-1 and

CD11b, BMCs were incubated with each PE Rat anti-mouse CD11b antibody (BD Biosciences) or PE Rat anti-mouse Gr-1 antibody (BD Biosciences) for 30 min at 4°C after blocking with 1% FBS. After three washes with PBS, BMCs were counterstained with Hoechst 33342 (Thermo Fisher Scientific). MRP8<sup>+</sup>, Gr-1<sup>+</sup> or CD11b<sup>+</sup> cells were counted and the ratio of each kind of cells to total cells was also expressed as percentage.

**Cell stimulation assay.** For assay of cellular response to LPS, BMCs ( $1 \times 10^6$  cells/ml) and SPCs ( $5 \times 10^6$  cells/ml) of MRP14-KO mice or WT mice were cultured in RPMI 1640 medium (Sigma-Aldrich) supplemented with 10% FBS (Thermo Fisher Scientific), 100 U/ml penicillin and 100 µg/ml streptomycin (Life Technologies), at 37°C in 5% CO<sub>2</sub>. BMCs and SPCs were treated with LPS (1 µg/ml, from *E. coli* 055:B5, Sigma-Aldrich), imiquimod (5 µg/ml, Sigma-Aldrich), CpG (1 µM, ODN1826, InvivoGen) or concanavalin A (conA: 3 µg/ml, Sigma-Aldrich). After incubation for 4 or 24 hr, supernatants were collected for determination of cytokine concentrations. For assay of BMC differentiation, BMCs ( $1 \times 10^6$  cells/ml) of WT mice were grown in DMEM (Sigma-Aldrich) supplemented with 10% FBS, 100 U/ml penicillin and 100 µg/ml streptomycin, and were treated with MRP8 (5 µg/ml), MRP14 (5 µg/ml), GM-CSF (50 ng/ml, PeproTech), M-CSF (80 ng/ml, PeproTech) or LPS (1 µg/ml) for 7 days at 37°C in 5% CO<sub>2</sub>. Cell proliferation was measured by Alamar Blue (Thermo Fisher Scientific).

**Determination of cytokines and hepatic enzymes.** Hepatic enzymes (AST and ALT), MRP14 or MRP8 concentration in serum were measured as described in chapter 1. IL-1β or TNF-α

concentration in serum and culture supernatants was measured by using commercial sandwich ELISA kit (eBioscience).

**Quantitative RT-PCR.** Quantitative RT-PCR analysis with the tissues were performed as described in chapter 1.

**Statistical analysis.** Statistical analysis was performed using GraphPad Prism 7.0 software package (GraphPad Software Inc.). Results are presented as mean + SD. The differences between MRP14-KO mice and WT mice were analyzed by two-way ANOVA followed by Sidak multiple comparisons test. Student's *t* test was used to compare the differences in the results from two independent groups. The difference in survival was analyzed with a Kaplan-Meier nonparametric model, and the curves were compared using the log-rank test. *P* value less than 0.05 were considered significantly different.

## Results

**Suppression of cellular MRP8 expression in MRP14-KO mice.** The expression of MRP8 and MRP14 in SPCs, BMCs and PECs of naïve MRP14-KO mice were analyzed by western blotting. It was demonstrated that MRP8 expression was suppressed in those cells of MRP14-KO mice compared with that of WT mice (Figure 19a and 19b). The absence of MRP14 expression was confirmed in MRP14-KO mice.

In immunohistochemical analysis, the cells expressing MRP8 were observed in the spleen and bone marrow of naïve MRP14-KO mice (Figure 19c). In the spleen and bone marrow of naïve WT mice, both of MRP8- and MRP14-expressing cells were observed. None of MRP14-expressing cells was observed in MRP14-KO mice. The expression of CD11b in MRP14-KO mice was comparable to WT mice. The basic structure of the spleen, bone marrow and other organs in MRP14-KO mice was similar to that of WT mice.

In order to compare BMC population, the cells expressing Gr-1, CD11 or MRP8 were analyzed by immunofluorescent assay (Figure 19d). The BMCs expressing Gr-1, CD11b or MRP8 were observed similarly in both of MRP14-KO mice and WT mice. The qualitative analysis showed that there was not significant difference in the percentage of the cells expressing Gr-1 (MRP14-KO:  $42.5 \pm 2.7\%$ , WT:  $52.1 \pm 3.2\%$ ), CD11b (MRP14-KO:  $53.0 \pm 9.3\%$ , WT:  $53.6 \pm 5.9\%$ ) or MRP8 (MRP14-KO:  $38.9 \pm 9.5\%$ , WT:  $43.5 \pm 9.4\%$ ) between MRP14-KO mice and WT mice (Figure 19e).

**The increased ratio of lymphocytes to neutrophils in peripheral blood leukocytes and PECs**

**of MRP14-KO mice.** The absence of MRP14 had no significant effect on the number of peripheral leukocytes (Figure 20a). The number of peripheral leukocytes was  $6,875 \pm 1,742$  cells/ $\mu$ l in MRP14-KO mice and  $8,575 \pm 1,899$  cells/ $\mu$ l in WT mice. The quantitative analysis of peripheral leukocytes showed that the percentage of neutrophils in MRP14-KO mice ( $15.0 \pm 2.5\%$ ) was significantly lower than that of WT mice ( $35.3 \pm 3.9\%$ ) (Figure 20b). In contrast, the percentage of lymphocytes in MRP14-KO mice ( $80.1 \pm 2.4\%$ ) was significantly higher than that of WT mice ( $57.2 \pm 7.2\%$ ). There was no significant difference in the number of monocytes between MRP14-KO mice and WT mice (MRP14-KO:  $4.9 \pm 1.4\%$ , WT:  $7.5 \pm 3.7\%$ ).

A similar pattern was observed in PECs; the quantitative analysis of PECs showed that the percentage of neutrophils in MRP14-KO mice ( $27.0 \pm 5.5\%$ ) was significantly lower than that of WT mice ( $45.7 \pm 1.7\%$ ), and that the percentage of lymphocytes in MRP14-KO mice ( $68.5 \pm 7.4\%$ ) was significantly higher than that of WT mice ( $48.4 \pm 3.4\%$ ) (Figure 20c and 20d). There was no significant difference in the number of monocytes between MRP14-KO mice and WT mice (MRP14-KO:  $4.6 \pm 2.0\%$ , WT:  $6.0 \pm 2.2\%$ ). In order to compare the protein expression pattern of PECs of MRP14-KO and WT mice, PEC lysates were analyzed by SDS-PAGE (Figure 20e). Although two major bands corresponding to the predicted molecular masses of MRP8 (8 kDa) and MRP14 (11 kDa) were observed in PEC lysates of WT mice, the bands were not detected in PEC lysates of MRP14-KO mice. Except for these two bands, apparent difference was not observed in protein pattern between PEC lysates of MRP14KO and WT mice.

On the other hand, the population of BMCs in MRP14-KO mice was comparable to WT mice (Figure 20f). The quantitative analysis of BMCs showed that there was not significant

difference in the percentage of the polymorphonuclear cells (MRP14-KO:  $9.3 \pm 7.9\%$ , WT:  $13.7 \pm 2.3\%$ ), mononuclear cells (MRP14-KO:  $80.7 \pm 8.0\%$ , WT:  $78.8 \pm 6.3\%$ ) or horseshoe-shaped nuclear cells (MRP14-KO:  $10.0 \pm 2.5\%$ , WT:  $7.5 \pm 4.2\%$ ) between MRP14-KO mice and WT mice (Figure 20g). SDS-PAGE analysis showed that no difference in BMC protein pattern between MRP14-KO mice and WT mice (Figure 20h).

**Enhanced TNF- $\alpha$  secretion by BMCs stimulated with LPS in MRP14-KO mice.** In order to analyze cellular response to LPS, BMCs of MRP14-KO mice or WT mice were stimulated with LPS *in vitro*. The secretion of TNF- $\alpha$  was significantly higher in BMCs of MRP14-KO mice than that of WT mice after stimulation with LPS at various concentrations (Figure 21a and 21b). The secretion of MRP8 was not dependent on LPS stimulation and MRP8 was secreted even before LPS stimulation (Figure 21c). MRP14 was not detected in culture supernatants of BMCs of MRP14-KO mice. Next, BMCs of MRP14-KO mice or WT mice were stimulated with other TLR agonists, i.e., imiquimod for TLR7 and CpG for TLR9. The secretion of TNF- $\alpha$  induced by those TLR agonists showed no significant difference between MRP14-KO and WT BMCs (Figure 21d and 21e).

In contrast to the results on BMCs, there was no significant difference in the secretion of TNF- $\alpha$  by SPCs after LPS stimulation between MRP14-KO and WT (Figure 21f). The secretion of TNF- $\alpha$  or IFN- $\gamma$  induced by other TLR agonists as well as conA showed no significant difference between SPCs of MRP14-KO and WT mice (Figure 21g).

**LPS-induced shock independent of MRP14 in BALB/c mice.** In order to examine whether MRP14 is also involved in endotoxin shock in mice with BALB/c background, survival rate was measured after intravenous injection of LPS in MRP14-KO mice and WT mice. Both of MRP14-KO and WT mice died within 9-13 hr after LPS injection, and there was no significant difference in survival rate between the two groups (Figure 22a). The numbers of peripheral leukocytes significantly decreased 8 hr after LPS injection, and showed no significant difference between MRP14-KO ( $4,220 \pm 783$  cells/ $\mu$ l) and WT mice ( $4,300 \pm 1,247$  cells/ $\mu$ l) (Figure 22b). The quantitative analysis showed that there was no significant difference in the percentage of the neutrophils (MRP14-KO:  $57.9 \pm 8.9\%$ , WT:  $50.6 \pm 15.9\%$ ), lymphocytes (MRP14-KO:  $38.9 \pm 8.7\%$ , WT:  $47.0 \pm 16.1\%$ ) or monocytes (MRP14-KO:  $3.2 \pm 1.6\%$ , WT:  $2.4 \pm 1.3\%$ ) in peripheral blood from MRP14-KO mice and WT mice (Figure 22c). Serum concentrations of IL-1 $\beta$  and TNF- $\alpha$  increased significantly at 8 hr after LPS injection in both mice (Figure 22d). Although there was no significant difference in serum IL-1 $\beta$  between MRP14-KO mice ( $320 \pm 84$  pg/ml) and WT mice ( $266 \pm 105$  pg/ml), serum TNF- $\alpha$  was significantly higher in MRP14-KO mice ( $302 \pm 47$  pg/ml) than WT mice ( $223 \pm 34$  pg/ml) at 8 hr after LPS injection. Serum concentration of MRP8 increased significantly at 8 hr after LPS injection in both mice, whereas its concentration was lower in MRP14-KO mice ( $295 \pm 82$  ng/ml) than WT mice ( $487 \pm 124$  ng/ml) (Figure 22e). MRP14 was not detected in serum of MRP14-KO mice. The serum concentration of MRP14 was  $2,957 \pm 884$  ng/ml in WT mice at 8 hr after LPS injection.

In histopathological analysis of the spleen and liver, no pathological difference was observed between MRP14-KO mice and WT mice (Figure 23a). In the liver of mice injected

with LPS, vasodilatation and remarkable cellular infiltration were observed in both groups. The quantitative analysis of accumulated cells in the liver showed that the migration of monocytes/macrophages was suppressed in MRP14-KO mice compared with WT mice at 8 hr after LPS injection (Figure 23b). The number of accumulated monocytes/macrophages in the liver was  $541 \pm 83$  cells/mm<sup>2</sup> in MRP14-KO mice and  $714 \pm 68$  cells/mm<sup>2</sup> in WT mice after LPS injection. Serum concentration of AST and ALT increased significantly at 8 hr after LPS injection (Figure 23c). No significant difference was observed in serum AST (MRP14-KO,  $157 \pm 22$  IU/L; WT,  $200 \pm 40$  IU/L) and ALT (MRP14-KO,  $59 \pm 4.8$  IU/L; WT,  $65 \pm 9.5$  IU/L) between MRP14-KO mice and WT mice after LPS injection. In both of MRP14-KO mice and WT mice, the mRNA expression of iNOS in the liver was significantly up-regulated after LPS injection, and there was no significant difference in iNOS expression level between the two groups (Figure 23d). The mRNA analysis in the spleen, liver and bone marrow showed that the expression level of IL-6 and IL-12 p40 was not different between MRP14-KO mice and WT mice injected with LPS. Though IL-1 $\beta$  in the liver and TNF- $\alpha$  in the bone marrow were slightly suppressed in MRP14-KO mice after LPS injection, the expression level of IL-1 $\beta$  and TNF- $\alpha$  in other tissues was not significantly different between MRP14-KO mice and WT controls (Figure 23e).

#### **Migration of the cells expressing MRP8 dependent on MRP14 in LPS-induced shock.**

Immunohistochemical analysis showed the accumulation of cells expressing MRP8 in the liver at 8 hr after LPS injection (Figure 24a). The quantitative analysis demonstrated that the number

of the MRP8<sup>+</sup> cells was significantly lower in MRP14-KO mice (spleen, 420 ± 40 cells/mm<sup>2</sup>; liver, 77 ± 8.5 cells/mm<sup>2</sup>) than WT mice (spleen, 1,293 ± 226 cells/mm<sup>2</sup>; liver, 341 ± 32 cells/mm<sup>2</sup>) after LPS injection (Figure 24b). The categorization of the MRP8<sup>+</sup> cells showed that population of the MRP8<sup>+</sup> cells was significantly different between MRP14-KO mice and WT mice (Figure 24c). In WT mice injected with LPS, mononuclear MRP8<sup>+</sup> cells (spleen, 64.5 ± 7.4%; liver, 70.0 ± 3.4%) were dominant to polymorphonuclear MRP8<sup>+</sup> cells (spleen, 35.5 ± 7.4%; liver, 30.0 ± 3.4%). In contrast, higher ratio of polymorphonuclear MRP8<sup>+</sup> cells (spleen, 53.5 ± 9.9%; liver, 49.6 ± 5.2%) was observed in MRP14-KO mice injected with LPS.

**Promotion of GM-CSF expression in BMCs stimulated with MRP14.** The assay of BMC differentiation of WT BALB/c mice showed that the secretion of TNF- $\alpha$  was promoted when BMCs were stimulated with MRP14 or GM-CSF for 7 days (Figure 25a). The mRNA expression of GM-CSF was significantly promoted in BMCs stimulated with MRP14 for 7 days (Figure 25b). MRP14-stimulated BMCs were adherent and differentiated to macrophages, which were morphologically similar to bone marrow-derived macrophages differentiated by GM-CSF. Although GM-CSF induced the proliferation of BMCs, BMCs stimulated with MRP14 did not proliferate for 7 days, which was confirmed also by Alamar Blue assay (Figure 25c). The promotion of TNF- $\alpha$  secretion was also observed when BMCs of C57BL/6 mice were stimulated with MRP14, GM-CSF or LPS (Figure 25d). The secretion of TNF- $\alpha$  was significantly higher in C57BL/6 BMCs than BALB/c BMCs when stimulated with MRP14 or LPS. In contrast, when stimulated with GM-CSF, the secretion of TNF- $\alpha$  was significantly higher in BALB/c BMCs

than C57BL/6 BMCs. In order to analyze the effect of MRP14 on BMC differentiation, the mRNA expression of CD11b, F4/80, CD68 and GM-CSF was measured in BMCs of MRP 14-KO mice and WT mice. It was shown that the expression level of CD11b, F4/80, CD68 and GM-CSF was not significantly different between MRP14-KO mice and WT mice (Figure 25e).

## Discussion

Since it is indicated that MRP14 deficiency induces not only the simple deletion of extracellular MRP14 function to promote inflammation but also affects intracellular MRP14 function in BALB/c mice, immunological characteristics of established MRP14-KO BALB/c mice were evaluated in this chapter by using an endotoxin shock model as reported on the KO mice with C57BL/6 background (28). Since it is known that MRP8 and MRP14 is expressed in BMCs, spleen, and PECs, MRP8 expression in these cell types was investigated in MRP14-KO BALB/c mice. In naïve MRP14-KO BALB/c mice, although the expression of MRP8 was suppressed in BMCs and PECs (Figure 19a, 19b and 20e), the protein was still at a detectable level in the spleen and bone marrow (Figure 19c-19e). Because the percentage of MRP8<sup>+</sup> cells in BMCs was comparable between MRP14-KO mice and WT mice (Figure 19d), these results indicate that expression of MRP8 in each cell is lower in MRP14-KO mice compared with WT mice. Hobbs *et al.* reported that MRP8 protein was not present in the myeloid cells of their MRP14-KO C57BL/6 mice (69). Manitz *et al.* reported that MRP8 was present in BMCs but not detectable in the peripheral blood cells, SPCs or PECs of their KO mice (68). These results suggest that MRP8<sup>+</sup> BMCs could not emigrate from bone marrow in MRP14-KO C57BL/6 mice, which is different from my results of the expression of MRP8 in peripheral tissues of MRP14-KO BALB/c mice. Manitz *et al.* also reported that MRP14 deficiency resulted in a 30% reduction of MRP8<sup>+</sup> cells in the bone marrow of their KO mice. In contrast, my MRP14-KO BALB/c mice showed unchanged ratio of MRP8<sup>+</sup> cells in BMCs (Figure 19e). Taken together, these results indicate that cellular MRP8 expression is suppressed in MRP14-KO BALB/c mice though

MRP8 expresses in their peripheral tissues.

The population of peripheral leukocytes seemed different between MRP14-KO BALB/c mice and the reported MRP14-KO C57BL/6 mice. While previous reports showed that deficiency of MRP14 did not affect the number and morphology of peripheral leukocytes (68, 69), here it was shown that the composition of neutrophils in peripheral leukocytes was significantly lower in MRP14-KO BALB/c mice than WT mice (Figure 20a-d). Because BMC population in MRP14-KO BALB/c mice was comparable to that of WT mice (Figure 20f-h), it is suggested that the emigration of peripheral neutrophils from bone marrow is dependent on MRP14 in naïve BALB/c mice. This is consistent with the report of Manitz *et al.* in which loss of MRP14 reduced the responsiveness of the neutrophils upon chemoattractant stimuli at least *in vitro* (68). The composition of lymphocytes in peripheral leukocytes was significantly higher in naïve MRP14-KO BALB/c mice than naïve WT mice (Figure 20a-d), indicating that lymphocytes emigrate into peripheral blood in compensate for the decrease of neutrophils. On the other hand, the composition of MRP8<sup>+</sup> neutrophils in liver was significantly higher in naïve MRP14-KO BALB/c mice than naïve WT mice (Figure 24c). The result suggests that the adherence of MRP8<sup>+</sup> neutrophils to sinusoid in the liver is also contributes to the decrease of peripheral neutrophils in naïve MRP14-KO mice.

The reaction to LPS is well-characterized model of endotoxin shock (83, 84, 89). In the report of Vogl *et al.*, LPS-induced shock model with MRP14-KO C57BL/6 mice demonstrated that MRP8 and MRP14 contribute to the pathogenesis of lethal endotoxic shock by amplifying the release of TNF- $\alpha$  (28). They showed that MRP14-KO C57BL/6 mice exhibited

a significantly higher survival rate compared to their WT controls in LPS-induced shock, and that TNF- $\alpha$  secretion by BMCs upon LPS stimulation *in vitro* was significantly lower in the MRP14-KO mice. Therefore, the survival rate and BMC activity to LPS of MRP14-KO BALB/c mice were compared with the reported results. In contrast, survival rate in LPS-induced shock was not significantly different between MRP14-KO BALB/c mice and WT BALB/c mice (Figure 22a), and that secretion of TNF- $\alpha$  by BMCs stimulated with LPS was significantly higher in BMCs of the MRP14-KO mice than the WT mice (Figure 21a, 21b, and 21d). Considering that the secretion of TNF- $\alpha$  induced by other TLR agonists showed no significant difference between MRP14-KO and WT BMCs (Figure 21d), it is suggested that the enhanced TNF- $\alpha$  secretion in MRP14-KO BMCs is LPS- or TLR4-specific reaction. Serum concentration of TNF- $\alpha$  was also significantly higher in the MRP14-KO mice than the WT mice after LPS injection (Figure 22d). The results may be explained by the hyporesponsiveness by MRP14. While MRP secretion from naïve BMC was low in the reported MRP14-KO C57BL/6 mice (28), MRP8 was constitutively secreted from BMC of MRP14-KO BALB/c mice (Figure 21c). It was reported that the pretreatment with nonactivating dose of MRP8 and MRP14 induced monocyte hyporesponsiveness in a TLR4-dependent manner (90). These facts suggest that the constitutively secreted MRP, TLR4 agonists, leads to the tolerance to TLR4 agonists in BMCs to some extent. It is anticipated that the MRP secretion was decreased in MRP14-KO mice, which attenuates the BMC hyporesponsiveness and leads stronger TLR4 signals than WT controls when BMCs are stimulated with high dose of LPS. The MRP8 secreted from MRP14-KO BMCs was higher than WT controls (Figure 21c) while the MRP8 expression was

suppressed in BMCs (Figure 19a), indicates that MRP8 gets secreted from the cells rapidly when MRP14 is missing, therefore stable expression in the cytosol is decreased. Since  $\text{Ca}^{2+}$  and  $\text{Zn}^{2+}$ -binding properties of MRP14 and MRP8 have a pivotal influence on their conformation and oligomerization state (15), including self-assembly into homo- and heterodimers, tetramers and larger oligomers, it is anticipated that the concentration of  $\text{Ca}^{2+}$  and  $\text{Zn}^{2+}$  can also influence the different stability of MRP8 in MRP14-KO mice. Besides, since MRP8 can form heterodimer with MRP14, it is also possible that MRP14 deletion technically increases the detection sensitivity of MRP8 by sandwich ELISA. Because it is well-known that LPS induces hepatic inflammation (91), the hepatic pathology of MRP14-KO BALB/c mice injected with LPS (Figure 23) was analyzed. There was no significant difference in pathology, serum hepatic enzymes and cytokines level between MRP14-KO mice and WT mice, which indicates that LPS-induced hepatic injury is independent of MRP14 in BALB/c mice. On the other hand, in an *E. coli*-induced sepsis model, it was reported that liver inflammation in MRP14-KO C57BL/6 mice was less profound compared with that in WT mice as reflected by lower total histology scores and serum hepatic enzymes (92). The present study demonstrates that MRP14 deficiency does not affect TNF- $\alpha$  secretion, pathology and lethality of LPS-induced shock in BALB/c mice. The number of peripheral leukocytes decreased after LPS-injection in both of MRP14-KO and WT mice (Figure 22b), indicating that the peripheral leukocytes immigrate and accumulated in tissues. The composition of peripheral neutrophils and lymphocytes were comparable between MRP14-KO and WT mice injected with LPS (Figure 22c) whereas the composition of neutrophils in peripheral leukocytes was significantly lower in naïve MRP14-KO BALB/c mice

than naïve WT mice (Figure 20b). It is indicated that MRP14 may be related to the leukocytes emigration from bone marrow. The deletion of MRP14, an TLR4 agonist, induces the overreaction of TLR4 signaling to LPS, which may promote the emigration of neutrophils from bone marrow in response to high concentration of LPS. On the other hand, the migration of MRP8<sup>+</sup> cells was dependent on MRP14 (Figure 24). The number of accumulated MRP8<sup>+</sup> cells in organs was significantly lower in the MRP14-KO mice than the WT controls after LPS injection, which was consistent with the reduced number of accumulated cells in the liver of the MRP14-KO mice after LPS injection (Figure 23b). The reduced number of accumulated cells in the liver of MRP14-KO mice was not consistent with the number of peripheral leukocytes which is comparable between MRP14-KO and WT mice (Figure 22b). The results indicate that MRP14 contributes to promote the expression of adherent molecules induced by LPS in the liver. Actually, it is reported that MRP14 promotes the up-regulation of ICAM-1 and VCAM-1 on the endothelial cells, which leads to macrophage adhesion (93). As described above, it is anticipated that TLR4 signals in BMCs are desensitized to some extent by MRP14 since MRP14 is expressed and secreted in bone marrow. In the bone marrow of MRP14-KO mice, instead of the BMC hyporesponsiveness to TLR4 agonists, the overreaction of TLR4 signaling can be induced in BMCs when stimulated by high dose of LPS. On the other hand, the hyporesponsiveness is not induced in the cells of naïve liver, in which MRP14 is rarely expressed in constitutive situation. In MRP14 KO mice, promotion of adherent molecules by MRP14 is suppressed during LPS injection. Besides, the population analysis of accumulated MRP8<sup>+</sup> cells showed that the monocytes were significantly dominant to neutrophils in WT mice compared with MRP14-KO

mice. These results suggest that MRP8<sup>+</sup> monocytes rather than MRP8<sup>+</sup> neutrophils immigrate and adhere in the liver in a manner dependent on MRP14 during LPS-induced shock. Besides, there was no significant difference in cytokine levels in the spleen and liver between MRP14-KO mice and WT mice (Figure 23e) whereas the accumulation of MRP8<sup>+</sup> cells in the organs was significantly suppressed in the MRP14-KO mice after LPS injection (Figure 24). It may be explained by the higher cellular capacity of BMCs from MRP14-KO mice to secrete TNF- $\alpha$  upon stimulation with LPS than WT controls (Figure 21).

Besides, it is demonstrated that MRP14 promotes GM-CSF expression in BMCs (Figure 25), which suggests that MRP14 is related to BMC differentiation. Because the Alamar Blue assay showed that MRP14 did not promote the proliferation of BMCs, it is indicated that MRP14 is related to the differentiation more than the proliferation of BMCs in myelopoiesis. In MRP14-KO BALB/c mice, the population of neutrophils and monocytes as well as expression of MRP8, CD11b, F4/80 and CD68 in BMCs were comparable to the WT controls (Figure 19d, 19e, 20f, 20g and 25e). Because the basal expression level of GM-CSF in bone marrow was also comparable between the two groups, these results suggest that there were other factors which promote GM-CSF in compensation for MRP14. Actually, it is known that GM-CSF is induced by IL-1 $\beta$ , IL-6 or TNF- $\alpha$  (94), and the expression of these cytokines in BMCs of MRP14-KO mice was comparable to WT controls (Figure 23e). Manitz *et al.* also reported that the proliferation of MRP14-KO BMCs was comparable to WT controls when stimulated by GM-CSF (68). Interestingly, I could not observe the production of GM-CSF when BMCs were stimulated with MRP8, even though MRP8 shows cell activity to RAW264.7 cells. Recently, it

was reported that MRP14 induces myelomonocytic cell differentiation, whereas MRP8 prevents differentiation induced by MRP14 activity and maintains immature phenotype in acute myeloid leukemia (47). Also, it is reported that MRP14 potentiates neutrophils to GM-CSF-induced cytokine production (95), which suggests that MRP14 amplify GM-CSF-induced cellular differentiation and activation. I showed that MRP8 was detected not only in BMCs of WT mice but also in BMCs of MRP14-KO mice (Figure 21c). The secretion of MRP8 was not dependent on LPS-stimulation, and MRP8 and MRP14 were secreted even in the absence of LPS, which suggests that these proteins are secreted by BMCs constitutively in bone marrow. While MRP14 and MRP8 have been characterized as inflammation-related proteins, my data give a new insight of MRP14 function in homeostatic myelopoiesis. Besides, the different reactivity of BMCs between BALB/c and C57BL/6 (Figure 25d) indicates that BMC phenotypes were different between the two mice strains.

The differences between BALB/c-background MRP14-KO mice and previously reported C57BL/6-background MRP14-KO mice are summarized in Table 1. Thus, MRP14-KO BALB/c mice model may help expand the existing insights on functions of MRP8 and MRP14 in immunological processes. The uncomplete absence of MRP8 in peripheral tissues of MRP14-KO BALB/c mice could be related to such differences, which indicates that MRP14-KO BALB/c mice is a valuable model for tracking MRP8<sup>+</sup> cells in the absence of MRP14. It is known that there are differences in inflammatory reactions, pathology and susceptibility to various diseases between C57BL/6 and BALB/c strains. For example, it was reported that C57BL/6 macrophages are far more sensitive to stimulus by IFN- $\gamma$  plus LPS for production of NO than are BALB/c

cells (96). Also, there are differences in expression of TLRs and responses to TLR agonists between BALB/c and C57BL/6 mice; dendritic cell (DC) isolated from the spleen of C57BL/6 mice preferentially expresses TLR9 mRNA, whereas DC from BALB/c mice strongly expresses TLR2, TLR4, TLR5, and TLR6 mRNAs (97). Besides, dynamics of MRP8/MRP14 expression during inflammatory responses are different between the two mouse strains. In *Leishmania major* infection, resistance C57BL/6 mice show a significantly lower percentage of MRP14<sup>+</sup> cells in the infiltrate during the early course of infection than in susceptible BALB/c mice (98). In the infection with *Ureaplasma parvum*, severe chorioamnionitis with cellular necrosis is the predominant lesion phenotype in BALB/c mice, which also exhibits a significant increase in placental expression of IL-1 $\alpha$ , IL-1 $\beta$ , IL-6, TNF- $\alpha$ , MRP8 and MRP14, though C57BL/6 predominantly exhibits mild to moderate chorioamnionitis with a significant reduction in placental expression of those cytokines (99). Because kinetics of MRP8<sup>+</sup> cells and MRP14<sup>+</sup> cells during inflammatory disorders are not uniform among disease types and among individuals (98, 100), indicating that immunological functions of MRP8 and MRP14 are affected by many factors including stimuli type of the pathogen and genetic background of the host. Therefore, the MRP14-KO mice with BALB/c background developed in the present study will complement the understanding of immunological functions of MRP14 as well as MRP8.

In chapter 3, it is revealed that MRP14 deficiency does not improve LPS-induced shock in BALB/c mice, although it is reported that MRP14-KO C57BL/6 mice were less severely affected and survived significantly longer (28). Besides, the hyperresponsiveness of TNF- $\alpha$  secretion from BMCs in MRP14-KO BALB/c mice was induced by LPS, which is contrast to

the suppression of TNF- $\alpha$  secretion from BMCs in MRP14-KO C57BL/6 mice. It is suggested that MRP14 deficiency induces not only the simple deletion of extracellular MRP14 function as an inflammation enhancer but also affects intracellular MRP14 function to maintain TLR4 signaling in myeloid cells of BALB/c mice.

## General discussion

In the present study, it is demonstrated that extracellular MRP14 exacerbates hepatic injury during rodent malaria. In chapter 1, it was shown that extracellular MRP14 promotes the accumulation of MRP8<sup>+</sup> and MRP14<sup>+</sup> macrophages and the up-regulation of pro-inflammatory molecules, which exacerbates hepatic injury during rodent malaria. It is indicated that the pro-inflammatory cytokines and NO induced by MRP14 are involved in the inflammatory response, which leads to hepatic injury during rodent malaria. Also, extracellular MRP14 induces the up-regulation CCR2 and CCL2, which suggests that these molecules are involved in the cellular recruitment to the tissue during rodent malaria. In chapter 2, MRP14 deficiency could not improve hepatic injury during rodent malaria. There was no significant difference in hepatic injury and pro-inflammatory cytokines levels between MRP14-KO BALB/c mice and WT mice. Those results suggest that MRP14 deficiency induces not only the simple deletion of extracellular MRP14 function to promote inflammation but also affects intracellular MRP14 function, which leads to other changes in immunological characters in myeloid cells of BALB/c mice. In chapter 3, it was revealed that MRP14 deficiency also could not improve the survival rate of LPS-induced shock in BALB/c mice, although it is reported that MRP14-KO C57BL/6 mice were less severely affected and survived significantly longer (28). BMCs in MRP14-KO BALB/c mice showed the hyperresponsiveness of TNF- $\alpha$  secretion, which is contrast to the suppression of TNF- $\alpha$  secretion from BMCs in MRP14-KO C57BL/6 mice (28). Those results suggest that intracellular MRP14 deficiency enhances TLR4 signaling in myeloid cells of BALB/c mice, which leads to hyperresponsiveness of myeloid cells in inflammation. The present

study elucidated that MRP14 has multiple functions not only to promote inflammation but also to maintain TLR4 signaling in myeloid cells of BALB/c mice.

Although MRP14 administration exacerbates liver inflammation and hepatic injury in chapter 1, MRP14 deficiency could not influence the levels of hepatic injury and pro-inflammatory molecules in chapter 2 and 3. BMCs from MRP14-KO BALB/c mice secreted higher TNF- $\alpha$  upon stimulation with LPS than WT controls (Figure 21) whereas TNF- $\alpha$  secretion induced by LPS was suppressed from BMCs in the reported MRP14-KO C57BL/6. The expression level of inflammatory cytokines in the liver was comparable between MRP14-KO and WT mice during both of Pb-infection and LPS-injection (Figure 16 and 23), which may be explained by the higher reactivity of TLR4 signaling in BMCs of MRP14-KO BALB/c mice. Actually, GPI anchor molecules of *Plasmodium* parasites as well as LPS is known to activate TLR4 as a PAMPs (101).

It is also suggested that other factors including PAMPs and DAMPs can compensate for MRP14 absence. As one of the factors, MRP8 cannot be excluded. MRP8, which is reported to work as a DAMP (15, 102), was still at a detectable level in the peripheral tissues of MRP14-KO BALB/c mice although MRP8 expression is absent in the peripheral tissues of MRP14-KO C57BL/6 mice (68, 69). Considering that cellular MRP8 expression is suppressed in MRP14-KO BALB/c mice (Figure 19), it is considered that even a small amount of MRP8 can act as a trigger of inflammatory cascade. Also, some studies reported that MRP14 deficiency does not influence the pathology and outcome of disease in several models such as epidermolysis bullosa acquisita, bullous pemphigoid, arthritis, and urinary tract bacterial infection (103–106). These

reports also indicate that other DAMPs can compensate for MRP14 deficiency in inflammatory responses involved in pathology. On the other hand, high level of MRP14 amplifies inflammatory responses and exacerbates hepatic injury. Besides, it was observed that mice injected with both of MRP14 and MRP8 showed severer hepatic injury and cellular accumulation than mice injected with MRP14 alone. Those results suggest that both of MRP14 and MRP8 are potent amplification factors for inflammatory cascade, and that the more MRPs there are, the stronger the positive feedback become. Thus, it is concluded that MRP14 has an important role as a DAMP which promotes inflammatory responses, leading to hepatic injury.

The differences between LPS-injected and Pb-infected models are summarized in Table 2. The accumulation level of MRP8<sup>+</sup> cells in the liver was different between Pb-infected and LPS-injected MRP14-KO mice (In chapter 2 and 3). At day 7 of Pb-infection, the number of the accumulated MRP8<sup>+</sup> cells in the liver was comparable between MRP14-KO mice and WT mice (Figure 15), whereas the number of the accumulated MRP8<sup>+</sup> cells was significantly lower in MRP14-KO mice than WT mice after 20 hr of LPS injection (Figure 24). It is indicated that migration of MRP8<sup>+</sup> cell is dependent on MRP14 in acute responses (for ~20 hr), but not in subacute responses (for ~7 days). The results may partially be explained by the different activation of inflammatory macrophages between liver and spleen (Figure 11). In acute responses in 20 hr of LPS-injection, M1 macrophage activation in the liver and M2 macrophage activation in the spleen is not promoted, MRP8<sup>+</sup> cells are recruited to the liver and spleen similarly. Since the number of MRP8<sup>+</sup> cells in bone marrow and peripheral leukocytes are comparable between naïve MRP14-KO mice and WT mice (Figure 19e), it is indicated that the adhesion of MRP8<sup>+</sup>

cells in liver is dependent on MRP14 during acute responses such as LPS-induced shock. On the other hand, in subacute responses in 7 days of Pb-injection, M1 macrophage activation is dominant in the liver and M2 macrophage activation is dominant in the spleen (figure 11). Since MRP14 promotes type 1 cytokines, it is considered that MRP14<sup>+</sup> macrophage is M1 macrophage. Considering that M1 macrophages activate type 1 cytokine cascade by positive feedback (78) and MRP14 deletion induces more activation of M2 macrophage in spleen during rodent malaria, it is anticipated that MRP8<sup>+</sup> macrophages are more likely to accumulate in the liver than spleen during malaria, which results in comparable number of accumulated MRP8<sup>+</sup> macrophages in the liver of MRP14-KO and WT mice during rodent malaria. Also, it is anticipated that other factors compensate for MRP14 absence and promote recruitment of MRP8<sup>+</sup> cells from bone marrow, showing comparable number of the cells between MRP14-KO and WT mice during Pb-infection. For example, it is reported that CCR2 is required for emigration of Ly6C<sup>high</sup> monocytes from bone marrow (107), and actually, the expression level of CCR2 was comparable between MRP14-KO mice and WT mice after Pb-infection (Figure 17).

Besides, the number of peripheral leukocytes in MRP14-KO mice was significantly lower than that in WT mice at day 7 of Pb-infection whereas the number of peripheral leukocytes was comparable in both of the two groups after 20hr of LPS injection (Figure 13e and 22b). The results indicate that BMC emigration from bone marrow is suppressed in MRP14-KO mice during Pb-infection. I first demonstrated that MRP14 up-regulates GM-CSF expression in BMCs (Figure 25), which suggests that MRP14 promotes GM-CSF-induced cellular differentiation and activation. GM-CSF promotes proliferation, differentiation and pro-inflammatory cytokine

production in macrophages (101). It is known that GM-CSF is low level in naïve mice but is induced by IL-1 $\beta$ , IL-6 or TNF- $\alpha$  during inflammation. During Pb-infection, MRP14 secretion is promoted in bone marrow, which induces GM-CSF up-regulation promoting BMC differentiation. It was reported that MRP14 induces myelomonocytic cell differentiation, whereas MRP8 prevents differentiation induced by MRP14 activity and maintains immature phenotype in acute myeloid leukemia (47). Thus, MRP8, which can be secreted rapidly when MRP14 is missing, may also be related to the suppression of BMC differentiation in MRP14-KO mice during Pb-infection. It is considered that the suppression of BMC differentiation by MRP14 during Pb-infection induces the suppression of BMC proliferation and emigration which followed by BMC differentiation. On the other hand, in acute responses in 20 hr of LPS-injection, there is not enough time for BMC differentiation by MRP14. Therefore, BMC population and the number of peripheral leukocytes were comparable between MRP14-KO mice and WT mice injected with LPS (Figure 22b and 25e), indicating that BMC differentiation and emigration is not induced yet in 20 hr of LPS-injection.

Taken together, hypothesized MRP14 function in hepatic injury during rodent malaria is illustrated in Figure 26. Extracellular MRP14 promotes the secretion of pro-inflammatory cytokines such as IL-1 $\beta$ , TNF- $\alpha$ , IL-6 and IL-12 from macrophages via TLR2 and TLR4. The pro-inflammatory cytokines induce the up-regulation of iNOS, which produces high concentration of NO. NOX2, which is expressed in macrophages, is also important to generate superoxide, which reacts with NO and leads to cytotoxic peroxynitrite (53). Actually, NOX2 was up-regulated by extracellular MRP14 in the liver of Pb-infected mice (Figure 8 and 9). High

levels of NO have cytotoxic and pro-inflammatory effects leading to necrosis of hepatocytes. IL-12 is a potent inducer of IFN- $\gamma$ , and IFN- $\gamma$  produced by Pb-pRBC antigen-specific T cells facilitates the production of NO. Extracellular MRP14 also promotes the accumulation of macrophages (including MRP8<sup>+</sup> and MRP14<sup>+</sup> macrophages) in the sinusoid of liver, to which CCR2 and CCL2 may contribute. Also, extracellular MRP14 may amplify GM-CSF-induced macrophage differentiation during Pb-infection. In this way, the accumulated macrophages promote the inflammatory cascade by positive feedback of cytokines and further macrophage recruitment, which leads to hepatic injury. MRP14 deficiency induces not only the simple deletion of extracellular MRP14 function to promote inflammation but also affects intracellular MRP14 function. Intracellular MRP14 deficiency induces the hyperresponsiveness of TLR4 signaling in myeloid cells, which keep comparable inflammatory cytokine levels to WT during inflammation.

In conclusion, the present study revealed that extracellular MRP14 is an one of key molecules for liver inflammation during rodent malaria. Besides, it is also elucidated that MRP14 deficiency induces not only the simple deletion of extracellular MRP14 function to promote inflammation but also affects intracellular MRP14 function to maintain TLR4 signaling in myeloid cells of BALB/c mice. Although most of previous studies have focused on the function of extracellular MRP14 as an inflammation enhancer, the present study gives a new insight of intracellular MRP14 function. More broad understanding of immunological function of MRP14 found in this study will leads to a new treatment of hepatic injury during malaria.

## **Acknowledgement**

I would like to express my gratitude to Assistant Professor Wataru Fujii (Laboratory of Applied Genetics, Graduate school of Agricultural and Life Sciences, the University of Tokyo) for producing and providing MRP14-KO BALB/c mice used in this study.

I'm also very grateful to Professor Yoshitsugu Matsumoto (Laboratory of Molecular Immunology, Graduate school of Agricultural and Life Sciences, the University of Tokyo) for giving me the constitutive advice and support during this study.

I also would like to show the deep appreciation to the Japan Society for the Promotion of Science for supports by DC1 fellowship programs and KAKENHI Grant (grant No. 15J08617).

I also want to express my sincere thanks to all the member of Laboratory of Molecular Immunology, for the warm and kind friendship.

Finally, I would like to express my gratitude to my supervisor, Associate Professor Yasuyuki Goto (Laboratory of Molecular Immunology, Graduate school of Agricultural and Life Sciences, the University of Tokyo) for providing invaluable discussions.

## References

1. Langhorne J, Ndungu FM, Sponaas A, Marsh K. 2008. Immunity to malaria : more questions than answers. *Nat Immunol* 9:725–732.
2. Das S, Mohapatra B, Mohanty R, Dash P, Kar K, Dash P. 2007. Malarial hepatitis as a component of multiorgan failure—a bad prognostic sign. *J Indian Med Assoc* 105:247–250.
3. World Health Organization. 2014. Severe Malaria. *Trop Med Int Heal* 19:7–131.
4. Anand A, Ramji C, Narula A, Singh W. 1992. Malarial hepatitis: a heterogeneous syndrome? *Natl Med J India* 5:59–62.
5. Anand A, Puri P. 2005. Jaundice in malaria. *J Gas- troenterology Hepatol* 20:1322–1332.
6. Kochar D, Singh P, Agarwal P, Kochar S, Pokharna R, Sa- reen P. 2003. Malarial Hepatitis. *J Assoc Physicians India* 51:1069–1072.
7. Rupani AB, Amarapurkar AD. 2009. Hepatic changes in fatal malaria : an emerging problem. *Ann Trop Med Parasitol* 103:119–127.
8. Prommano O, Chaisri U, Turner G, Wilairatana P, Ferguson D, Viriyavejakul P, White N, Pongponratn E. 2005. A quantitative ultrastructural study of the liver and the spleen in fatal falciparum malaria. *South East Asian J Trop Med Public Heal* 36:1359–1370.
9. Mackey LJ, Hochmann A, June CH, Contreras CE, Lambert PH. 1980. Immunopathological aspects of Plasmodium berghei infection in five strains of mice. *Clin Exp Immunol* 42:412–420.
10. Yoshimoto T, Takahama Y, Wang C, Yoneto T, Waki S, Nariuchi H, Alerts E. 1998. A

Pathogenic Role of IL-12 in Blood-Stage Murine Malaria Lethal Strain *Plasmodium berghei* NK65 Infection. *J Immunol* 160:5500–5505.

11. Adachi K, Tsutsui H, Kashiwamura S, Seki E, Nakano H, Takeuchi O, Okumura K, Kaer L Van, Okamura H, Akira S, Nakanishi K, Alerts E. 2001. *Plasmodium berghei* Infection in Mice Induces Liver Injury by an IL-12- and Toll-Like Receptor/Myeloid Differentiation Factor 88-Dependent Mechanism. *J Immunol* 167:5928–5934.
12. Haque A, Best SE, Amante FH, Ammerdorffer A, Labastida F De, Pereira T, Ramm GA, Engwerda CR. 2011. High parasite burdens cause liver damage in mice following *Plasmodium berghei* ANKA infection independently of CD8(+) T cell-mediated immune pathology. *Infect Immun* 79:1882–1888.
13. Gebhardt C, Németh J, Angel P, Hess J. 2006. S100A8 and S100A9 in inflammation and cancer. *Biochem Pharmacol* 72:1622–1631.
14. Ehrchen JM, Sunderkotter C, Foell D, Vogl T, Roth J. 2009. The endogenous Toll-like receptor 4 agonist S100A8/S100A9 (calprotectin) as innate amplifier of infection, autoimmunity, and cancer. *J Leukoc Biol* 86:557–566.
15. Vogl T, Gharibyan AL, Morozova-Roche LA. 2012. Pro-inflammatory S100A8 and S100A9 proteins: Self-assembly into multifunctional native and amyloid complexes. *Int J Mol Sci* 13:2893–2917.
16. Edgeworth J, Gorman M, Bennett R, Freemont P, Hogg N. 1991. Identification of p8,14 as a highly abundant heterodimeric calcium binding protein complex of myeloid cells. *J Biol Chem* 266:7706–7713.

17. Goebeler M, Roth J, Henseleit U, Sunderkötter C, Sorg C. 1993. Expression and complex assembly of calcium-binding proteins MRP8 and MRP14 during differentiation of murine myelomonocytic cells. *J Leukoc Biol* 53:11–18.
18. Hunter MJ, Chazin WJ. 1998. High level expression and dimer characterization of the S100 EF-hand proteins, migration inhibitory factor-related proteins 8 and 14. *J Biol Chem* 273:12427–12435.
19. Hessian P, Edgeworth J, Hogg N. 1993. MRP-8 and MRP-14, two abundant Ca<sup>2+</sup>-binding proteins of neutrophils and monocytes. *J Leukoc Biol* 53:197–204.
20. Frosch M, Strey A, Vogl T, Wulffraat NM, Kuis W, Sunderkötter C, Harms E, Sorg C, Roth J. 2000. Myeloid-related proteins 8 and 14 are specifically secreted during interaction of phagocytes and activated endothelium and are useful markers for monitoring disease activity in pauciarticular-onset juvenile rheumatoid arthritis. *Arthritis Rheum* 43:628–637.
21. Frosch M, Vogl T, Seeliger S, Wulffraat N, Kuis W, Viemann D, Foell D, Sorg C, Sunderkötter C, Roth J. 2003. Expression of myeloid-related proteins 8 and 14 in systemic-onset juvenile rheumatoid arthritis. *Arthritis Rheum* 48:2622–2626.
22. van Lent PLEM, Grevers L, Blom AB, Sloetjes A, Mort JS, Vogl T, Nacken W, van den Berg WB, Roth J. 2008. Myeloid-related proteins S100A8/S100A9 regulate joint inflammation and cartilage destruction during antigen-induced arthritis. *Ann Rheum Dis* 67:1750–1758.
23. Rammes A, Roth J, Goebeler M, Klempt M, Hartmann M, Sorg C. 1997. Myeloid-related

protein (MRP) 8 and MRP14, calcium-binding proteins of the S100 family, are secreted by activated monocytes via a novel, tubulin- dependent pathway. *J Biol Chem* 272:9496–9502.

24. Altwegg LA, Neidhart M, Hersberger M, Müller S, Eberli FR, Corti R, Roffi M, Sütsch G, Gay S, Von Eckardstein A, Wischnewsky MB, Lüscher TF, Maier W. 2007. Myeloid-related protein 8/14 complex is released by monocytes and granulocytes at the site of coronary occlusion: A novel, early, and sensitive marker of acute coronary syndromes. *Eur Heart J* 28:941–948.
25. Benoit S, Toksoy A, Ahlmann M, Schmidt M, Sunderkötter C, Foell D, Pasparakis M, Roth J, Goebeler M. 2006. Elevated serum levels of calcium-binding S100 proteins A8 and A9 reflect disease activity and abnormal differentiation of keratinocytes in psoriasis. *Br J Dermatol* 155:62–66.
26. Chen B, Miller AL, Rebelatto M, Brewah Y, Rowe DC, Clarke L, Czapiga M, Rosenthal K, Imamichi T, Chen Y. 2015. S100A9 Induced Inflammatory Responses Are Mediated by Distinct Damage Associated Molecular Patterns ( DAMP ) Receptors In Vitro and In Vivo. *PLoS One* 10:e0115828.
27. Bordmann G, Burmeister G, Saladin S, Urassa H, Mwankyusye S, Weiss N, Tanner M. 1997. MRP 8 / 14 as Marker for Plasmodium falciparum -Induced Malaria Episodes in Individuals in a Holoendemic Area. *Clin Diagnostic Laboratory Immunol* 4:435–439.
28. Vogl T, Tenbrock K, Ludwig S, Leukert N, Ehrhardt C, van Zoelen MAD, Nacken W, Foell D, van der Poll T, Sorg C, Roth J. 2007. Mrp8 and Mrp14 are endogenous activators

- of Toll-like receptor 4, promoting lethal, endotoxin-induced shock. *Nat Med* 13:1042–1049.
29. Roth J, Vogl T, Sorg C, Sunderko C. 2003. Phagocyte-specific S100 proteins: a novel group of proinflammatory molecules. *Trends Immunol* 24:155–158.
  30. Mizobuchi H, Yamakoshi S, Omachi S, Osada Y, Sanjoba C, Goto Y, Matsumoto Y. 2014. The accumulation of macrophages expressing myeloid-related protein 8 (MRP8) and MRP14 in the spleen of BALB/cA mice during infection with *Plasmodium berghei*. *Exp Parasitol* 138:1–8.
  31. Clark I, Nicholas H, Butcher GA. 1987. Inhibition of murine malaria (*Plasmodium chabaudi*) in vivo by recombinant interferon-gamma or tumor necrosis factor, and its enhancement by butylated hydroxyanisole. *J Immunol* 139:3493–3496.
  32. Stevenson M, Tam M, Belosevic M, van der Meide P, Podoba J. 1990. Role of Endogenous Gamma Interferon in Host Response to Infection with Blood-Stage *Plasmodium chabaudi* AS. *Infect Immun* 58:3225–3232.
  33. Meding SJ, Cheng SHICHI, Simon-haarhaus B, Langhorne J. 1990. Role of Gamma Interferon during Infection with *Plasmodium chabaudi chabaudi*. *Infect Immun* 58:3671–3678.
  34. Waki S, Uehara S, Kanbe K, Ono K, Suzuki M, Departments HN. 1992. The role of T cells in pathogenesis and protective immunity to murine malaria. *Immunology* 75:646–651.
  35. Finley RW, Mackey J, Lambert PH. 1982. Virulent *P. berghei* malaria: prolonged

- survival and decreased cerebral pathology in cell-dependent nude mice. *J Immunol* 129:2213–2218.
36. Hon W, Lee K, Khoo H. 2002. Nitric Oxide in Liver Diseases Friend, Foe, or Just Passerby ? *Ann New York Acad Sci* 295:275–295.
  37. Guzik T, Korb R, Adamek-Guzik T. 2003. Nitric oxide and superoxide in inflammation and immune regulation. *J Physiol Pharmacol* 54:469–487.
  38. Akira S, Takeda K. 2004. Toll-like receptor signalling. *Nat Rev Immunol* 4:499–511.
  39. Kawai T, Akira S. 2006. TLR signaling. *Cell Death Differ* 13:816–825.
  40. Riva M, Källberg E, Björk P, Hancz D, Vogl T, Roth J, Ivars F, Leanderson T. 2012. Induction of nuclear factor- $\kappa$ B responses by the S100A9 protein is Toll-like receptor-4-dependent. *Immunology* 137:172–182.
  41. Basir R, Rahiman S, Hasballah K, Chong W, Talib H, Yam M, Jabbarzare M, Tie T, Othman F, Moklas M, Abdullah W, Ahman Z. 2012. Plasmodium berghei ANKA Infection in ICR Mice as a Model of Cerebral Malaria. *Iran J Parasitol* 7:62–74.
  42. Loser K, Vogl T, Voskort M, Lueken A, Kupas V, Nacken W, Klenner L, Kuhn A, Foell D, Sorokin L, Luger TA, Roth J, Beissert S. 2010. The Toll-like receptor 4 ligands Mrp8 and Mrp14 are crucial in the development of autoreactive CD8<sup>+</sup> T cells. *Nat Med* 16:713–717.
  43. Barton GM, Kagan JC. 2009. A cell biological view of Toll-like receptor function: regulation through compartmentalization. *Nat Rev Immunol* 9:535–542.
  44. Coban C, Ishii KJ, Kawai T, Hemmi H, Sato S, Uematsu S, Yamamoto M, Takeuchi O,

- Itagaki S, Kumar N, Horii T, Akira S. 2005. Toll-like receptor 9 mediates innate immune activation by the malaria pigment hemozoin. *J Exp Med* 201:19–25.
45. Takeuchi A, Mühlradt PF, Takeda K, Shintaro Sato S, Nomura F, Kawai T, Sato S, Takeuchi O, Mühlradt PF, Akira S. 2000. Synergy and Cross-Tolerance Between Toll-Like Receptor (TLR) 2-and TLR4-Mediated Signaling Pathways. *J Immunol* 165:7096–7101.
46. De Nardo D, De Nardo CM, Nguyen T, Hamilton JA, Scholz GM. 2009. Signaling Crosstalk during Sequential TLR4 and TLR9 Activation Amplifies the Inflammatory Response of Mouse Macrophages. *J Immunol* 183:8110–8118.
47. Laouedj M, Tardif MR, Gil L, Raquil M-A, Lachaab A, Pelletier M, Tessier PA, Barabé F. 2017. S100A9 induces differentiation of acute myeloid leukemia cells through TLR4. *Blood* 129:blood-2016-09-738005.
48. Vandal K, Rouleau P, Boivin A, Ryckman C, Talbot M, Tessier PA. 2003. Blockade of S100A8 and S100A9 Suppresses Neutrophil Migration in Response to Lipopolysaccharide. *J Immunol* 171:2602–2609.
49. Schnekenburger J, Schick V, Krüger B, Manitz MP, Sorg C, Nacken W, Kerkhoff C, Kahlert A, Mayerle J, Domschke W, Lerch MM. 2008. The calcium binding protein S100A9 is essential for pancreatic leukocyte infiltration and induces disruption of cell-cell contacts. *J Cell Physiol* 216:558–567.
50. De Jong H, Achouiti A, Koh G, Parry C, Baker S, Faiz M, van Dissel J, Vollaard A, van Leeuwen E, Roelofs J, se Vos A, Roth J, van der Poll T, Vogl T, Wiersinga W. 2015.

Expression and Function of S100A8 / A9 ( Calprotectin ) in Human Typhoid Fever and the Murine Salmonella Model. PLoS Negl Trop Dis 9:e0003663.

51. Fukumura D, Kashiwagi S, Jain RK. 2006. The role of nitric oxide in tumour progression. *Nat Rev Cancer* 6:521–534.
52. Gabrilovich DI, Nagaraj S. 2009. Myeloid-derived suppressor cells as regulators of the immune system. *Nat Rev Immunol* 9:162–174.
53. Drummond GR, Sobey CG. 2014. Endothelial NADPH oxidases : which NOX to target in vascular disease ? *Trends Endocrinol Metab* 25:452–463.
54. Ryckman C, Vandal K, Rouleau P, Tessier PA, Ryckman C, Vandal K, Rouleau P, Tessier PA. 2003. Proinflammatory Activities of S100: Proteins S100A8, S100A9, and S100A8/A9 Induce Neutrophil Chemotaxis and Adhesion. *J Immunol* 170:3233–3242.
55. Ryckman C, Mccoll SR, Vandal K, Me R De, Poubelle PE, Tessier PA. 2003. Role of S100A8 and S100A9 in Neutrophil Recruitment in Response to Monosodium Urate Monohydrate Crystals in the Air-Pouch Model of Acute Gouty Arthritis. *Arthritis Rheum* 48:2310–2320.
56. Vogl T, Ludwig S, Goebeler M, Strey A, Thorey IS, Reichelt R, Foell D, Gerke V, Manitz MP, Nacken W, Werner S, Sorg C, Roth J, Sa MRP. 2004. MRP8 and MRP14 control microtubule reorganization during transendothelial migration of phagocytes. *Blood* 104:4260–4269.
57. Raquil M, Anceriz N, Rouleau P, Tessier PA, Raquil M, Anceriz N, Rouleau P, Tessier PA. 2008. Blockade of Antimicrobial Proteins S100A8 and S100A9 Inhibits Phagocyte

- Migration to the Alveoli in Streptococcal Pneumonia Marie-Astrid. *J Immunol* 180:3366–3374.
58. Mossanen J, Krenkel O, Ergen C, Govaere O, Liepelt A, Puengel T, Heymann F, Kalthoff S, Lefebvre E, Eulberg D, Luedde T, Marx G, Strassburg C, Roskams T, Trautwein C, Tacke F. 2016. Chemokine (C-C Motif) Receptor 2–Positive Monocytes Aggravate the Early Phase of Acetaminophen-Induced Acute Liver Injury. *Hepatology* 64:1667–1682.
59. Baeck C, Wehr A, Karlmark KR, Heymann F, Vucur M, Gassler N, Huss S, Klussmann S, Eulberg D, Luedde T, Trautwein C, Tacke F. 2012. Pharmacological inhibition of the chemokine CCL2 ( MCP-1 ) diminishes liver macrophage infiltration and steatohepatitis in chronic hepatic injury. *Gut* 61:416–26.
60. Sisto F, Miluzio A, Leopardi O, Mirra M, Boelaert JR, Taramelli D. 2003. Differential Cytokine Pattern in the Spleens and Livers of BALB / c Mice Infected with *Penicillium marneffeii* : Protective Role of Gamma Interferon. *Infect Immun* 71:465–473.
61. Ohmori Y, Hamilton TA. 2016. Requirement for STAT1 in LPS-induced gene expression in macrophages. *J Leukoc Biol* 69:598–604.
62. Davies LC, Jenkins SJ, Allen JE, Taylor PR. 2013. Tissue-resident macrophages. *Nat Immunol* 14:986–995.
63. Okabe Y, Medzhitov R. 2014. Tissue-Specific Signals Control Reversible Program of Localization and Functional Polarization of Macrophages. *Cell* 157:832–844.
64. Rosas M, Davies LC, Giles PJ, Liao C, Kharfan B, Stone TC, O’Donnell VB, Fraser DJ, Jones SA, Taylor PR. 2014. The transcription factor Gata6 links tissue macrophage

- phenotype and proliferative renewal. *Science* (80- ) 344:645–8.
65. Mantovani A, Sozzani S, Locati M, Allavena P, Sica A, Mantovani A. 2002. Macrophage polarization: tumor-associated macrophages as a paradigm for polarized M2 mononuclear phagocytes. *Trends Immunol* 23:549–555.
  66. Liu G, Yang HUI. 2013. Modulation of Macrophage Activation and Programming in Immunity. *J Cell Physiol* 228:502–512.
  67. Schlaepfer E, Rochat M, Duo L, Speck R. 2014. Triggering TLR2, -3, -4, -5, and -8 Reinforces the Restrictive Nature of M1- and M2-Polarized Macrophages to HIV. *J Virol* 88:9769–9781.
  68. Manitz M-P, Horst B, Seeliger S, Strey A, Skryabin B V., Gunzer M, Frings W, Schonlau F, Roth J, Sorg C, Nacken W. 2003. Loss of S100A9 (MRP14) Results in Reduced Interleukin-8-Induced CD11b Surface Expression, a Polarized Microfilament System, and Diminished Responsiveness to Chemoattractants In Vitro. *Mol Cell Biol* 23:1034–1043.
  69. Hobbs J, May R, Tanousis K, Mathies M, Gebhardt C, Robinson MJ, Hogg N, Mcneill E, Henderson R. 2003. Myeloid Cell Function in MRP-14 ( S100A9 ) Null Mice. *Mol Cell Biol* 14:2564–2576.
  70. Passey RJ, Williams E, Lichanska a M, Wells C, Hu S, Geczy CL, Little MH, Hume D a. 1999. A null mutation in the inflammation-associated S100 protein S100A8 causes early resorption of the mouse embryo. *J Immunol* 163:2209–2216.
  71. Croce K, Gao H, Wang Y, Mooroka T, Sakuma M, Shi C, Sukhova GK, Packard RRS, Hogg N, Libby P, Simon DI. 2009. Myeloid-related protein-8/14 is critical for the

- biological response to vascular injury. *Circulation* 120:427–436.
72. Achouiti A, Vogl T, Endeman H, Mortensen BL, Laterre P-F, Wittebole X, van Zoelen MAD, Zhang Y, Hoogerwerf JJ, Florquin S, Schultz MJ, Grutters JC, Biesma DH, Roth J, Skaar EP, van 't Veer C, de Vos AF, van der Poll T. 2014. Myeloid-related protein-8/14 facilitates bacterial growth during pneumococcal pneumonia. *Thorax* 69:1034–1042.
  73. Van Den Bosch MH, Blom AB, Schelbergen RFP, Vogl T, Roth JP, Sløetjes AW, Van Den Berg WB, Van Der Kraan PM, Van Lent PLEM. 2016. Induction of Canonical Wnt Signaling by the Alarmins S100A8/A9 in Murine Knee Joints: Implications for Osteoarthritis. *Arthritis Rheumatol* 68:152–163.
  74. Grevers LC, De Vries TJ, Vogl T, Abdollahi-Roodsaz S, Sloetjes AW, Leenen PJM, Roth J, Everts V, Van Den Berg WB, Van Lent PLEM. 2011. S100A8 enhances osteoclastic bone resorption in vitro through activation of Toll-like receptor 4: Implications for bone destruction in murine antigen-induced arthritis. *Arthritis Rheum* 63:1365–1375.
  75. Wache C, Klein M, Ostergaard C, Angele B, Häcker H, Pfister HW, Pruenster M, Sperandio M, Leanderson T, Roth J, Vogl T, Koedel U. 2015. Myeloid-related protein 14 promotes inflammation and injury in meningitis. *J Infect Dis* 212:247–257.
  76. Fujii W, Onuma A, Sugiura K, Naito K. 2014. Efficient generation of genome-modified mice via offset-nicking by CRISPR/Cas system. *Biochem Biophys Res Commun* 445:791–794.
  77. Björk P, Björk A, Vogl T, Stenstro M, Liberg D, Olsson A, Roth J, Ivars F, Leanderson T. 2009. Identification of Human S100A9 as a Novel Target for Treatment of

- Autoimmune Disease via Binding to Quinoline-3-Carboxamides. *PLoS Biol* 7:e1000097.
78. Tisoncik JR, Korth MJ, Simmons CP, Farrar J, Martin TR, Katze MG. 2012. Into the Eye of the Cytokine Storm. *Microbiol Mol Biol Rev* 76:16–32.
79. De Ponti A, Wiechert L, Stojanovic A, Longerich T, Marhenke S, Hogg N, Vogel A, Cerwenka A, Schirmacher P, Hess J, Angel P. 2015. Chronic liver inflammation and hepatocellular carcinogenesis are independent of S100A9. *Int J Cancer* 136:2458–2463.
80. Moles A, Murphy L, Wilson CL, Chakraborty JB, Fox C, Park EJ, Mann J, Oakley F, Howarth R, Brain J, Masson S, Karin M, Seki E, Mann DA. 2014. A TLR2 / S100A9 / CXCL-2 signaling network is necessary for neutrophil recruitment in acute and chronic liver injury in the mouse. *J Hepatol* 60:782–791.
81. Bianchi ME. 2007. DAMPs, PAMPs and alarmins: all we need to know about danger. *J Leukoc Biol* 81:1–5.
82. Tsai SY, Segovia JA, Chang TH, Morris IR, Berton MT, Tessier PA, Tardif MR, Cesaro A, Bose S. 2014. DAMP Molecule S100A9 Acts as a Molecular Pattern to Enhance Inflammation during Influenza A Virus Infection: Role of DDX21-TRIF-TLR4-MyD88 Pathway. *PLoS Pathog* 10.
83. Buras JA, Holzmann B, Sitkovsky M. 2005. Model organisms: Animal Models of sepsis: setting the stage. *Nat Rev Drug Discov* 4:854–865.
84. Schulte W, Bernhagen J, Bucala R. 2013. Cytokines in sepsis: Potent immunoregulators and potential therapeutic targets - An updated view. *Mediators Inflamm* 2013.
85. Suzuki R, Kohno H, Sugie S, Nakagama H, Tanaka T. 2006. Strain differences in the

- susceptibility to azoxymethane and dextran sodium sulfate-induced colon carcinogenesis in mice. *Carcinogenesis* 27:162–169.
86. Nials AT, Uddin S. 2008. Mouse models of allergic asthma: acute and chronic allergen challenge. *Dis Model Mech* 1:213–220.
87. Walkin L, Herrick SE, Summers A, Brenchley PE, Hoff CM, Korstanje R, Margetts PJ. 2013. The role of mouse strain differences in the susceptibility to fibrosis: a systematic review. *Fibrogenesis Tissue Repair* 6:16–18.
88. Goto Y, Sanjoba C, Asada M, Saeki K, Onodera T, Matsumoto Y. 2008. Adhesion of MRP8/14 to amastigotes in skin lesions of *Leishmania major*-infected mice. *Exp Parasitol* 119:80–86.
89. MacMicking JD, Nathan C, Hom G, Chartrain N, Fletcher DS, Trumbauer M, Stevens K, Xie Q wen, Sokol K, Hutchinson N, Chen H, Mudgett JS. 1995. Altered responses to bacterial infection and endotoxic shock in mice lacking inducible nitric oxide synthase. *Cell* 81:641–650.
90. Austermann J, Friesenhagen J, Fassl SK, Ortkras T, Burgmann J, Barczyk-Kahlert K, Faist E, Zedler S, Pirr S, Rohde C, Müller-Tidow C, vonKöckritz-Blickwede M, vonKaisenberg CS, Flohé SB, Ulas T, Schultze JL, Roth J, Vogl T, Viemann D. 2014. Alarmins MRP8 and MRP14 Induce Stress Tolerance in Phagocytes under Sterile Inflammatory Conditions. *Cell Rep* 9:2112–2124.
91. Sass G, Heinlein S, Agli A, Bang R, Schümann J, Tiegs G. 2002. Cytokine Expression in Three Mouse Models of Experimental Hepatitis. *Cytokine* 19:115–120.

92. Van Zoelen MAD, Vogl T, Foell D, Van Veen SQ, Van Till JWO, Florquin S, Tanck MW, Wittebole X, Laterre PF, Boermeester MA, Roth J, Van Poll T Der. 2009. Expression and role of myeloid-related protein-14 in clinical and experimental sepsis. *Am J Respir Crit Care Med* 180:1098–1106.
93. Viemann D, Strey A, Janning A, Jurk K, Klimmek K, Vogl T, Hirono K, Ichida F, Foell D, Kehrel B, Gerke V, Sorg C, Roth J, Mrp M. 2005. Myeloid-related proteins 8 and 14 induce a specific inflammatory response in human microvascular endothelial cells. *Blood* 105:2955–2963.
94. Shi Y, Liu CH, Roberts AI, Das J, Xu G, Ren G, Zhang Y, Zhang L, Yuan ZR, Tan HSW, Das G, Devadas S. 2006. Granulocyte-macrophage colony-stimulating factor (GM-CSF) and T-cell responses: what we do and don't know. *Cell Res* 16:126–133.
95. Simard JC, Noël C, Tessier PA, Girard D. 2014. Human S100A9 potentiates IL-8 production in response to GM-CSF or fMLP via activation of a different set of transcription factors in neutrophils. *FEBS Lett* 588:2141–2146.
96. Santos JL, Andrade A a, Dias A a M, Bonjardim C a, Reis LFL, Teixeira SMR, Horta MF. 2006. Differential sensitivity of C57BL/6 (M-1) and BALB/c (M-2) macrophages to the stimuli of IFN-gamma/LPS for the production of NO: correlation with iNOS mRNA and protein expression. *J Interf cytokine Res* 26:682–688.
97. Liu T, Matsuguchi T, Tsuboi N, Yajima T, Yoshikai Y. 2002. Differences in Expression of Toll-Like Receptors and Their Reactivities in Dendritic Cells in BALB/c and C57BL/6 Mice. *Infect Immun* 70:6638–6645.

98. Sunderkötter C, Kunz M, Steinbrink K, Meinardus-Hager G, Goebeler M, Bildau H, Sorg C. 1993. Resistance of mice to experimental leishmaniasis is associated with more rapid appearance of mature macrophages in vitro and in vivo. *J Immunol* 151:4891–901.
99. von Chamier M, Allam A, Brown MB, Reinhard MK, Reyes L. 2012. Host Genetic Background Impacts Disease Outcome During Intrauterine Infection with *Ureaplasma parvum*. *PLoS One* 7:1–10.
100. Delabie J, de Wolf-Peeters C, van den Oord JJ, Desmet VJ. 1990. Differential expression of the calcium-binding proteins MRP8 and MRP14 in granulomatous conditions: an immunohistochemical study. *Clin Exp Immunol* 81:123–6.
101. Krishnegowda G, Hajjar AM, Zhu J, Douglass EJ, Uematsu S, Akira S, Woods AS, Gowda DC. 2005. Induction of Proinflammatory Responses in Macrophages by the Glycosylphosphatidylinositols of *Plasmodium falciparum*. *J Biol Chem* 280:8606–8616.
102. Schiopu A, Cotoi OS. 2013. S100A8 and S100A9 : DAMPs at the Crossroads between Innate Immunity , Traditional Risk Factors , and Cardiovascular Disease. *Mediators Inflamm* 2013.
103. Akbarzadeh R, Yu X, Vogl T, Ludwig RJ, Schmidt E, Zillikens D, Petersen F. 2016. Myeloid-related proteins-8 and -14 are expressed but dispensable in the pathogenesis of experimental epidermolysis bullosa acquisita and bullous pemphigoid. *J Dermatol Sci* 81:165–172.
104. van Lent P, Blom A, Schelbergen R, Slöetjes A, Lafeber F, Lems W, Cats H, Vogl T, Roth J, van den Berg W. 2012. Active Involvement of Alarmins S100A8 and S100A9 in

the Regulation of Synovial Activation and Joint Destruction During Mouse and Human Osteoarthritis. *Arthritis Rheum* 64:1466–1476.

105. Dessing MC, Butter LM, Teske GJ, Claessen N, Van der Loos CM, Vogl T, Roth J, Van der Poll T, Florquin S, Leemans JC. 2010. S100A8/A9 is not involved in host defense against murine urinary tract infection. *PLoS One* 5:3–9.
106. Rampersad R, Esserman D, McGinnis M, Lee D, Patel D, Tarrant T. 2009. S100A9 is not essential for disease expression in an acute ( K / BxN ) or chronic ( CIA ) model of inflammatory arthritis. *Scand J Rheumatol* 38:445–449.
107. Serbina N V, Pamer EG. 2006. Monocyte emigration from bone marrow during bacterial infection requires signals mediated by chemokine receptor CCR2. *Nat Immunol* 7:311–317.
108. Hamilton JA. 2008. Colony-stimulating factors in inflammation and autoimmunity. *Nat Rev Immunol* 8:533–544.

## Figure legends

**Figure 1. Hepatic injury regulated by T cells during rodent malaria.** (a) Kinetics of pRBC rate in peripheral blood after infection of  $10^6$  pRBCs in *nu/nu* mice and WT mice (n=5). (b) Hematocrit in *nu/nu* mice and WT mice after Pb-infection (n=5). (c) The body weight change of *nu/nu* mice and WT mice after Pb-infection (n=5). (d) Serum concentration of AST (left) and ALT (right) of *nu/nu* mice and WT mice after Pb-infection (n=5). (e) mRNA expression of iNOS (left) and IFN- $\gamma$  (right) in the liver of *nu/nu* mice and WT mice treated with LPS (n=5). (f) IFN- $\gamma$  produced by Pb-pRBC antigen-specific T cells. SPCs ( $5 \times 10^6$  cells/ml) of Pb-infected mice or naïve mice were stimulated by Pb-pRBC ( $1 \times 10^8$  cells/ml), nRBC ( $1 \times 10^8$  cells/ml) or conA (3  $\mu$ g/ml) and the concentration of IFN- $\gamma$  secreted in supernatant was measured by ELISA. Graphs show mean and SD of each group. Data are representative of two independent experiments. \* $P < 0.05$ ; n.s., not significant.

**Figure 2. Increase of extracellular MRP14 depend on T cells during rodent malaria.** (a) Serum concentration of MRP8 (left) and MRP14 (right) of *nu/nu* mice and WT mice after Pb-infection (n=5). (b) The accumulation of MRP14<sup>+</sup> cells in the liver and spleen of *nu/nu* mice and WT mice after Pb-infection. RP, red pulp; WP, white pulp. Bars; 50  $\mu$ m. (c) The accumulation of MRP14<sup>+</sup> cells, CD3<sup>+</sup> cells and CD45<sup>+</sup> cells in the liver and spleen of Pb-infected mice. RP, red pulp; WP, white pulp. Bars; 50  $\mu$ m. Graphs show mean and SD of each group. Data are representative of two independent experiments. \* $P < 0.05$ ; n.s., not significant.

**Figure 3. Macrophage activation induced by MRP14.** (a) Increase of TNF- $\alpha$  secretion dependent on MRP14 concentration in RAW264.7 cells. RAW264.7 cells ( $2 \times 10^5$  cells/ml) were stimulated by MRP14 or MRP8 (0.15 - 5  $\mu\text{g/ml}$ ) and the concentration of secreted TNF- $\alpha$  in supernatant was measured by ELISA. (b) The increase of TNF- $\alpha$  by MRP14 and MRP8 could not be blocked by addition of polymyxin B. RAW264.7 cells ( $2 \times 10^5$  cells/ml) were stimulated by MRP14 (100 ng/ml), rMRP8 (100 ng/ml), EGFP (100 ng/ml) or LPS (2.5 ng/ml) incubated with or without polymyxin B (50  $\mu\text{g/ml}$ ), which is a LPS inhibitor. EGFP is recombinant proteins with polyhistidine-tag, which was used as a negative control. (c) The increase of TNF- $\alpha$  by MRP14 blocked by addition of paquinimod. RAW264.7 cells ( $2 \times 10^5$  cells/ml) were stimulated by MRP14 (5  $\mu\text{g/ml}$ ), MRP8 (5  $\mu\text{g/ml}$ ), EGFP (5  $\mu\text{g/ml}$ ) or LPS (5 ng/ml) incubated with or without paquinimod (250  $\mu\text{g/ml}$ ), which is a MRP14 inhibitor. (d) MRP14 as an agonist of TLR2 and TLR4. HEK293 cells transfected with murine TLR gene were stimulated by MRP14 (5  $\mu\text{g/ml}$ ) and SEAP induced by NF- $\kappa\text{B}$  activation through TLR was measured. Different letters on the bars represent statistical difference between groups. (e) mRNA expression of IL-1 $\beta$ , TNF- $\alpha$ , IL-6, CCL2, CCR2, iNOS and  $\beta$ -actin in RAW264.7 cells ( $2 \times 10^5$  cells/ml) stimulated by MRP14 (5  $\mu\text{g/ml}$ ) or MRP8 (5  $\mu\text{g/ml}$ ). (f) Enhanced NO production by RAW264.7 cells stimulated by MRP with IFN- $\gamma$ . RAW264.7 cells ( $2 \times 10^5$  cells/ml) were stimulated with MRP14 (5  $\mu\text{g/ml}$ ), MRP8 (5  $\mu\text{g/ml}$ ) or LPS (5 ng/ml) incubated with or without IFN- $\gamma$  (20 ng/ml), and the concentration of NO in supernatant was measured by Griess test. Graphs show mean and SD of triplicates or duplicates. Data are representative of three independent experiments. \* $P < 0.05$ ; n.s., not significant.

**Figure 4. Weight loss exacerbated by MRP14 during rodent malaria.** (a) Kinetics of pRBC rate in peripheral blood after infection of  $10^6$  pRBCs in MRP14-injected mice and PBS-injected controls (n=5). (b) Hematocrit in mice injected with MRP14 or PBS after Pb-infection (n=5). (c) The body weight change of mice injected with MRP14 or PBS after Pb-infection (n=5). (d) The spleen weight of mice injected with MRP14 or PBS after Pb-infection (n=5). (e) Serum concentration of MRP8 (left) and MRP14 (right) of mice injected with MRP14 or PBS after Pb-infection (n=5). Graphs show mean and SD of each group. Data are representative of two independent experiments. \* $P < 0.05$ ; n.s., not significant.

**Figure 5. Exacerbation of hepatic injury by MRP14 during rodent malaria.** (a) Histopathology of the liver of mice injected with MRP14 or PBS after Pb-infection analyzed by HE staining. The area surrounded by dotted line shows focal necrosis. Bar; 50  $\mu\text{m}$ . (b)(c) Serum concentration of AST (b) and ALT (c) of mice injected with MRP14 or PBS after Pb-infection (n=5). Graphs show mean and SD of each group. Data are representative of two independent experiments. \* $P < 0.05$ ; n.s., not significant.

**Figure 6. The accumulation of MRP8<sup>+</sup> and MRP14<sup>+</sup> cells promoted by MRP14 during rodent malaria.** (a) The accumulation of MRP14<sup>+</sup> cells in the liver and spleen of mice injected with MRP14 or PBS after Pb-infection. RP, red pulp; WP, white pulp. Bars; 50  $\mu\text{m}$ . (b)(c) The number of accumulated MRP8<sup>+</sup> and MRP14<sup>+</sup> cells in the liver (b) and spleen (c) of mice injected

with MRP14 or PBS after Pb-infection (n=5). (d) The number of peripheral blood leukocytes of mice injected with MRP14 or PBS after Pb-infection (n=5). (e) The accumulation of MRP14<sup>+</sup> cells in focal necrosis area of the liver in mice injected with MRP14 or PBS after Pb-infection. Bars; 50 μm. Graphs show mean and SD of each group. Data are representative of two independent experiments. \**P* < 0.05; n.s., not significant.

**Figure 7. The accumulation of MRP8<sup>+</sup> and MRP14<sup>++</sup> cells promoted by MRP14 in the absence of Plasmodium infection.** (a) The accumulation of MRP14<sup>+</sup> cells in the liver and spleen of MRP14-injected mice and PBS-injected controls. RP, red pulp; WP, white pulp. Bars; 50 μm. (b)(c) The number of accumulated MRP8<sup>+</sup> and MRP14<sup>+</sup> cells in the liver (b) and spleen (c) of MRP14-injected mice and PBS-injected controls (n=5). (d) The number of peripheral blood leukocytes of MRP14-injected mice and PBS-injected controls (n=5). (e) The spleen weight of MRP14-injected mice and PBS-injected controls (n=5). Graphs show mean and SD of each group. Data are representative of two independent experiments. \**P* < 0.05; n.s., not significant.

**Figure 8. The expression of pro-inflammatory molecules promoted by MRP14 injection.** mRNA expression of iNOS, IL-1β, IL-6, IL-12 p40, TNF-α, Arg-1, FIZZ-1, IL-10, TGF-β, NOX2, CCR2, CCL2, IFN-γ and IL-4 in the liver and spleen of mice injected with MRP14 or PBS (n=5). Graphs show mean and SD of each group. Data are representative of two independent experiments. \**P* < 0.05; n.s., not significant.

**Figure 9. The expression of iNOS and pro-inflammatory molecules in the liver promoted by MRP14 during rodent malaria.** mRNA expression of iNOS, IL-1 $\beta$ , IL-6, IL-12 p40, TNF- $\alpha$ , Arg-1, FIZZ-1, IL-10, TGF- $\beta$ , NOX2, CCR2, CCL2, IFN- $\gamma$  and IL-4 in the liver of mice injected with MRP14 or PBS after Pb-infection (n=5). Graphs show mean and SD of each group. Data are representative of two independent experiments. \* $P < 0.05$ ; n.s., not significant.

**Figure 10. The expression of pro-inflammatory molecules suppressed in the spleen during rodent malaria.** mRNA expression of iNOS, IL-1 $\beta$ , IL-6, IL-12 p40, TNF- $\alpha$ , Arg-1, FIZZ-1, IL-10, TGF- $\beta$ , NOX2, CCR2, CCL2, IFN- $\gamma$  and IL-4 in the spleen of mice injected with MRP14 or PBS after Pb-infection (n=5). Graphs show mean and SD of each group. Data are representative of two independent experiments. \* $P < 0.05$ ; n.s., not significant.

**Figure 11. The expression pattern of inflammatory molecules in the liver and spleen.** The mRNA expression pattern of inflammatory molecules in the liver and spleen was summarized. Cells colored with red indicate up-regulation, and cells colored with blue indicate down-regulation. Color graduation is dependent on the relative fold change rate; cells with darker red represent larger increase rate, and cells with darker blue represent larger decrease rate.

**Figure 12. Targeted inactivation of MRP14 gene in BALB/c mice.** (a) Exon 2 of the MRP14 locus, which includes EF-hand region, was deleted by offset-nicking method of CRISPR/Cas

system using the four gRNAs which designed at the following loci; 5'-GGCCACTGTTAGGCAAGATAAGGAGGGG, 5'-GAGACTAGGTCAGGGAAGCTTGG, 5'-GGCAGAGCCCTACTGCCCCCGG, and 5'-GCAGTAGGGCTCTGCCATTAGAGG. (b) Analysis of PCR products from total DNA of the tails for genotyping. Genotyping was performed by the genomic PCR using the primers (forward primer, 5'-GTCAA AATTCTGTTTTGTGTATATGTGGAG-3', and reverse primer, 5'-AATTCCTTGTGTTCTTAAAGTTATGTGTC-3') and sequencing of the PCR amplicons. Expected product sizes are 585 bp (WT) and 242 bp (target-deletion).

**Figure 13. No effect of MRP14 deficiency on weight loss during rodent malaria.** (a) Kinetics of pRBC rate in peripheral blood after infection of  $10^6$  pRBCs in MRP14-KO mice and WT mice (n=5). (b) Hematocrit in MRP14-KO mice and WT mice after Pb-infection (n=5). (c) The body weight change of MRP14-KO mice and WT mice after Pb-infection (n=5). (d) The spleen weight of MRP14-KO mice and WT mice after Pb-infection (n=5). (e) The number of peripheral blood leukocytes of MRP14-KO mice and WT mice after Pb-infection (n=5). (f) The population of peripheral blood leukocytes categorized by nuclear morphology in MRP14-KO mice and WT mice after Pb-infection (n=5). Graphs show mean and SD of each group. Data are representative of two independent experiments. \*  $P < 0.05$ ; n.s., not significant.

**Figure 14. Unimproved hepatic injury in MRP14-KO BALB/c mice during rodent malaria.**

(a) Histopathology of the liver and spleen of MRP14-KO mice and WT mice after Pb-infection

analyzed by HE staining. RP, red pulp; WP, white pulp. Bars; 50  $\mu$ m. (b) Serum concentration of AST (left) and ALT (right) of MRP14-KO mice and WT mice after Pb-infection (n=5). Graphs show mean and SD of each group. Data are representative of two independent experiments. \* $P$  < 0.05; n.s., not significant.

**Figure 15. The accumulation of MRP8<sup>+</sup> cells in the liver of MRP14-KO BALB/c mice during rodent malaria.** (a) The accumulation of MRP8<sup>+</sup> cells in the liver and spleen of MRP14-KO mice and WT mice after Pb-infection. RP, red pulp; WP, white pulp. Bars; 50  $\mu$ m. (b) The number of accumulated MRP8<sup>+</sup> cells in the liver (left) and spleen (right) of MRP14-KO mice and WT mice after Pb-infection (n=5). (c) The population of accumulated leukocytes categorized by morphological characters in the liver (left) and spleen (right) of MRP14-KO mice and WT mice after Pb-infection (n=5). (d) Serum concentration of MRP8 (left) and MRP14 (right) of MRP14-KO mice and WT mice after Pb-infection (n=5). Graphs show mean and SD of each group. Data are representative of two independent experiments. \* $P$  < 0.05; n.s., not significant.

**Figure 16. Enhanced pro-inflammatory molecules in the liver of MRP14-KO BALB/c mice during rodent malaria.** mRNA expression of iNOS, IL-1 $\beta$ , IL-6, IL-12 p40, TNF- $\alpha$ , Arg-1, FIZZ-1, IL-10, TGF- $\beta$ , CCR2, CCL2, IFN- $\gamma$  and IL-4 in the liver of MRP14-KO mice and WT mice after Pb-infection (n=5). Graphs show mean and SD of each group. Data are representative of two independent experiments. \* $P$  < 0.05; n.s., not significant.

**Figure 17. The suppression of pro-inflammatory molecules in the spleen of MRP14-KO BALB/c mice during rodent malaria.** mRNA expression of iNOS, IL-1 $\beta$ , IL-6, IL-12 p40, TNF- $\alpha$ , Arg-1, FIZZ-1, IL-10, TGF- $\beta$ , CCR2, CCL2, IFN- $\gamma$  and IL-4 in the spleen of MRP14-KO mice and WT mice after Pb-infection (n=5). Graphs show mean and SD of each group. Data are representative of two independent experiments. \* $P < 0.05$ ; n.s., not significant.

**Figure 18. The administration of paquinimod failed to suppress MRP14 *in vivo*.** (a) Kinetics of pRBC rate in peripheral blood after infection of  $10^6$  pRBCs in Paquinimod-injected mice and PBS-injected controls (n=5). (b) Hematocrit in mice injected with Paquinimod or PBS during Pb-infection (n=5). (c) The body weight change of mice injected with Paquinimod or PBS during Pb-infection (n=5). (d) The spleen weight of mice injected with Paquinimod or PBS during Pb-infection (n=5). (e) The number of peripheral blood leukocytes of mice injected with Paquinimod or PBS during Pb-infection (n=5). (f) Serum concentration of MRP14 of mice injected with Paquinimod or PBS during Pb-infection (n=5). (g) Left: the accumulation of MRP14<sup>+</sup> cells in the liver and spleen of mice injected with Paquinimod or PBS during Pb-infection. Bars; 50  $\mu$ m. Right: the number of accumulated MRP8<sup>+</sup> and MRP14<sup>+</sup> cells in the liver and spleen of mice injected with Paquinimod or PBS during Pb-infection (n=5). (h) Serum concentration of AST (left) and ALT (right) of mice injected with Paquinimod or PBS during Pb-infection (n=5). Paquinimod, which is a MRP14 inhibitor, was injected intraperitoneally every day from 3 days before Pb-infection to the 7<sup>th</sup> day after Pb-infection (25 mg/kg/day). The liver, spleen and serum were collected at day 7 of infection. Graphs show mean and SD of each group. Data are

representative of two independent experiments. \* $P < 0.05$ ; n.s., not significant.

**Figure 19. Suppression of cellular MRP8 expression in MRP14-KO mice.** (a) MRP8 and MRP14 levels in SPCs ( $5 \times 10^4$  cells/lane) and BMCs ( $5 \times 10^3$  cells/lane) of MRP14-KO mice and WT mice analyzed by western blotting. (b) MRP8 and MRP14 levels in PECs ( $5 \times 10^3$  cells/lane) of MRP14-KO and WT mice analyzed by western blotting. (c) The expression of MRP8, MRP14 or CD11b in spleens and bone marrows of MRP14-KO mice and WT mice. Bars; 50  $\mu\text{m}$  (spleen) or 200  $\mu\text{m}$  (BM). (d) Expression of Gr-1, CD11b and MRP8 in BMCs of MRP14-KO mice and WT mice. Bars; 20  $\mu\text{m}$ . (e) The population of Gr-1<sup>+</sup>, CD11b<sup>+</sup> and MRP8<sup>+</sup> cells in BMCs of MRP14-KO mice and WT mice (n=5). Graphs show mean and SD of each group. Data are representative of two independent experiments. \* $P < 0.05$ ; n.s., not significant.

**Figure 20. Increased ratio of lymphocytes in peripheral blood leukocytes and PECs of MRP14-KO mice.** (a) The number of peripheral blood leukocytes of MRP14-KO mice and WT mice (n=5). (b) The population of peripheral blood leukocytes categorized by nuclear morphology in MRP14-KO mice and WT mice (n=5). (c) Giemsa-stained peritoneal PECs of MRP14-KO mice and WT mice. Bar; 5  $\mu\text{m}$ . (d) The population of PECs categorized by morphological nuclear characters in MRP14-KO mice and WT mice (n=5). (e) SDS-PAGE of PEC lysates (1  $\mu\text{g}$ /lane) of MRP14-KO mice and WT mice (n=3). (f) Giemsa-stained BMCs of MRP14-KO mice and WT mice. Bar; 5  $\mu\text{m}$ . (g) The population of BMCs categorized by morphological nuclear characters in MRP14-KO mice and WT mice (n=5). (h) SDS-PAGE of

BMCs ( $5 \times 10^4$  cells/lane) of MRP14-KO mice and WT mice ( $n=3$ ). Graphs show mean and SD of each group. Data are representative of two independent experiments. \* $P < 0.05$ ; n.s., not significant.

**Figure 21. Enhanced TNF- $\alpha$  secretion by BMCs stimulated with LPS in MRP14-KO mice.**

(a) TNF- $\alpha$  secretion by BMCs stimulated with different concentrations of LPS. BMCs ( $1 \times 10^6$  cells/ml) of MRP14-KO mice or WT mice were stimulated by LPS (1 - 1,000 ng/ml) for 4 hr and the concentration of secreted TNF- $\alpha$  in supernatant was measured by ELISA. (b) Temporal kinetics of TNF- $\alpha$  secretion by BMCs stimulated with LPS. BMCs ( $1 \times 10^6$  cells/ml) of MRP14-KO mice or WT were stimulated by LPS (1  $\mu$ g/ml) and the concentration of secreted TNF- $\alpha$  in supernatant was measured by ELISA. (c) MRP8 (left) and MRP14 (right) secretion by BMCs stimulated with LPS. BMCs ( $1 \times 10^6$  cells/ml) of MRP14-KO mice or WT were stimulated by LPS (1  $\mu$ g/ml) for 4 hr and the concentration of secreted TNF- $\alpha$  in supernatant was measured by ELISA. (d, e) TNF- $\alpha$  secretion by BMCs stimulated with TLR agonists. BMCs ( $1 \times 10^6$  cells/ml) of MRP14-KO mice or WT were stimulated by LPS (1  $\mu$ g/ml), imiquimod (5  $\mu$ g/ml), CpG (1  $\mu$ M) for 4 hr (d) or 24 hr (e) and the concentration of secreted TNF- $\alpha$  in supernatant was measured by ELISA. (f) TNF- $\alpha$  secretion from SPCs stimulated with LPS. SPCs ( $5 \times 10^6$  cells/ml) of MRP14-KO mice or WT mice were stimulated by LPS (1  $\mu$ g/ml) and the concentration of secreted TNF- $\alpha$  in supernatant was measured by ELISA. (g) TNF- $\alpha$  (left) or IFN- $\gamma$  (right) secretion from SPCs stimulated with TLR agonists. SPCs ( $5 \times 10^6$  cells/ml) of MRP14-KO mice or WT were stimulated by LPS (1  $\mu$ g/ml), imiquimod (5  $\mu$ g/ml), CpG (1  $\mu$ M)

for 24 hr. Graphs show mean and SD of each group (n=5). Data are representative of three independent experiments. \* $P < 0.05$ ; n.s., not significant; n.d., not detected.

**Figure 22. Unimproved LPS-induced shock in MRP14-KO BALB/c mice.** (a) Survival of MRP14-KO mice and WT mice treated with LPS (30 mg/kg) (n=5). Data are representative of three independent experiments. (b) The number of peripheral blood leukocytes of MRP14-KO mice and WT mice treated with LPS (n=5). (c) The population of peripheral blood leukocytes categorized by morphological nuclear characters in MRP14-KO mice and WT mice (n=5). (d) Serum concentration of IL-1 $\beta$  (left) and TNF- $\alpha$  (right) of MRP14-KO mice and WT mice treated with LPS (n=5). (e) Serum concentration of MRP8 (left) and MRP14 (right) of MRP14-KO mice and WT mice treated with LPS (n=5). Graphs show mean and SD of each group. Data are representative of two independent experiments. \* $P < 0.05$ ; n.s., not significant; n.d.: not detected.

**Figure 23. Unimproved LPS-induced hepatic injury in MRP14-KO BALB/c mice.** (a) Histopathology of spleens and livers of MRP14-KO mice and WT mice treated with LPS analyzed by HE staining. Bar; 50  $\mu$ m. (b) The population of accumulated leukocytes categorized by morphological characters in livers of MRP14-KO mice and WT mice treated with LPS (n=5). (c) Serum concentration of AST (left) and ALT (right) of MRP14-KO mice and WT mice treated with LPS (n=5). (d) mRNA expression of iNOS in the liver (left) and spleen (right) of MRP14-KO mice and WT mice treated with LPS (n=5). (e) mRNA expression of IL-1 $\beta$ , IL-6, IL-12 p40 and TNF- $\alpha$  in the liver, spleen and BMCs of MRP14-KO mice and WT mice treated with LPS

(n=5). Graphs show mean and SD of each group. Data are representative of two independent experiments. \* $P < 0.05$ ; n.s., not significant.

**Figure 24. Migration of the monocytes expressing MRP8 dependent on MRP14.** (a) The expression of MRP8 or MRP14 in the spleen and liver of MRP14-KO mice and WT mice treated with LPS. Bars; 50  $\mu\text{m}$ . (b) The number of accumulated MRP8<sup>+</sup> cells in the spleen (left) and liver (right) of MRP14-KO mice and WT mice treated with LPS (n=5). (c) The population of accumulated MRP8<sup>+</sup> cells categorized by morphological characters in the spleen (left) and liver (right) of MRP14-KO mice and WT mice treated with LPS (n=5). Graphs show mean and SD of each group. Data are representative of two independent experiments. \* $P < 0.05$ ; n.s., not significant.

**Figure 25. Promotion of GM-CSF expression in BMCs stimulated with MRP14.** (a) Increase of TNF- $\alpha$  secretion from WT BMCs stimulated with MRP14 or GM-CSF for 7 days. Different letters on the bars represent statistical difference between groups. (b) mRNA expression of GM-CSF in WT BMCs stimulated with MRP14, MRP8, GM-CSF or LPS for 7 days. (c) WT BMC proliferation stimulated with MRP14, MRP8 or GM-CSF for 7 days analyzed by AlamarBlue. (d) TNF- $\alpha$  secretion by BMCs of WT BALB/c or C57BL/6 mice stimulated with MRP14, MRP8, GM-CSF or LPS for 7 days. BMCs ( $1 \times 10^6$  cells/ml) were stimulated by MRP14 (5  $\mu\text{g/ml}$ ), MRP8 (5  $\mu\text{g/ml}$ ), GM-CSF (50 ng/ml), M-CSF (80 ng/ml) or LPS (1  $\mu\text{g/ml}$ ). (e) mRNA expression of CD11b, F4/80, CD68 and GM-CSF in BMCs of MRP14-KO mice and WT mice

treated with LPS (n=5). Graphs show mean and SD of each group. Data are representative of two independent experiments. \*  $P < 0.05$ ; n.s., not significant.

**Figure 26. Hypothesized MRP14 function in pathology of hepatic injury during rodent malaria.** MRP14 promotes the secretion of pro-inflammatory cytokines such as IL-1 $\beta$ , TNF- $\alpha$ , IL-6 and IL-12 from macrophages via TLR2 and TLR4. The pro-inflammatory cytokines induce the up-regulation of iNOS, which produces high concentration of NO. High levels of NO have cytotoxic and pro-inflammatory effects leading to necrosis of hepatocytes. IL-12 is a potent inducer of IFN- $\gamma$ , and IFN- $\gamma$  produced by Pb-pRBC antigen specific T cells facilitates the production of NO. MRP14 also promotes the accumulation of macrophages (including MRP8<sup>+</sup> and MRP14<sup>+</sup> macrophages) in the sinusoid of liver, to which CCR2 and CCL2 may contribute. The accumulated macrophages promote inflammatory cascade, which leads to hepatic injury. MRP14 deficiency induces not only the simple deletion of extracellular MRP14 function to promote inflammation but also affects intracellular MRP14 function. Intracellular MRP14 deficiency induces the hyperresponsiveness of TLR4 signaling in myeloid cells, which keep comparable inflammatory cytokine levels to WT during inflammation. M $\Phi$ , macrophage; T, T cell; HC, hepatocyte; Mo, monocyte; O<sub>2</sub><sup>-•</sup>, superoxide; NO<sup>•</sup>, nitric oxide; ONOO<sup>-</sup>, peroxynitrite.

## Figures

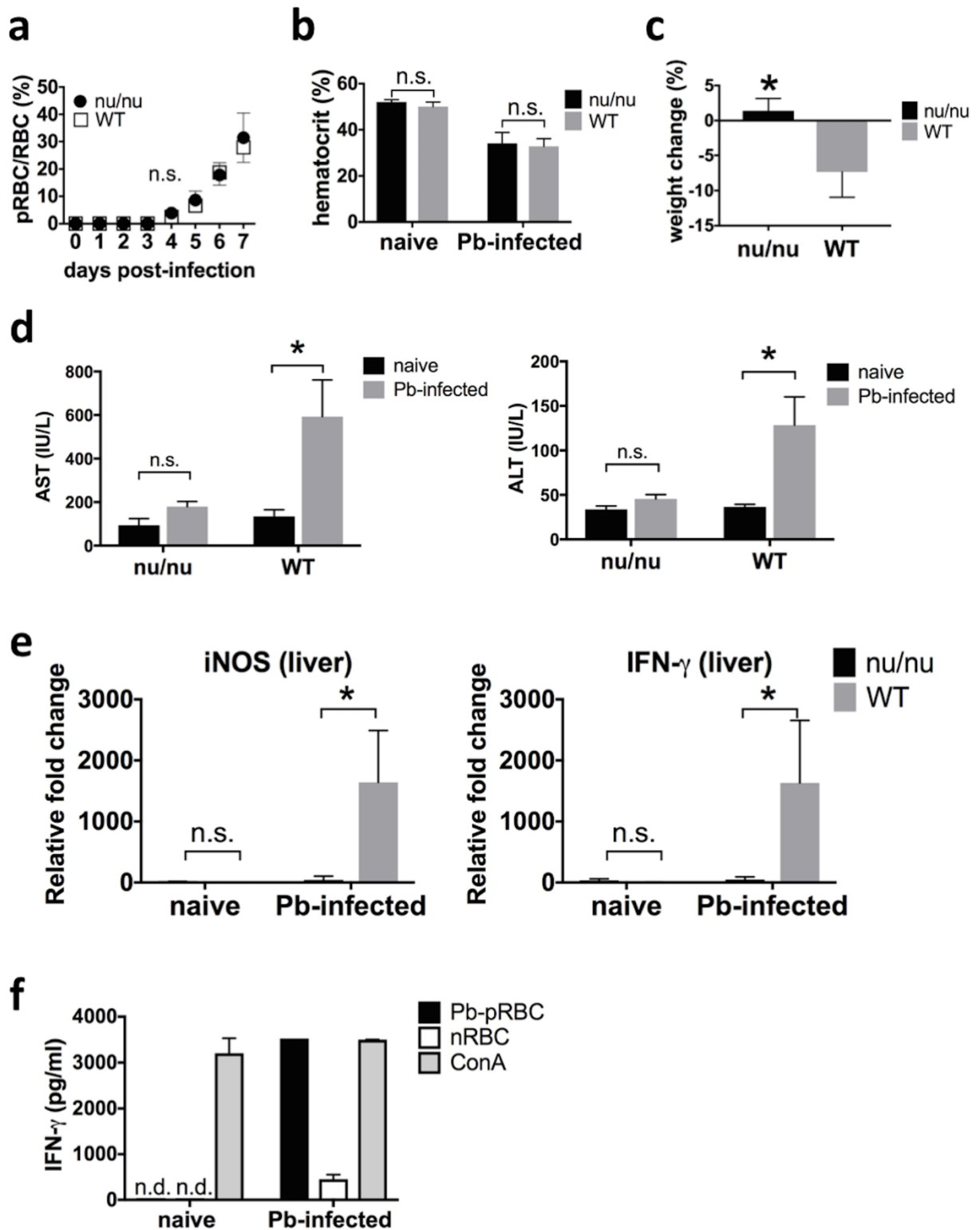
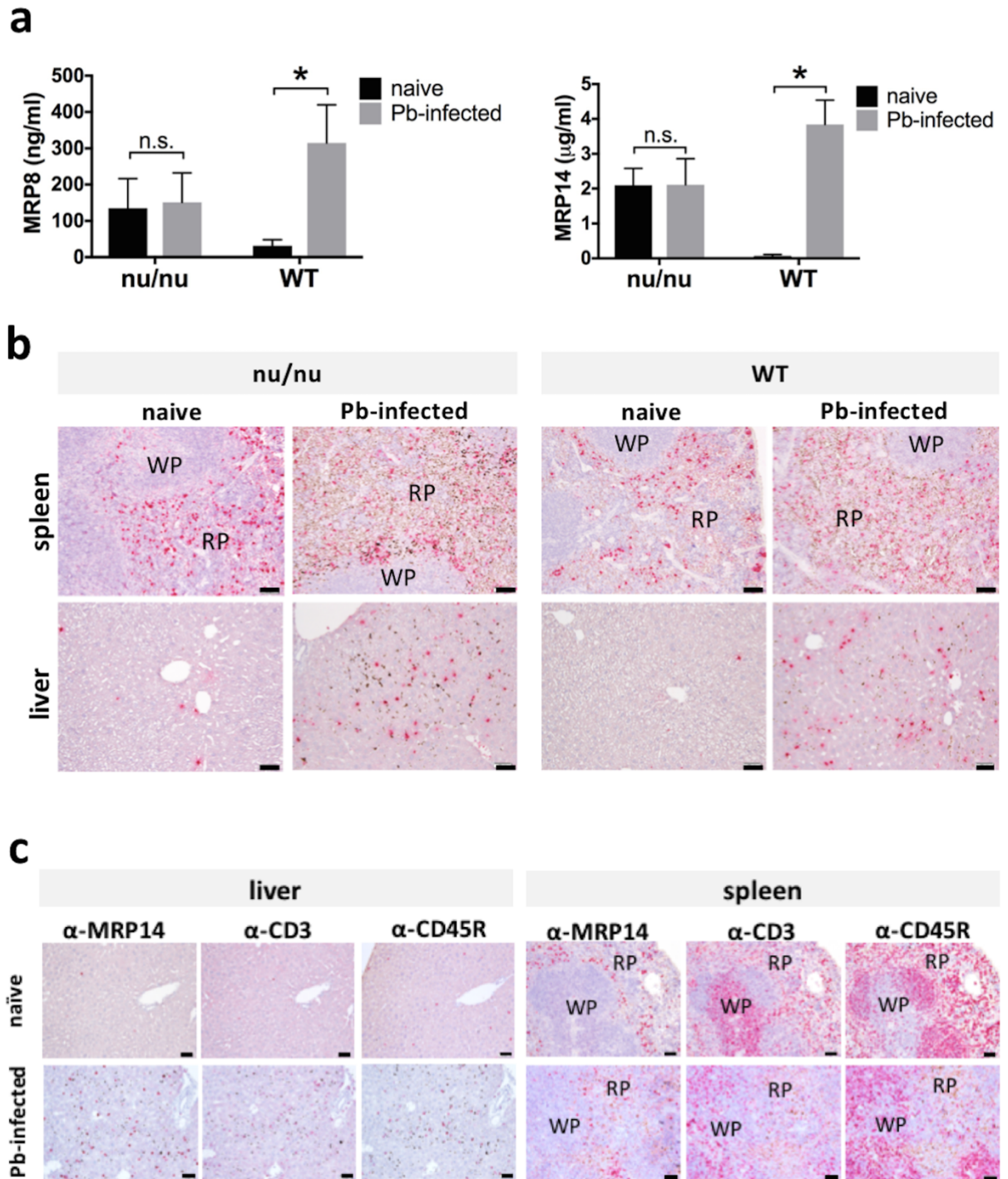


Figure 1. Hepatic injury regulated by T cells during rodent malaria.



**Figure 2. Increase of extracellular MRP14 depend on T cells during rodent malaria.**

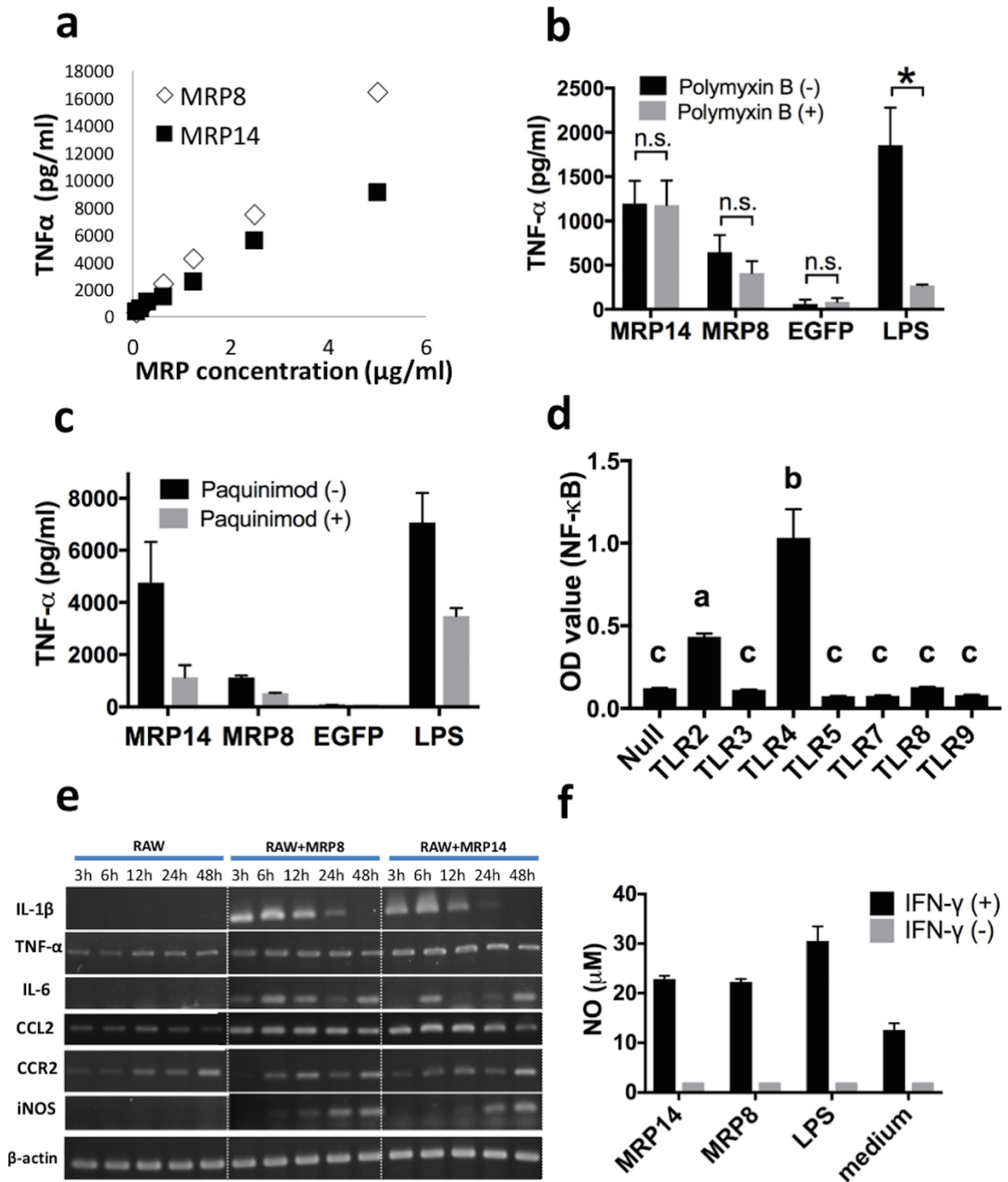


Figure 3. Macrophage activation induced by MRP14.

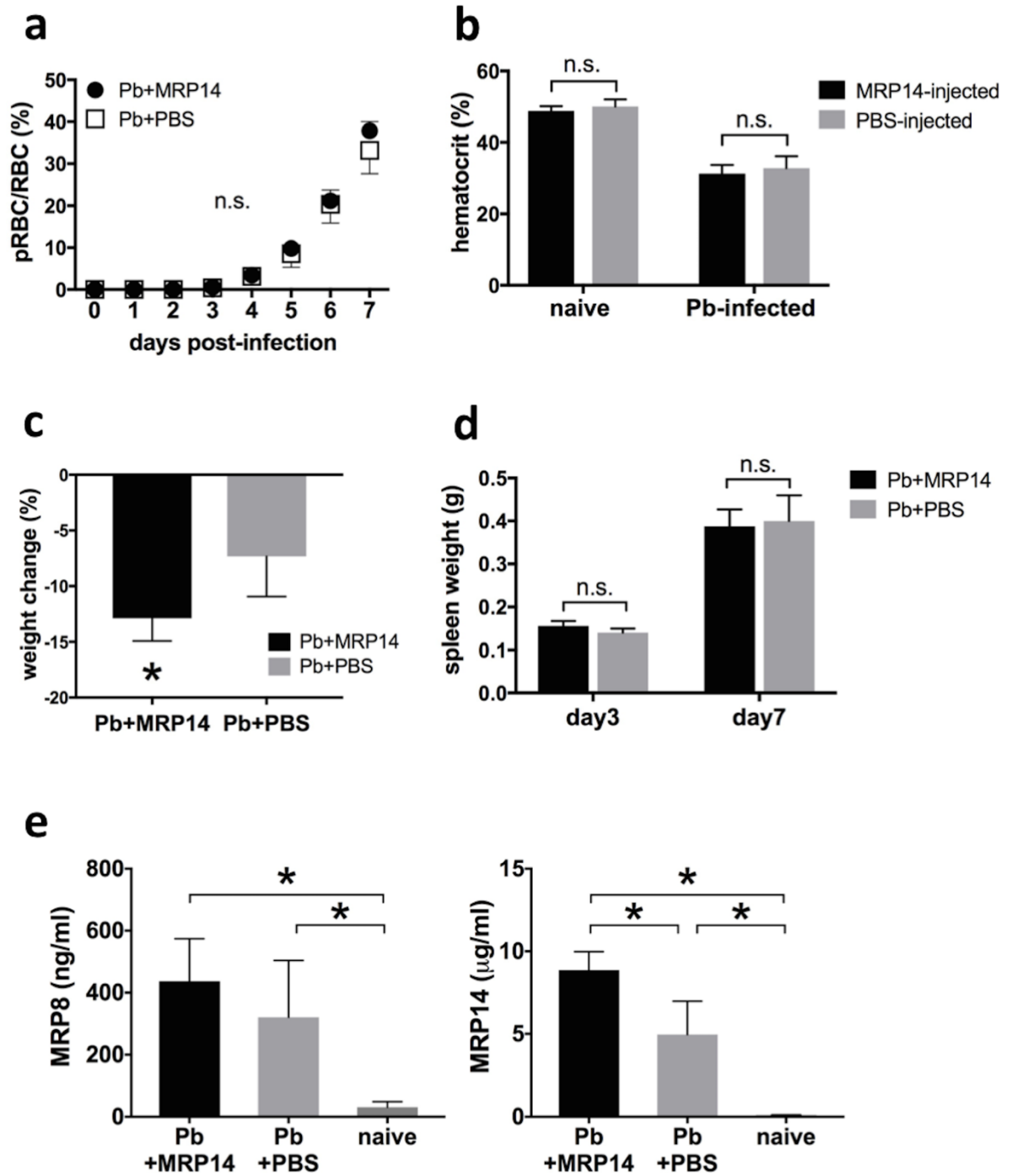
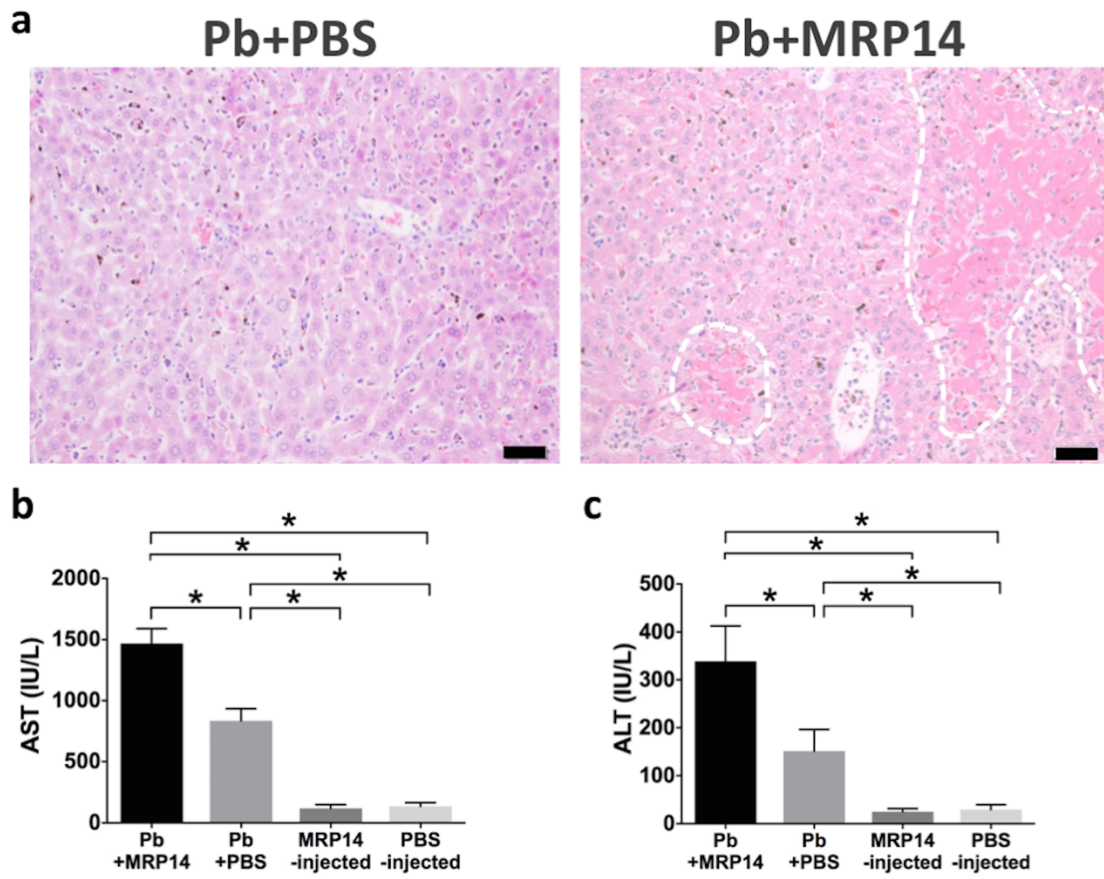


Figure 4. Weight loss exacerbated by MRP14 during rodent malaria.



**Figure 5. Exacerbation of hepatic injury by MRP14 during rodent malaria.**

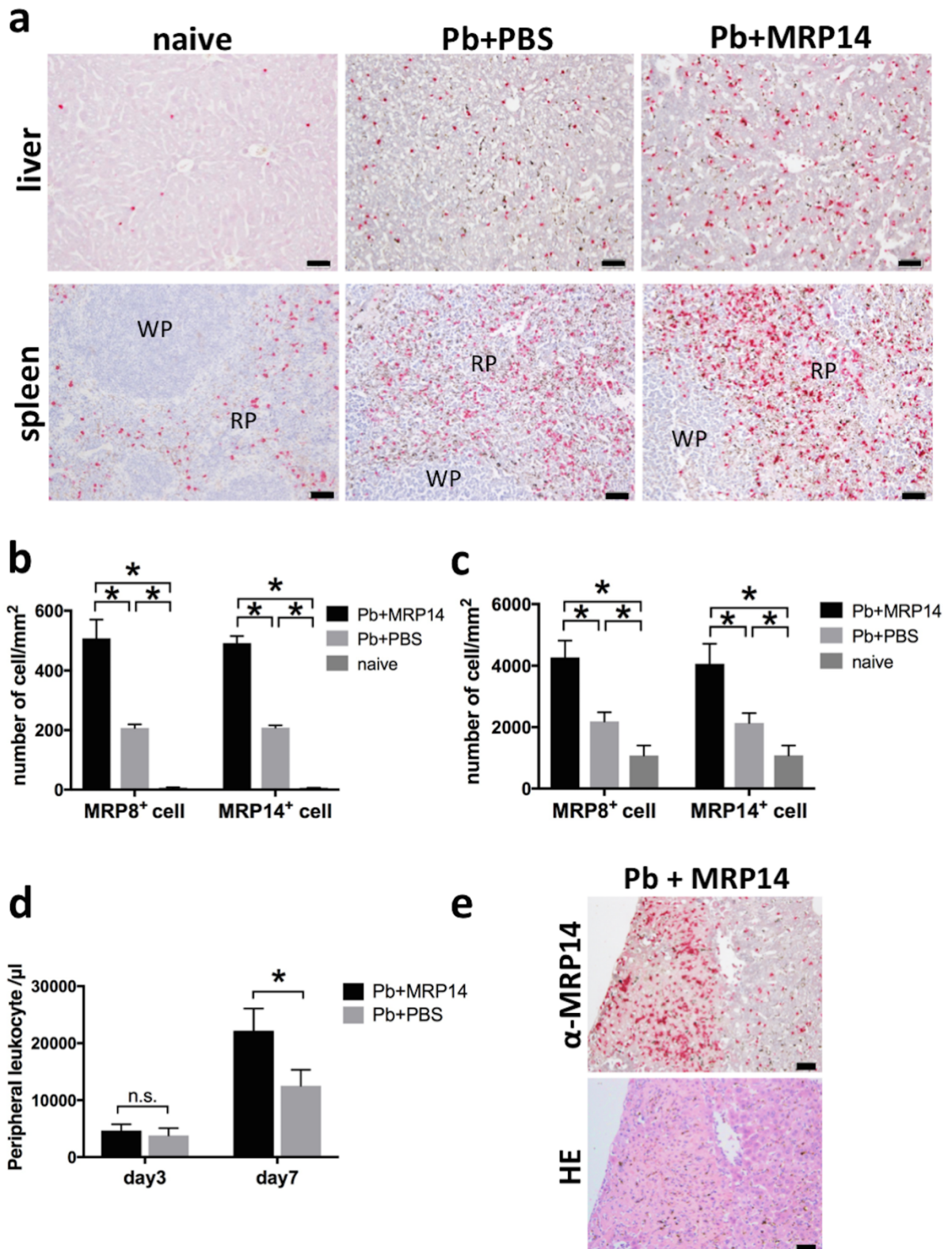


Figure 6. The accumulation of MRP8<sup>+</sup> and MRP14<sup>+</sup> cells promoted by MRP14 during rodent malaria.

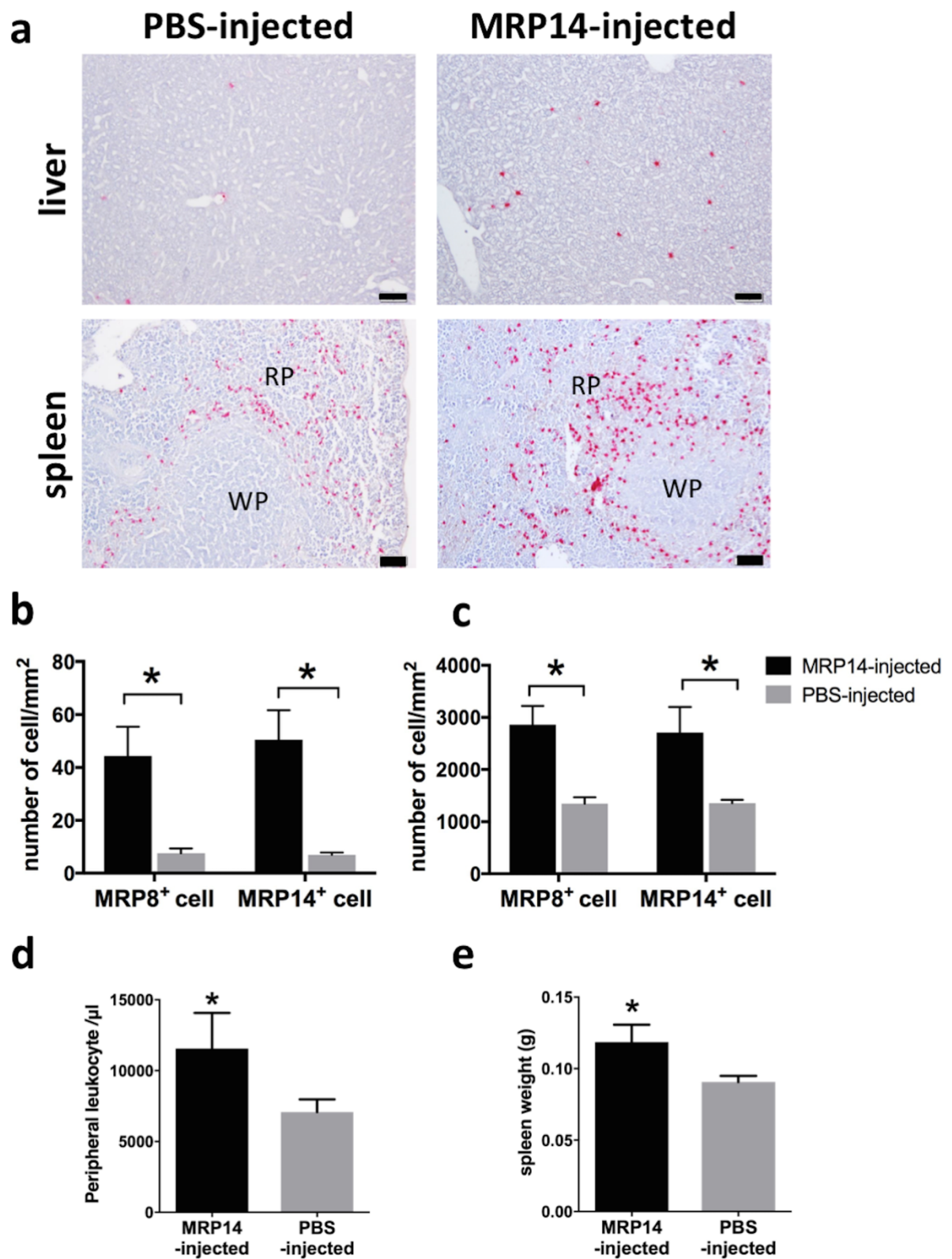


Figure 7. The accumulation of MRP8<sup>+</sup> and MRP14<sup>+</sup> cells promoted by MRP14 in the absence of Plasmodium infection.

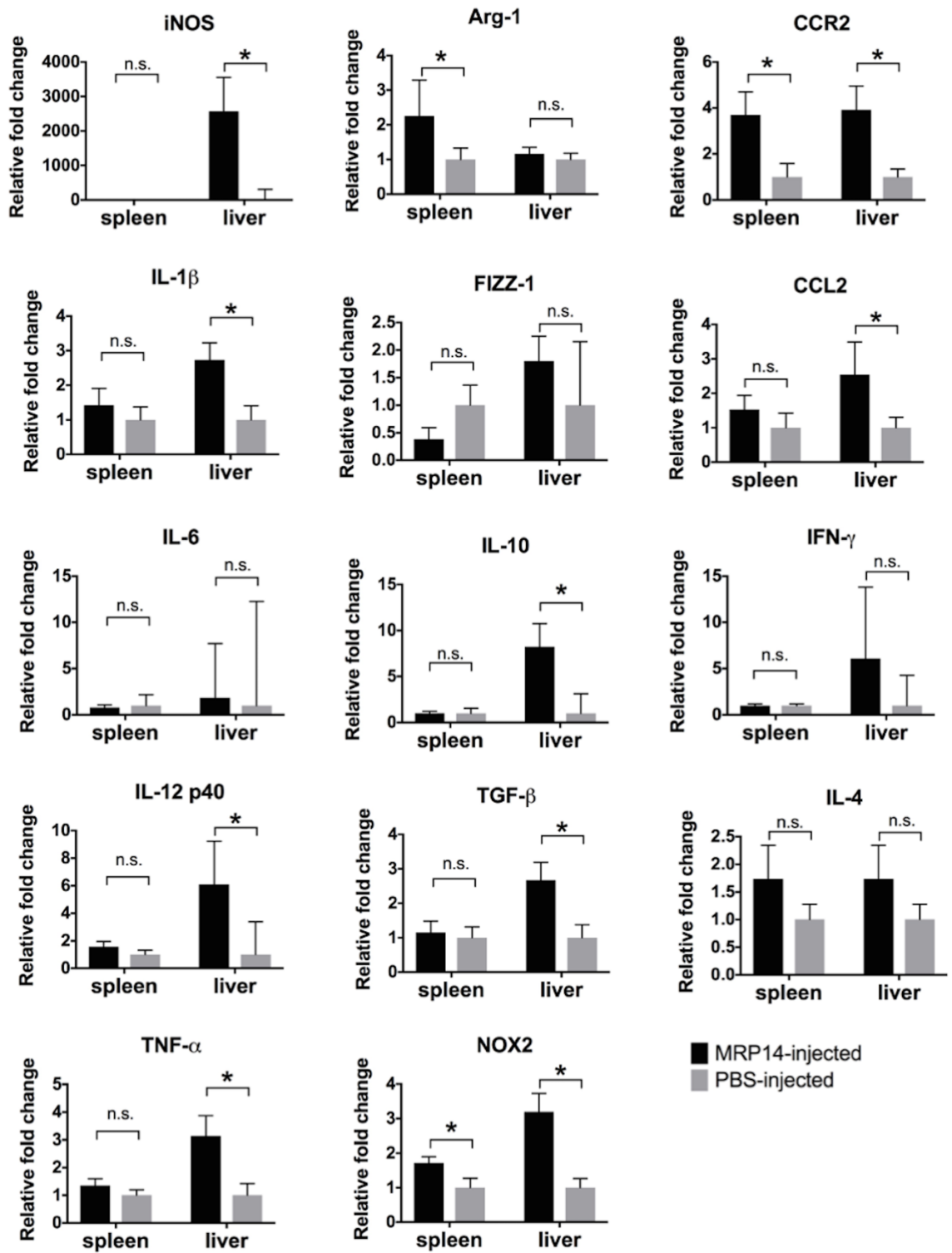


Figure 8. The expression of pro-inflammatory molecules promoted by MRP14 injection.

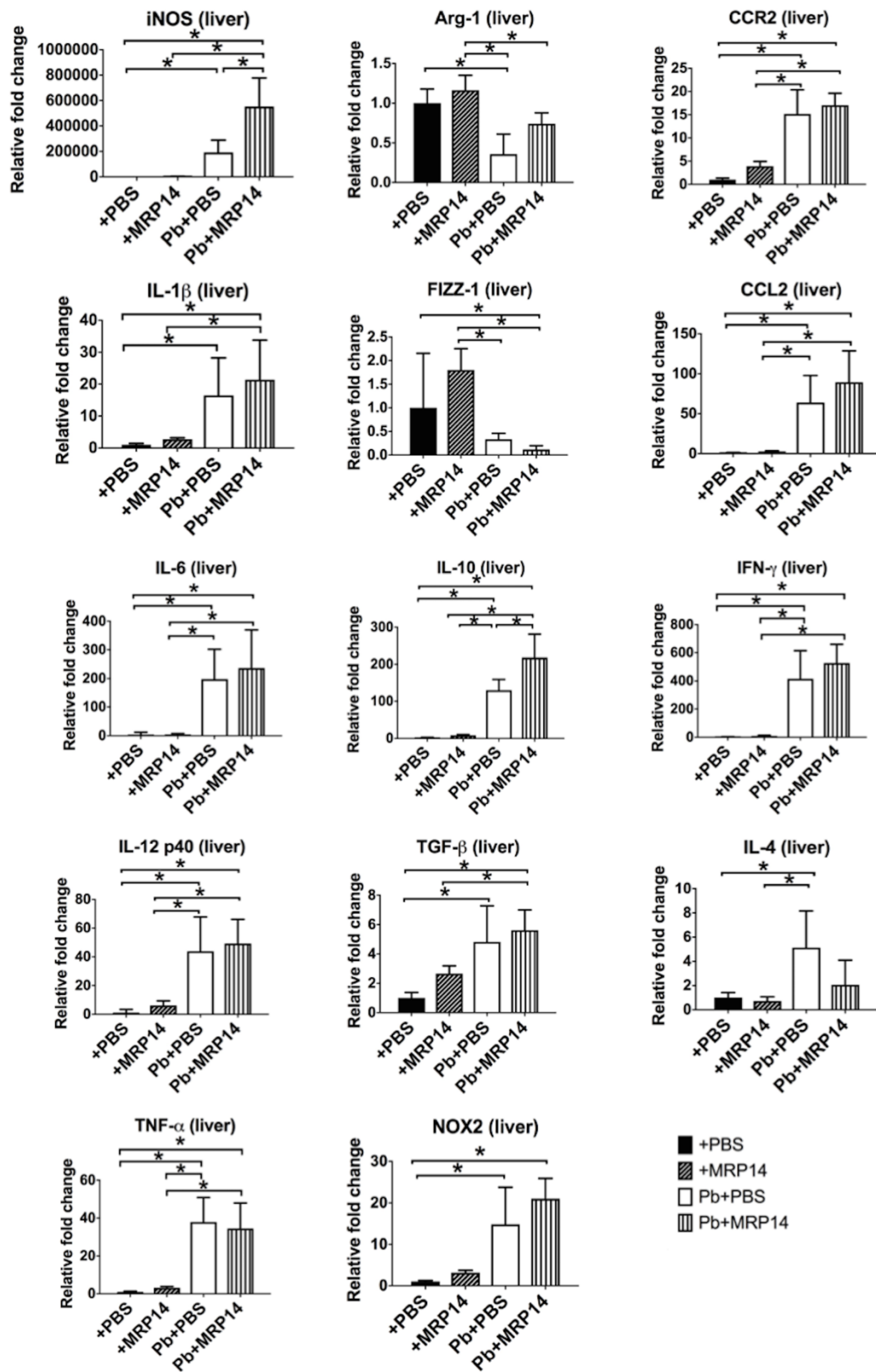


Figure 9. The expression of iNOS and pro-inflammatory molecules in the liver promoted by MRP14 during rodent malaria.

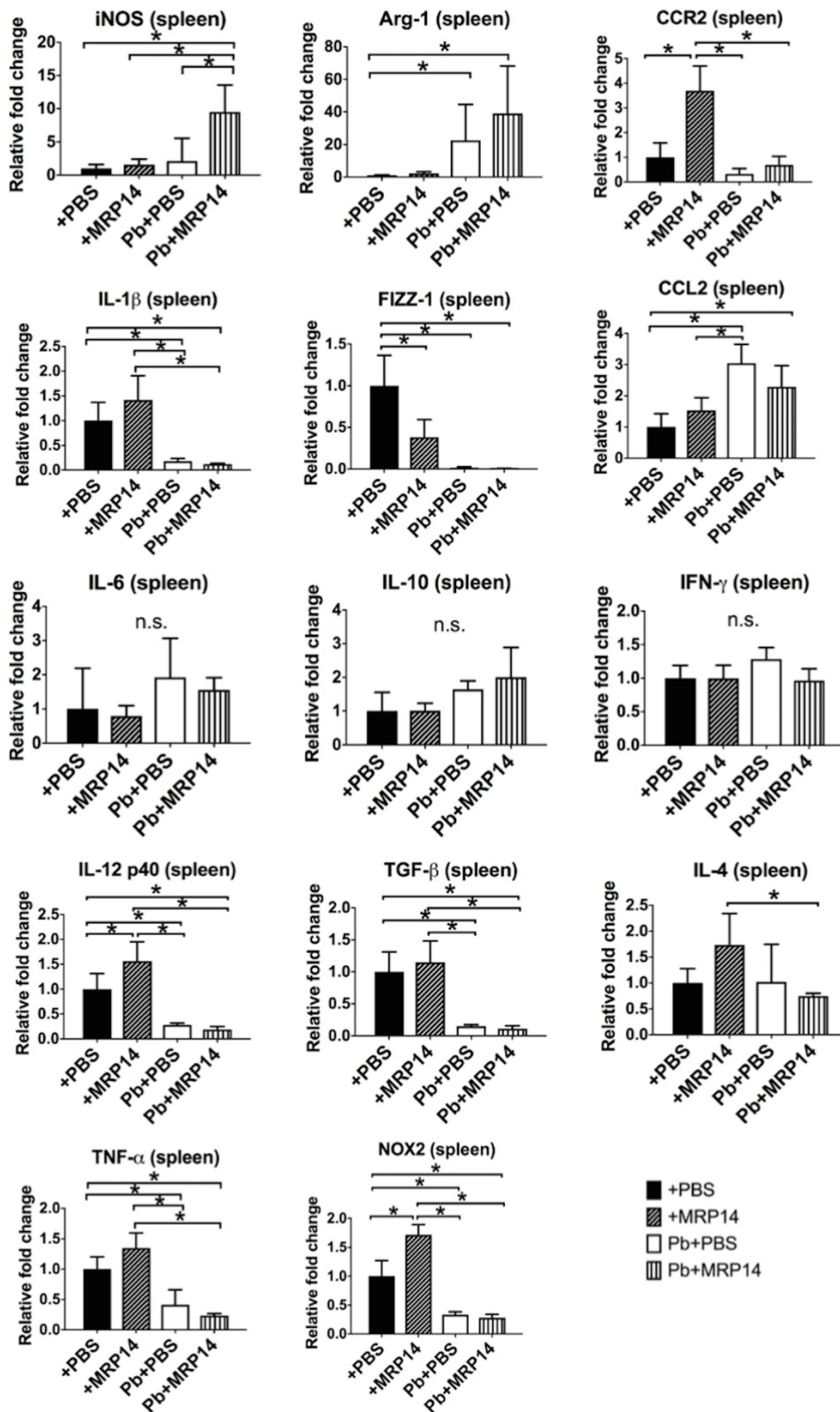
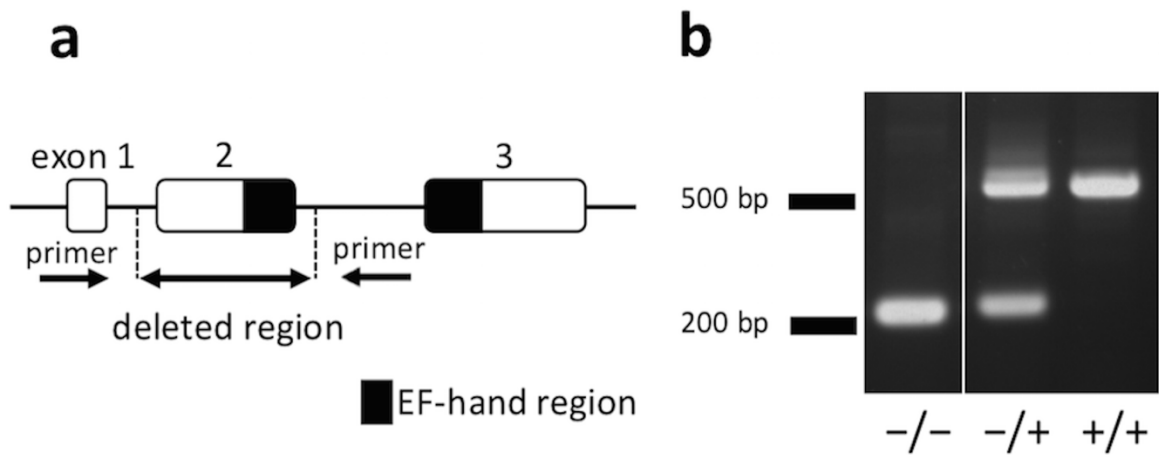


Figure 10. The expression of pro-inflammatory molecules suppressed in the spleen during rodent malaria.

	spleen		liver	
	Pb-infected	MRP14 i.v.	Pb-infected	MRP14 i.v.
M1 marker	iNOS	iNOS	iNOS	iNOS
	IL-1 $\beta$	IL-1 $\beta$	IL-1 $\beta$	IL-1 $\beta$
	IL-6	IL-6	IL-6	IL-6
	IL-12	IL-12	IL-12	IL-12
	TNF- $\alpha$	TNF- $\alpha$	TNF- $\alpha$	TNF- $\alpha$
M2 marker	Arg-1	Arg-1	Arg-1	Arg-1
	FIZZ1	FIZZ1	FIZZ1	FIZZ1
	IL-10	IL-10	IL-10	IL-10
	TGF- $\beta$	TGF- $\beta$	TGF- $\beta$	TGF- $\beta$
ROS production	NOX2	NOX2	NOX2	NOX2
M $\Phi$ chemotaxis	CCR2	CCR2	CCR2	CCR2
	CCL2	CCL2	CCL2	CCL2
T cell cytokines	IFN- $\gamma$	IFN- $\gamma$	IFN- $\gamma$	IFN- $\gamma$
	IL-4	IL-4	IL-4	IL-4

x1000~
x100~x1000
x10~x100
x1.5~x10
No change
x1/2~x1/10
~x1/100

**Figure 11. The expression pattern of inflammatory molecules in the liver and spleen.**



**Figure 12. Targeted inactivation of MRP14 gene in BALB/c mice.**

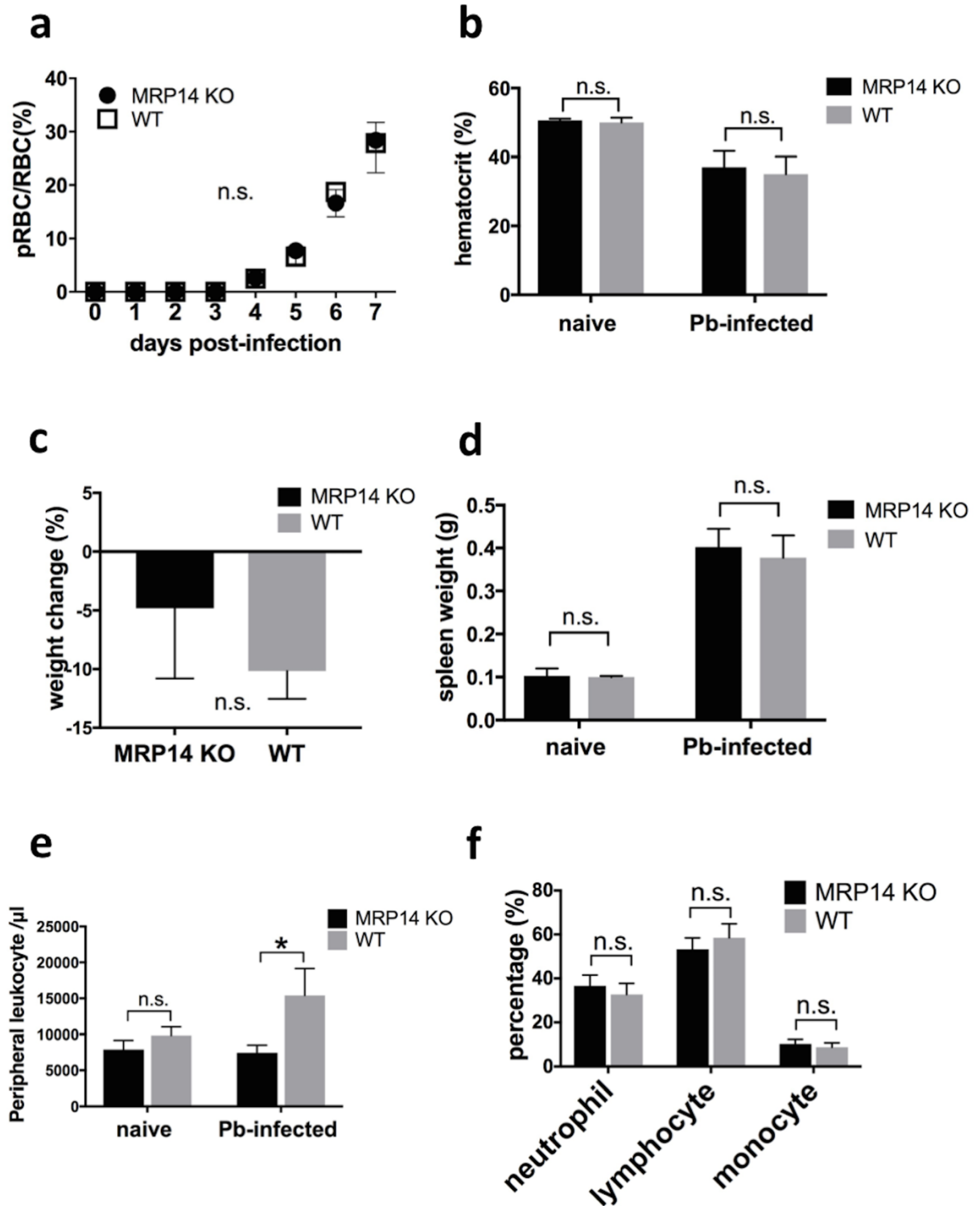
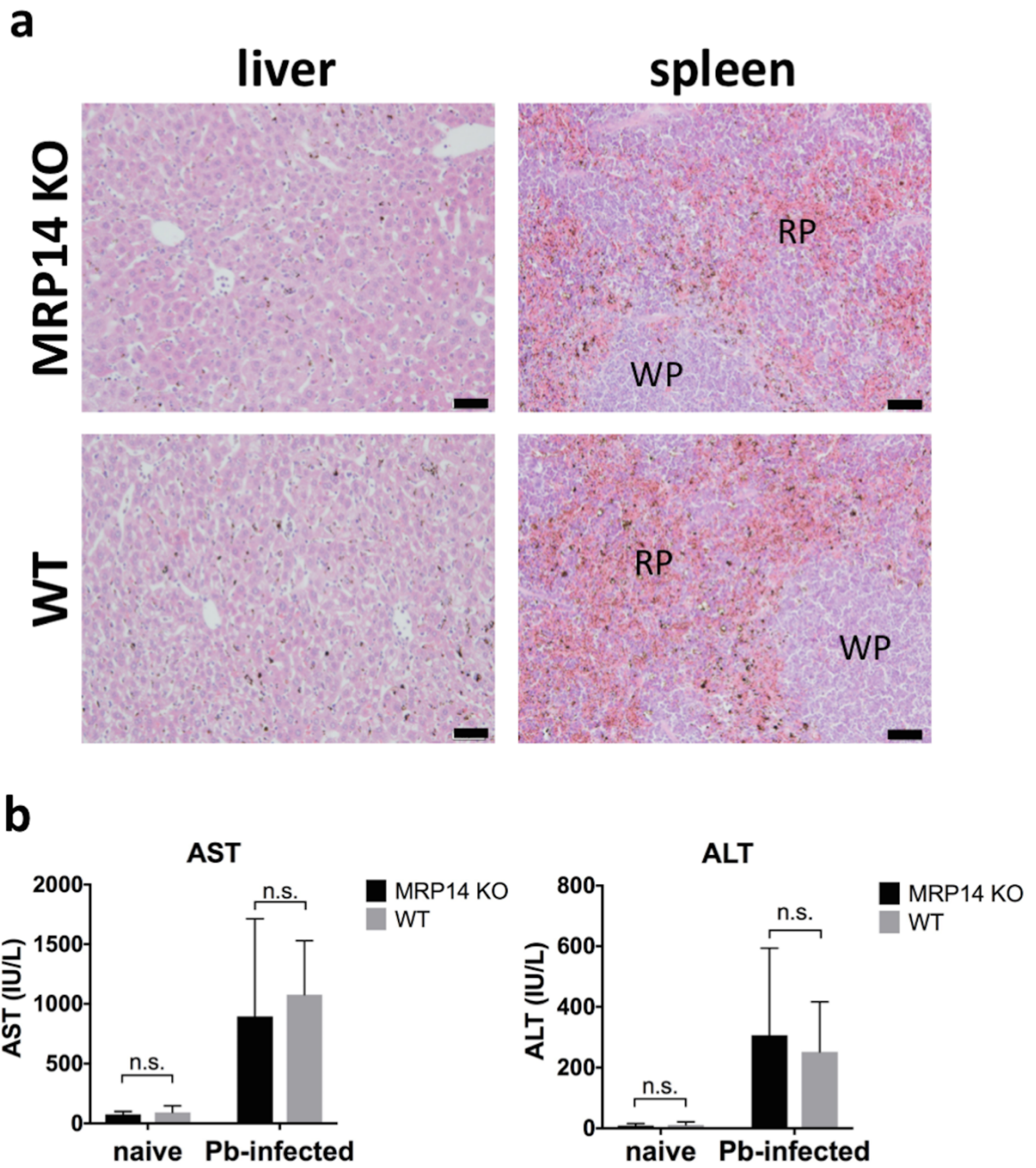


Figure 13. No effect of MRP14 deficiency on weight loss during rodent malaria.



**Figure 14. Unimproved hepatic injury in MRP14-KO BALB/c mice during rodent malaria.**

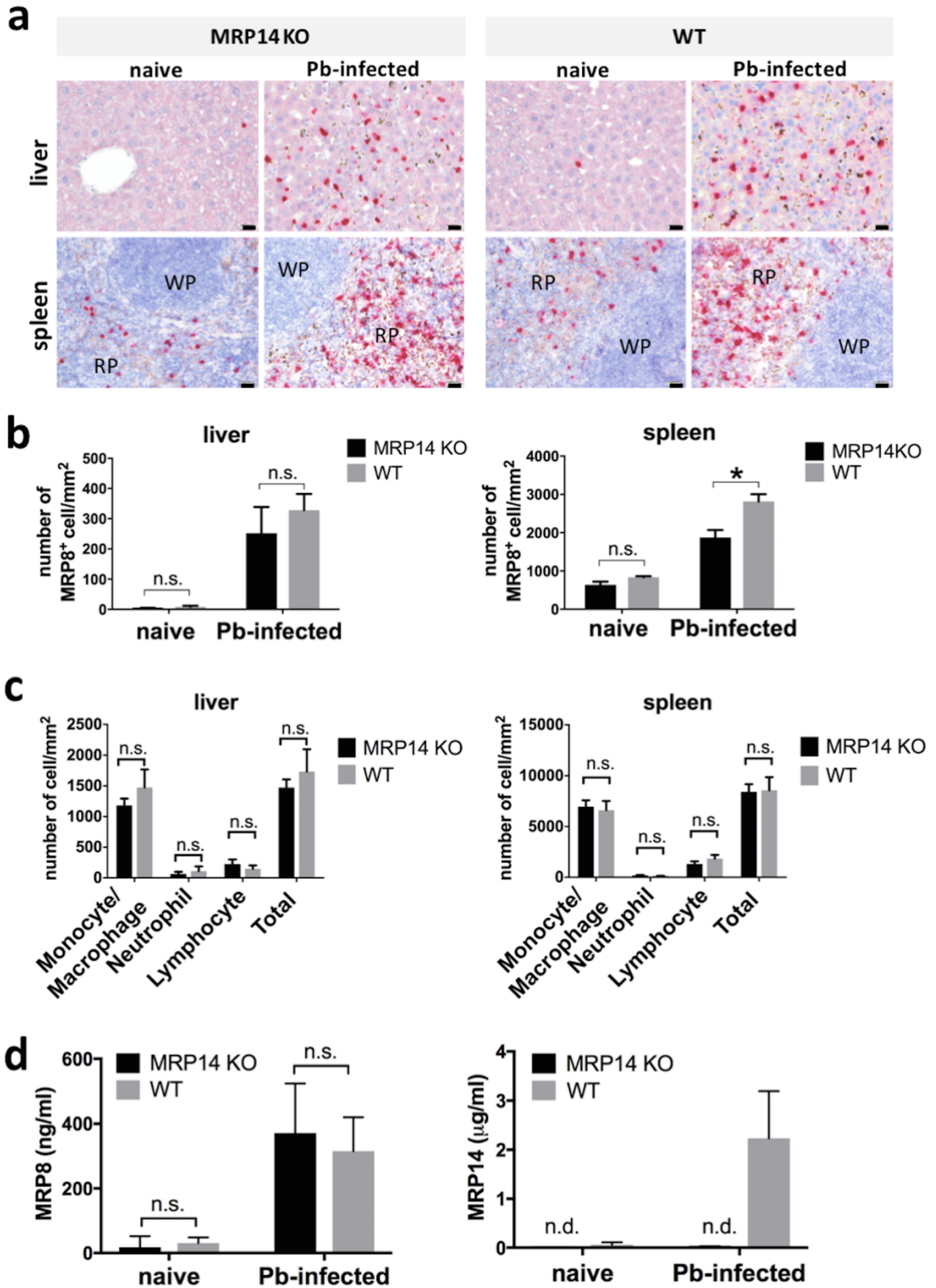


Figure 15. The accumulation of MRP8<sup>+</sup> cells in the liver of MRP14-KO BALB/c mice during rodent malaria.

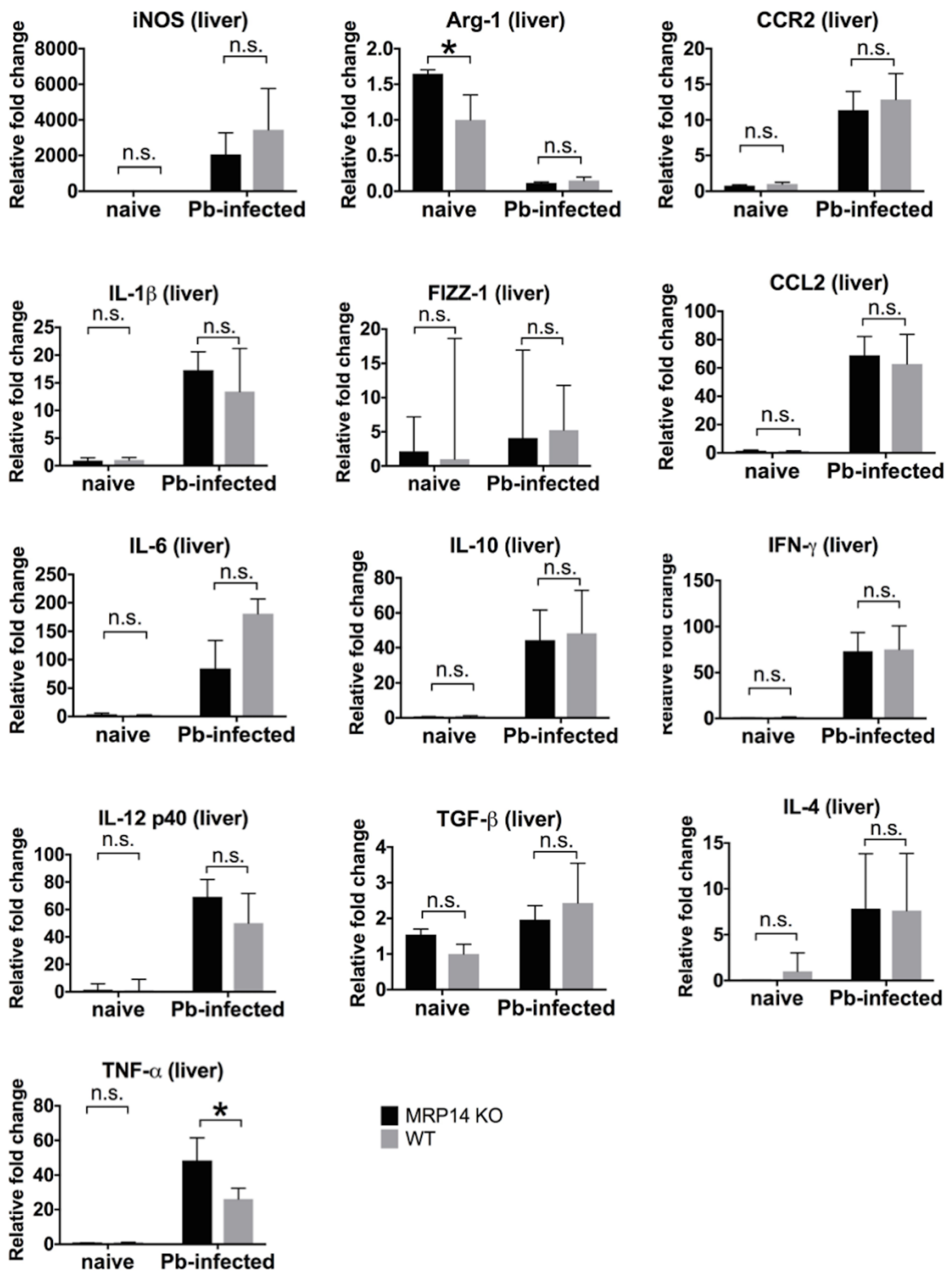


Figure 16. Enhanced pro-inflammatory molecules in the liver of MRP14-KO BALB/c mice during rodent malaria.

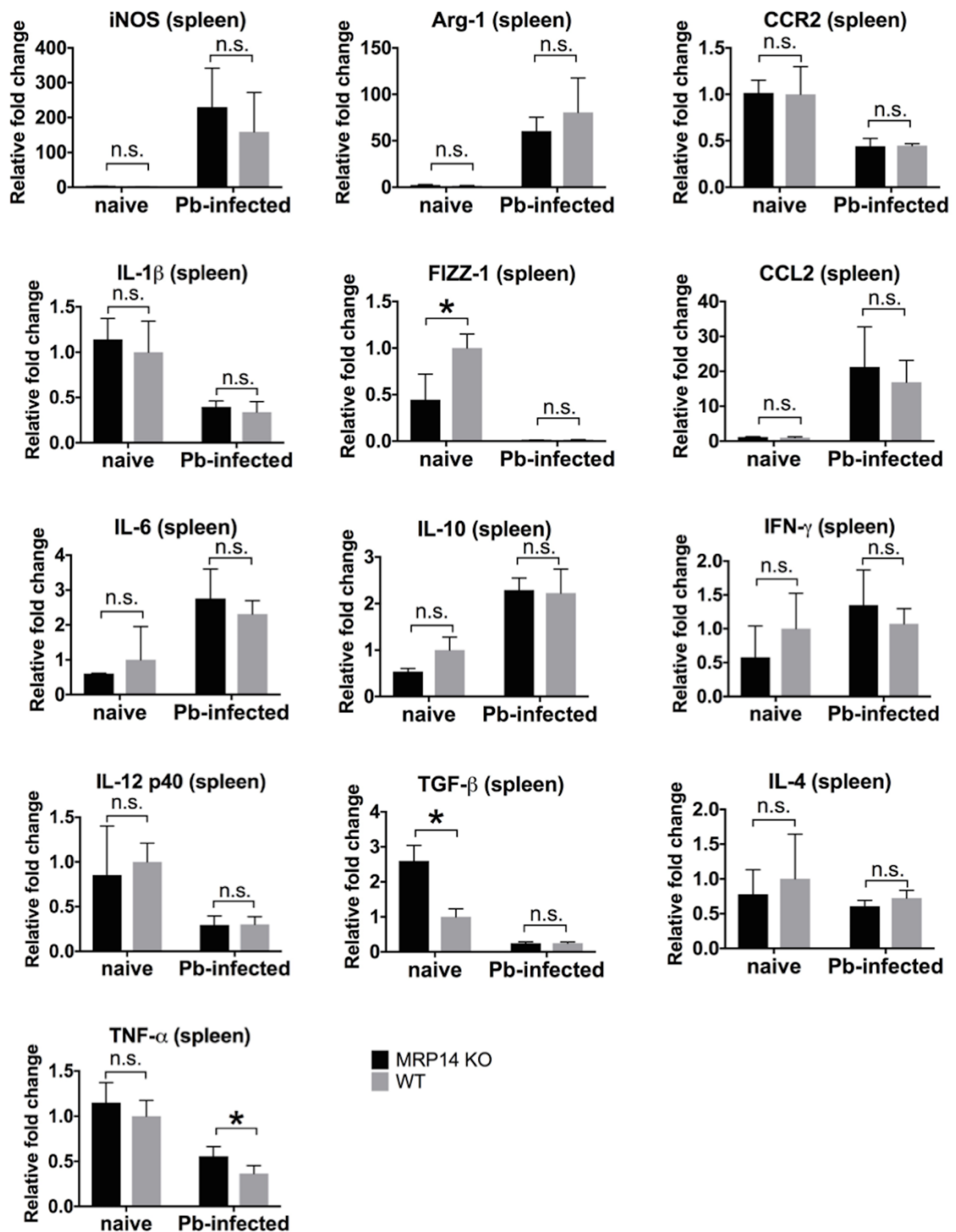


Figure 17. The suppression of pro-inflammatory molecules in the spleen of MRP14-KO BALB/c mice during rodent malaria.

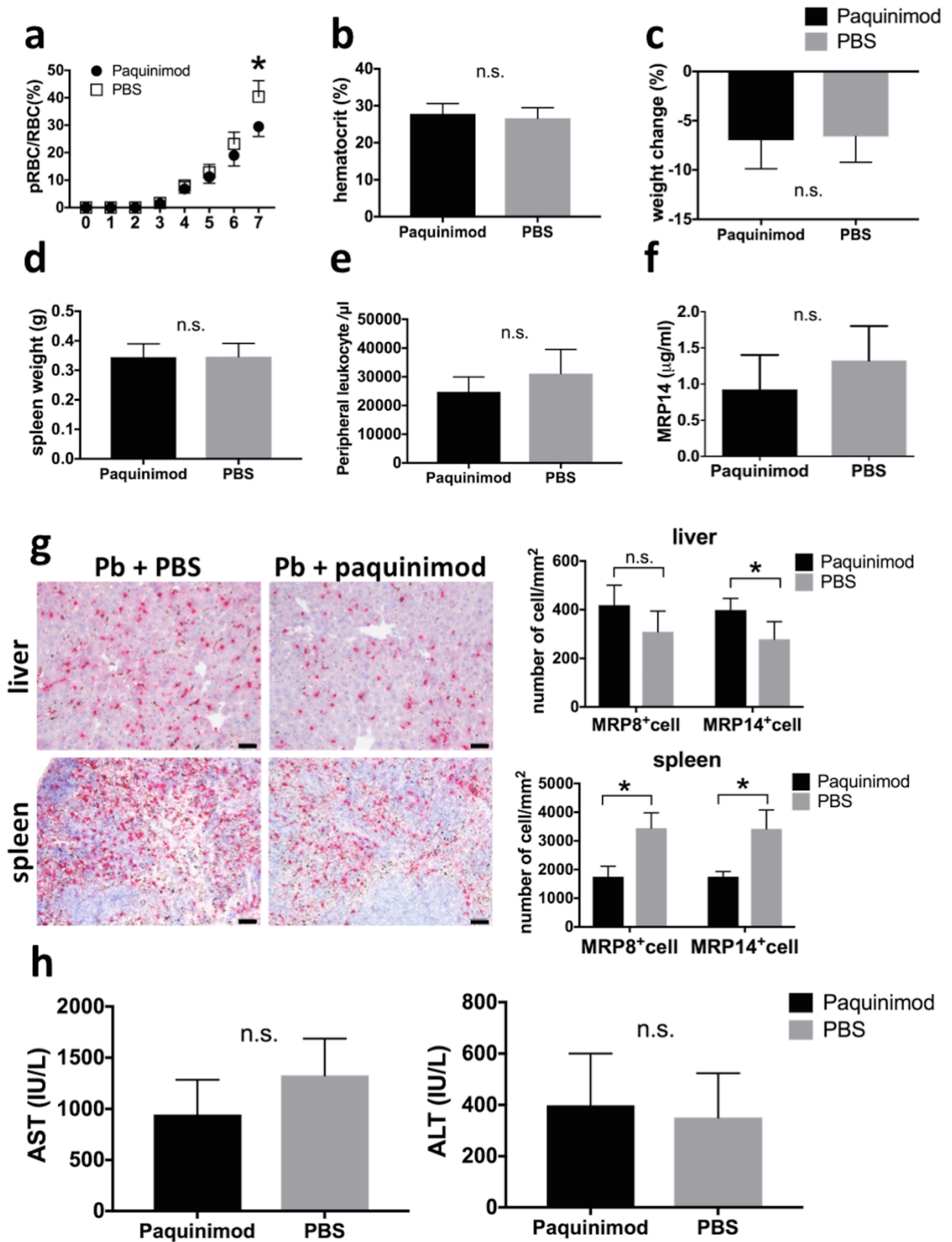


Figure 18. The administration of paquinimod failed to suppress MRP14 *in vivo*.

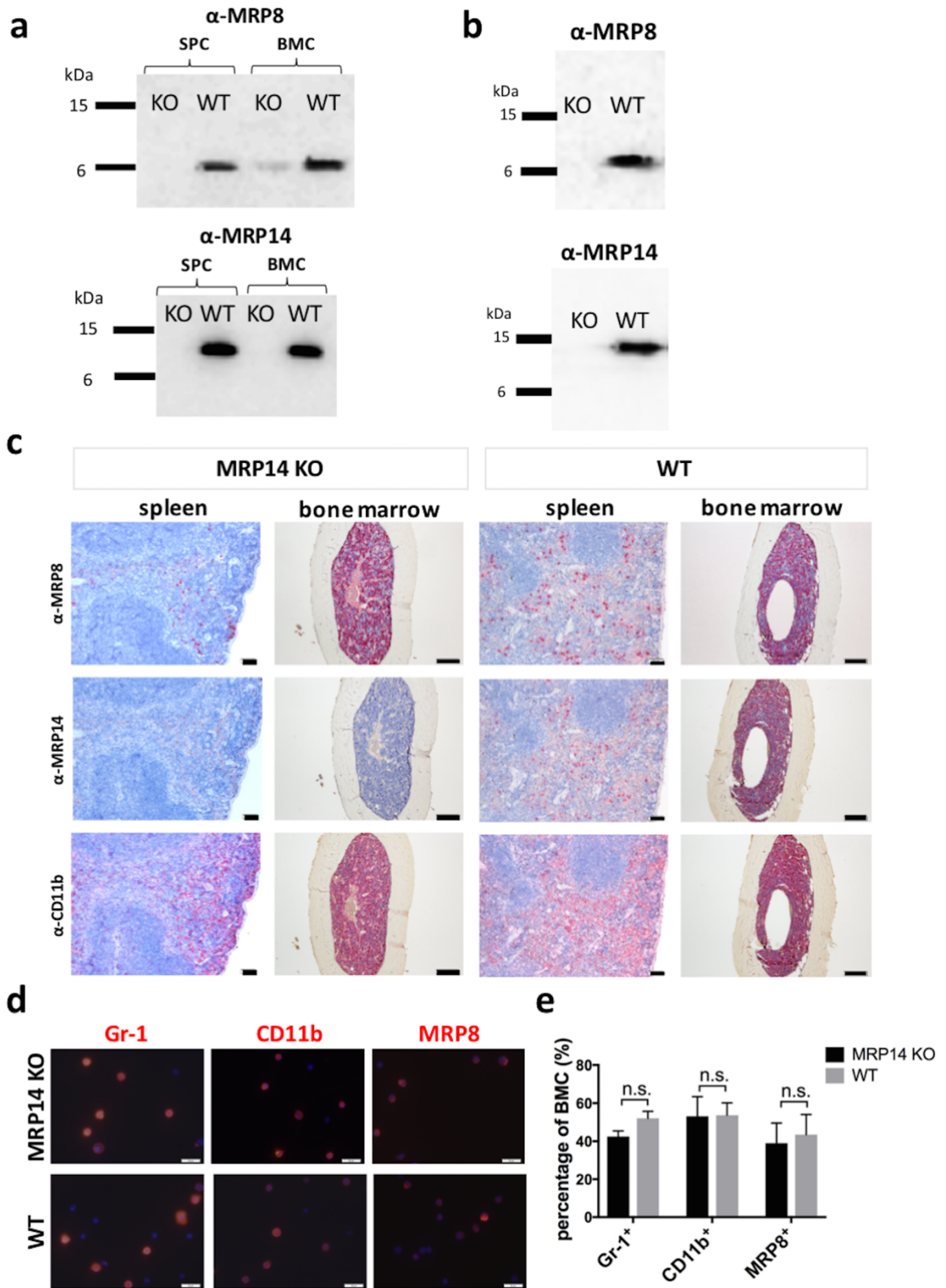
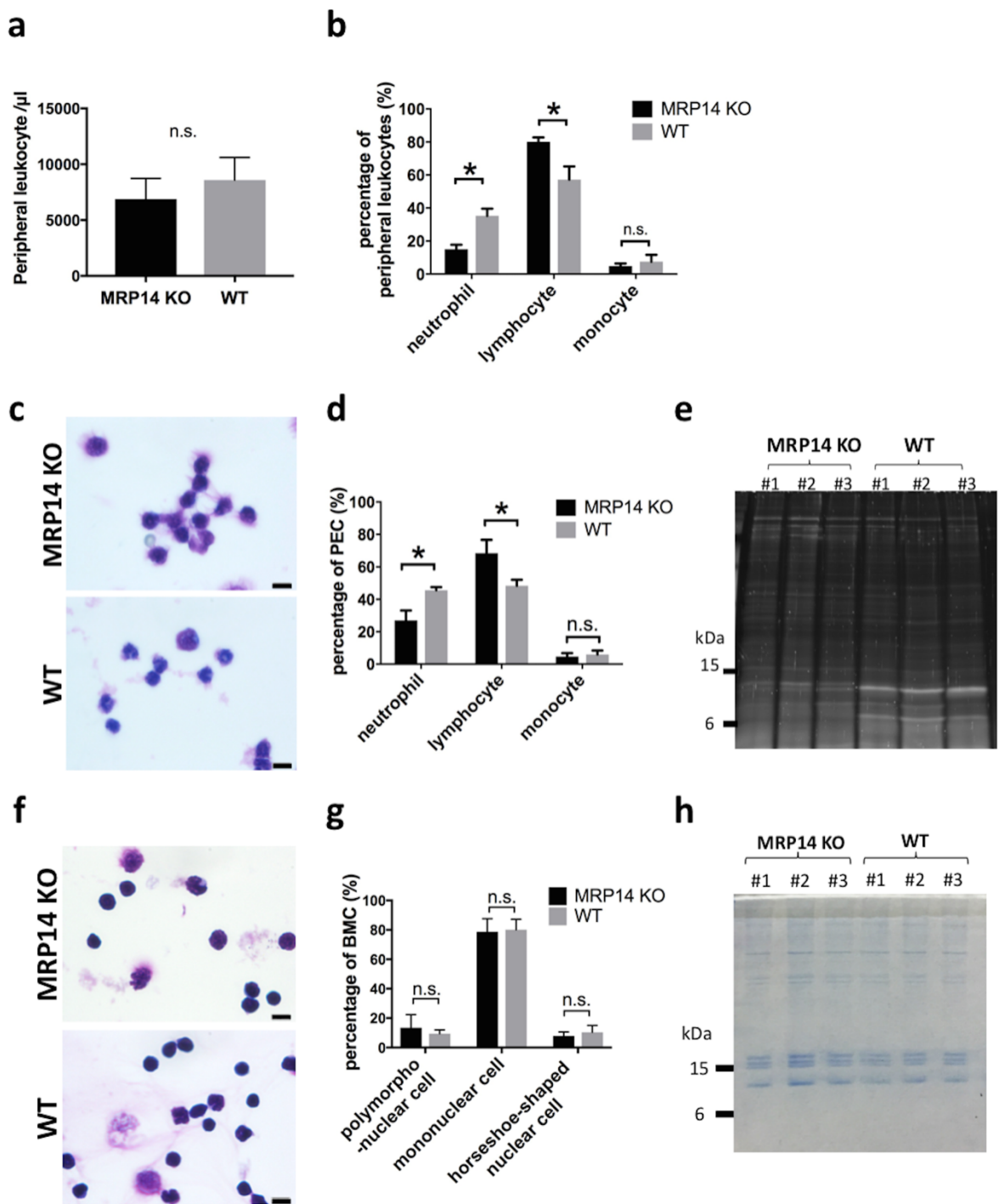


Figure 19. Suppression of cellular MRP8 expression in MRP14-KO mice.



**Figure 20. Increased ratio of lymphocytes in peripheral blood leukocytes and PECs of MRP14-KO mice.**

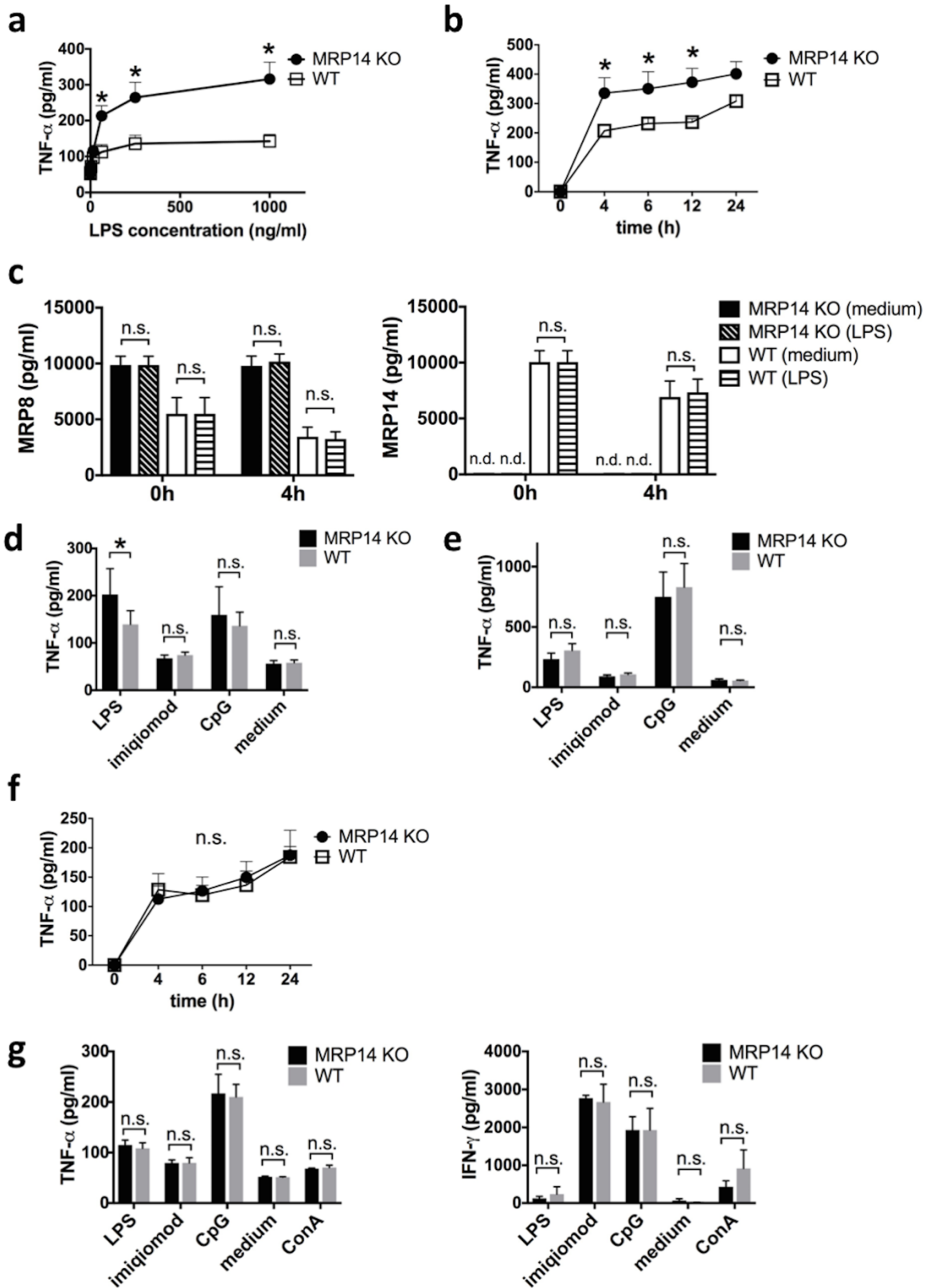


Figure 21. Enhanced TNF- $\alpha$  secretion by BMCs stimulated with LPS in MRP14-KO mice.

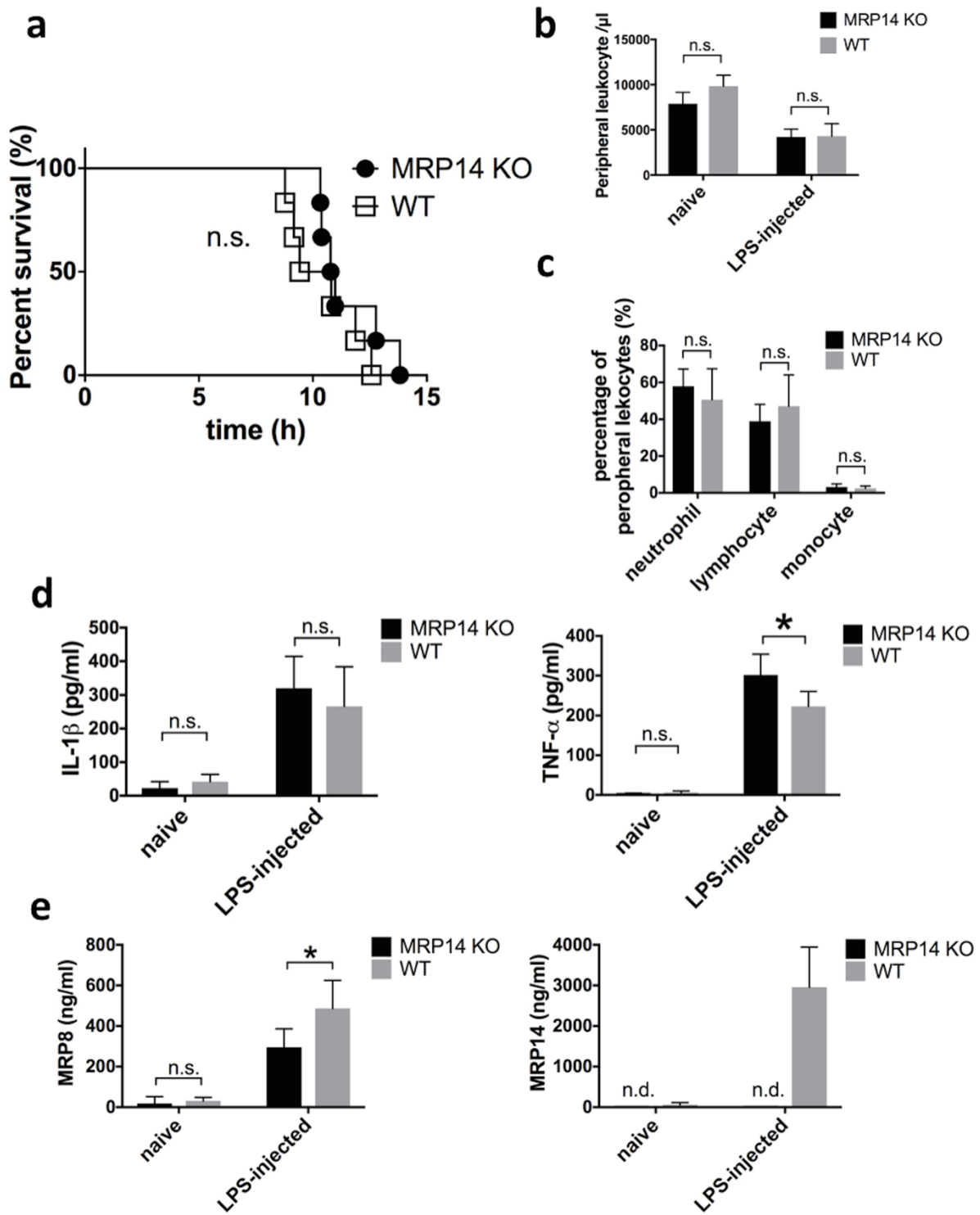


Figure 22. Unimproved LPS-induced shock in MRP14-KO BALB/c mice.

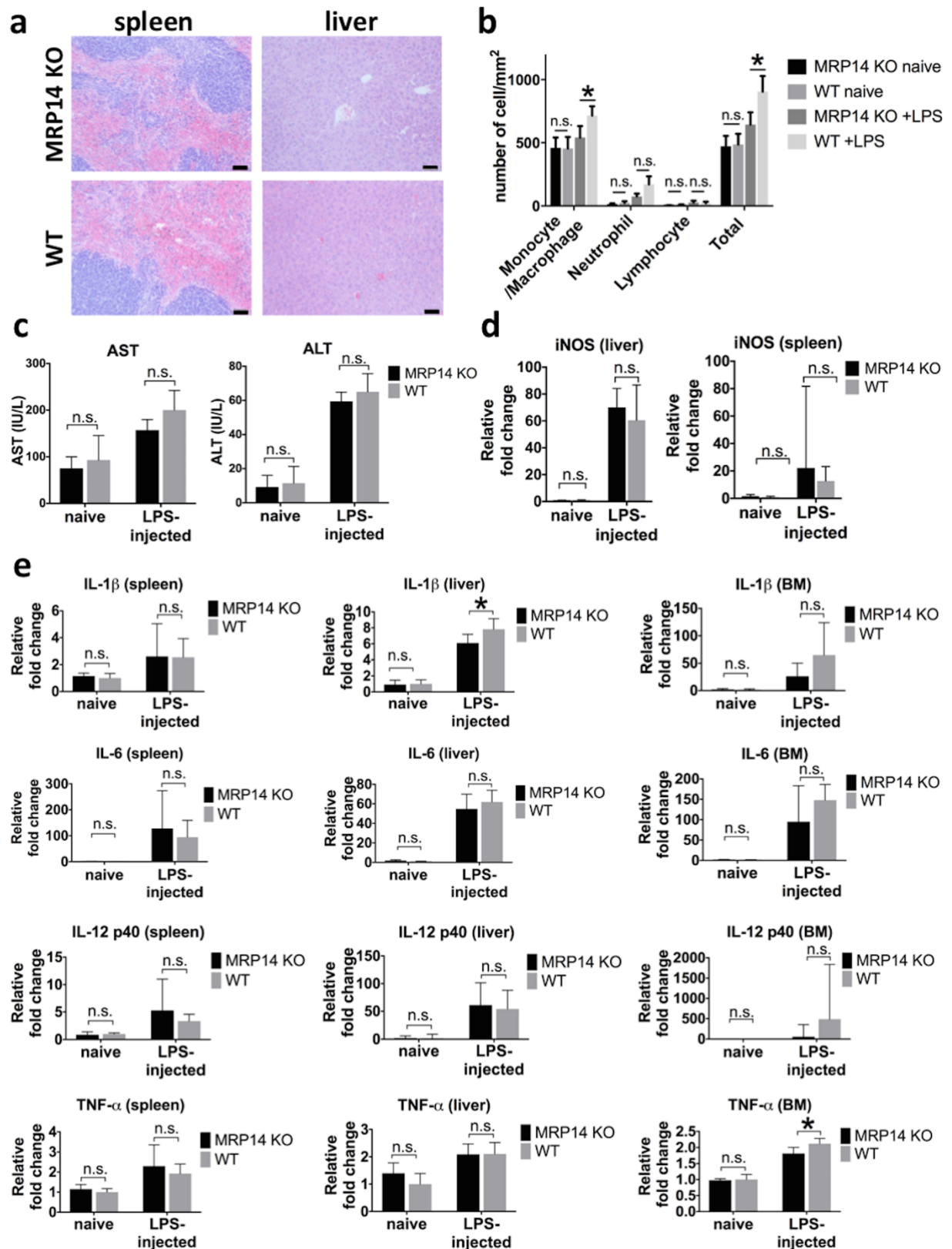
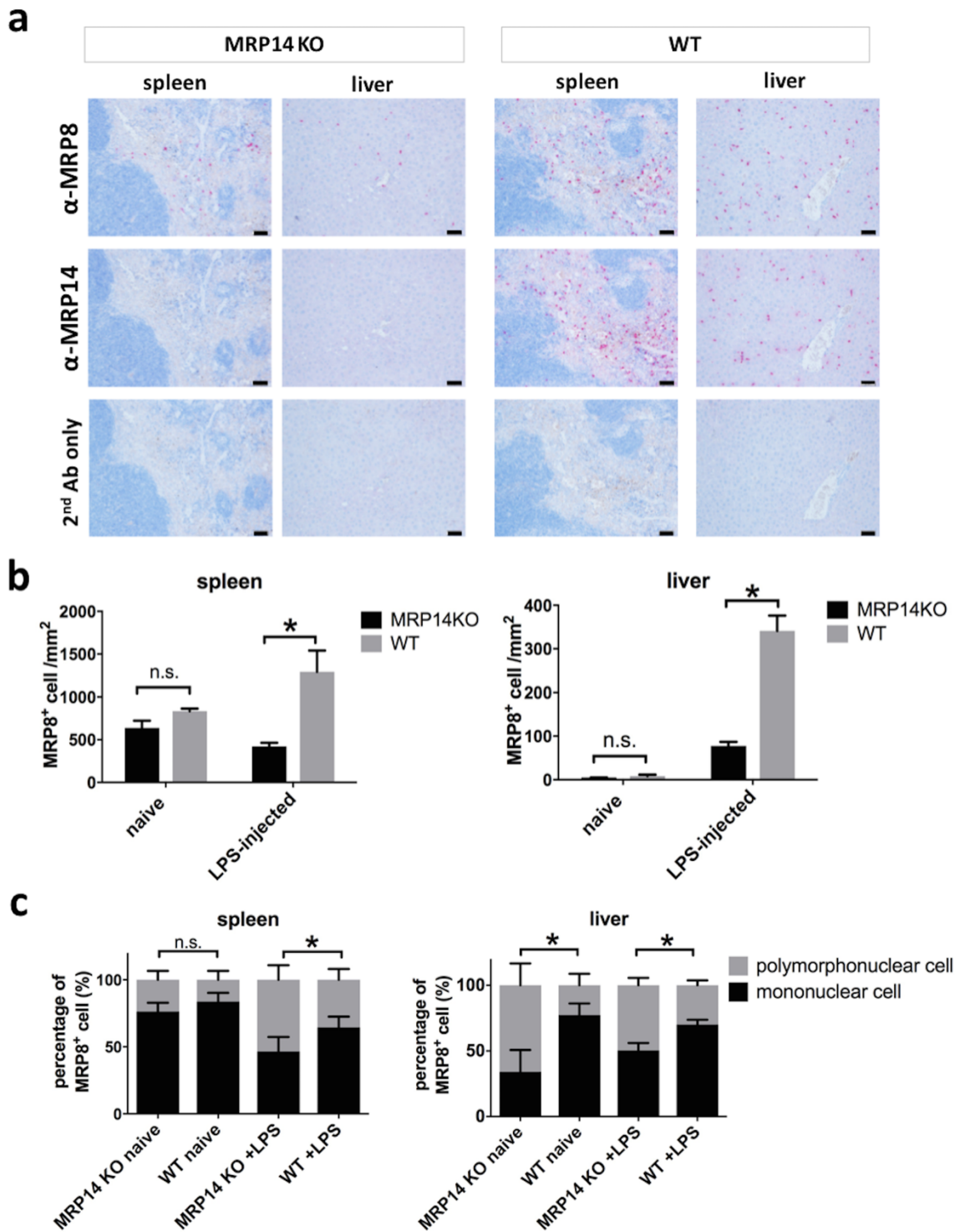


Figure 23. Unimproved LPS-induced hepatic injury in MRP14-KO BALB/c mice.



**Figure 24. Migration of the monocytes expressing MRP8 dependent on MRP14.**

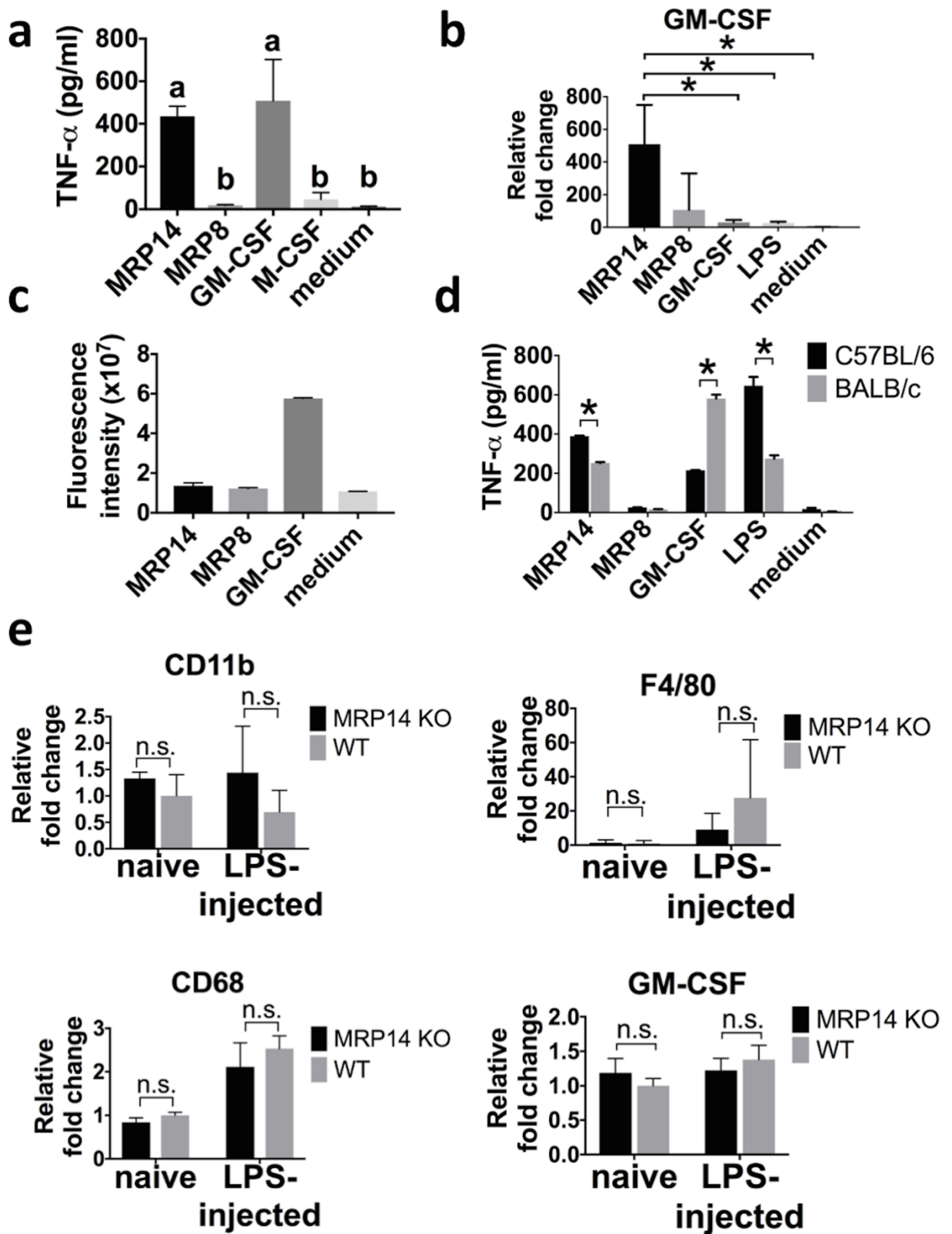
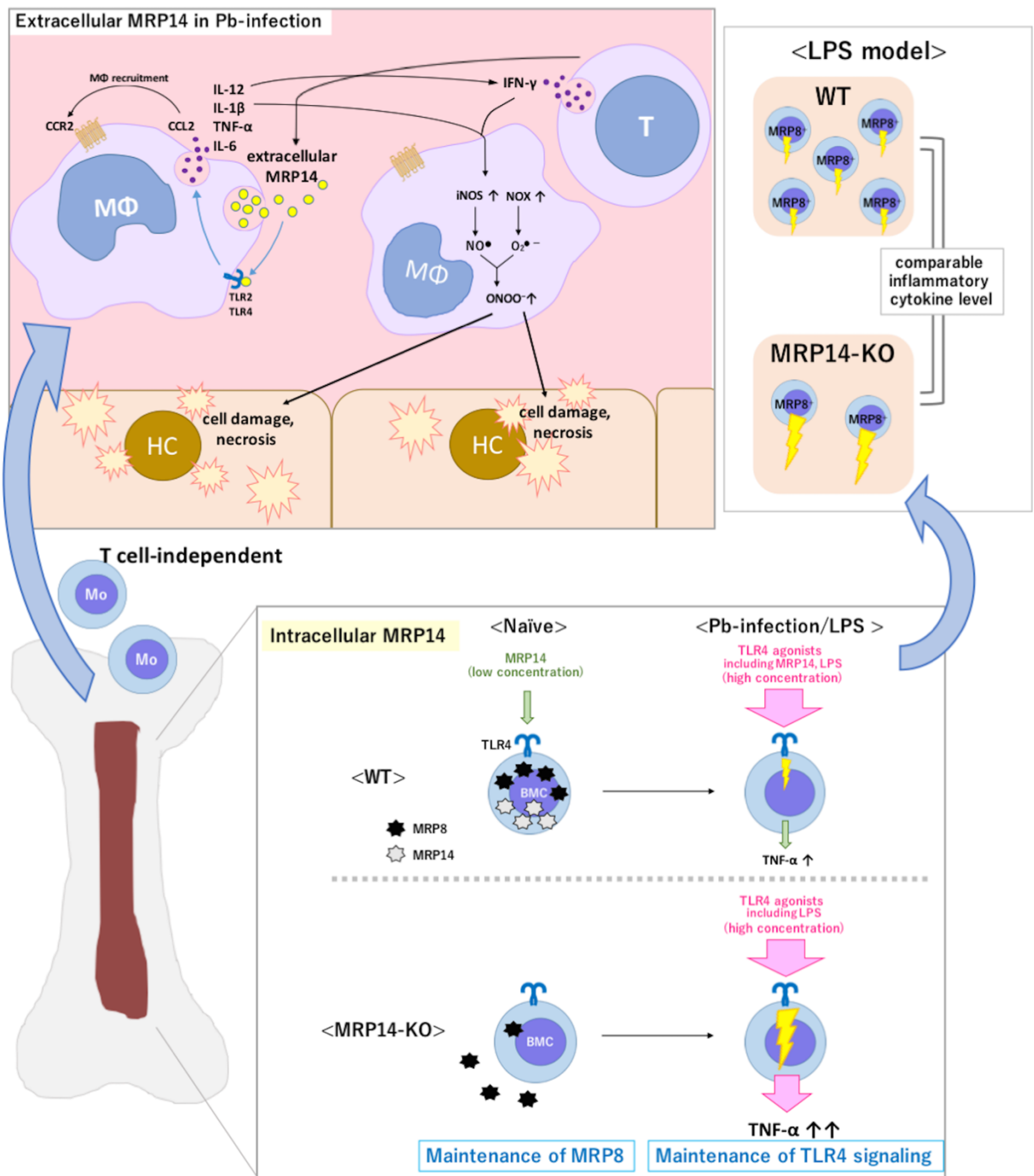


Figure 25. Promotion of GM-CSF expression in BMCs stimulated with MRP14.



**Figure 26. Hypothesized MRP14 function in pathology of hepatic injury during rodent malaria.**

## Tables

**Table 1. The comparison between BALB/c-background and C57BL/6-back ground MRP14**

**KO mice.**

	BALB/c	C57BL/6 (68, 69)
Peripheral leukocytes, PEC	Neu ↓, Lym ↑	Neu →, Lym →
MRP8 <sup>+</sup> cells in spleen	(+)	(-)
MRP8 <sup>+</sup> cells in bone marrow	(+)	(+)
Survival rate in LPS-induced shock	MRP14 KO = WT	MRP14 KO > WT
Migration of MRP8 <sup>+</sup> cell in tissues in LPS-induced shock	MRP14 KO < WT (Mo > Neu)	No expression of MRP8 in MRP14 KO mice
LPS-induced TNF- $\alpha$ secretion by BMC	MRP14 KO > WT Independent of MRP14	MRP14 KO < WT Dependent on MRP14
MRP secretion by BMC	Independent of LPS	Dependent on LPS
Sensitivity to GM-CSF	high	low

Neu: neutrophil, Lym: lymphocyte, Mo: Monocyte

**Table 2. The comparison of peripheral leukocytes and MRP8<sup>+</sup> cells accumulation between LPS-injected and Pb-infected models.**

	Naïve	LPS-injected	Pb-infected
The number of peripheral leukocytes	MRP14 KO = WT (MRP14 KO: Neu < Lym)	MRP14 KO = WT (MRP14 KO: Neu = Lym)	MRP14 KO < WT
Accumulated MRP8 <sup>+</sup> cell in liver	MRP14 KO < WT (MRP14 KO: Neu > Mo)	MRP14 KO < WT (MRP14 KO: Neu > Mo)	MRP14 KO = WT (in spleen: MRP14 KO < WT)

Neu: neutrophil, Lym: lymphocyte, Mo: Monocyte

### Supplemental table 1. Primer list.

Gene	Forward	Reverse
IL-1 $\beta$	5'-GAAAGACGGCACACCCACCCT-3'	5'-GCTCTGCTTGTGAGGTGCTGATGTA-3'
IL-6	5'-CCAGAGATACAAAGAAATGATGG-3'	5'-ACTCCAGAAGACCAGAGGAAAT-3'
IL-12 p40	5'-ACAGCACCAGCTTCTTCATCAG-3'	5'-TCTTCAAAGGCTTCATCTGCAA-3'
TNF- $\alpha$	5'-CTGTGAAGGGAATGGGTGTT-3'	5'-GGTCACTGTCCCAGCATCTT-3'
iNOS	5'-GTTCTCAGCCCAACAATACAAGA-3'	5'-GTGGACGGGTCGATGTCAC-3'
Arg-1	5'-CTCCAAGCCAAAGTCCTTAGAG-3'	5'-AGGAGCTGTCATTAGGGACATC-3'
FIZZ-1	5'-CCAATCCAGCTAACTATCCCTCC-3'	5'-CCAGTCAACGAGTAAGCACAG-3'
IL-10	5'-GCTGGACAACATACTGCTAACCC-3'	5'-CCCAAGTAACCCTTAAAGTCCTG-3'
TGF- $\beta$	5'-GTCAGACATTCGGGAAGCAG-3'	5'-GCGTATCAGTGGGGGTCA-3'
CCR2	5'-TGCCATCATAAAGGAGCCAT-3'	5'-TTTGTTTTTGCAGATGATTCAA-3'
CCL2	5'-GTTGGCTCAGCCAGATGCA-3'	5'-AGCCTACTCATTGGGATCATCTTG-3'
IFN- $\gamma$	5'-GGCCATCAGCAACAACATAAGCG-3'	5'-TGGGTTGTTGACCTCAAACCTGG-3'
IL-4	5'-GGCATTTTGAACGAGGTCAC-3'	5'-AAATATGCGAAGCACCTTGG-3'
CD11b	5'-ATGGACGCTGATGGCAATACC-3'	5'-TCCCCATTACGTCTCCCA-3'
F4/80	5'-AATCGCTGCTGGTTGAATACAG-3'	5'-CCAGGCAAGGAGGACAGAGTT-3'
CD68	5'-CAAGGTCCAGGGAGGTTGTG-3'	5'-CCAAAGGTAAGCTGTCCATAAGGA-3'
GM-CSF	5'-CAACTCCGAAACGGACTGTG-3'	5'-GCTGTGCCACATCTCTTGGTC-3'
GAPDH	5'-CGACTTCAACAGCAACTCCCCTCTTCC-3'	5'-TGGGTGGTCCAGGGTTTCTTACTCCTT-3'
$\beta$ -actin	5'-GTTACCAACTGGGACGACA-3'	5'-TGGCCATCTCTGCTCGAA-3'
NOX2	5'-AGCTATGAGGTGGTGTGTTAGTGG-3'	5'-CACAATATTTGTACCAGACAGACTTGAG-3'

## Summary (in Japanese)

### 論文の内容の要旨

獣医学専攻  
平成 26 年度 博士課程進学  
氏名 溝渕 悠代  
指導教員名 後藤 康之

### 論文題目

Exacerbation of hepatic injury during rodent malaria by myeloid-related protein 14  
(myeloid-related protein 14 によるローデントマラリア肝障害の悪化)

#### 【背景と目的】

マラリアは *Plasmodium* 属原虫の感染により発症する原虫感染症であり、赤内期に認められる重篤な症状の一つとして肝障害が挙げられる。マクロファージの集簇はマラリアの肝臓における典型的な病理像であることから、マラリアにおける肝障害にマクロファージが関与すると考えられてきた。しかしながら、マラリア肝障害の病態機序は未だ明らかになっていない。一方、myeloid-related protein 14 (MRP14) および MRP8 は炎症性マクロファージの細胞質に発現する蛋白質であり、細胞活性化により分泌される。現在、関節リウマチや動脈硬化症などの様々な炎症性疾患において、病態悪化に伴う MRP14 陽性マクロファージの炎症部位への集簇が報告されているが、マラリアにおける MRP14 陽性マクロファージの動態については、ほとんど明らかになっていなかった。筆者は卒業論文において、*P. berghei* 感染 BALB/c マウスの肝臓における MRP14 陽性及び MRP8 陽性マクロファージの増加を明らかにした。また、感染マウスにおいて血中 MRP14 濃度が上昇することも示した。以上の結果から MRP14 陽性マクロファージより分泌された MRP14 がマラリアの肝障害に関与していると考えられた。本研究では、*P. berghei* の赤内期感染によって引き起こされるマラリア肝障害への MRP14 の関与を明らかにすることを目的とした。

#### 【第 1 章】

第 1 章では、細胞外 MRP14 が肝障害へもたらす影響を解析した。*P. berghei* 感染マウスにおいて、肝障害の指標である血清中 AST・ALT の上昇及びマクロファージの浸潤を伴う巣状壊死が認められたことから、肝障害が示された。さらに免疫組織学的解

析では、感染マウスの肝臓類洞において MRP14 陽性マクロファージの顕著な集簇が認められた。T 細胞を欠損するヌードマウスにおいてはこのような肝障害が生じず、血中 MRP14 の上昇も認められなかった。一方、MRP14 陽性マクロファージの集簇はヌードマウスでも認められたことから、MRP14 陽性マクロファージは T 細胞に依存しない機構で集簇するが、MRP14 の分泌は T 細胞依存性に誘導されることが明らかになった。また、*in vitro* 解析では、MRP14 が toll-like receptor (TLR) 2 及び TLR4 の新規内因性アゴニストであり、damage-associated molecular patterns (DAMPs) の一つとして機能することが明らかになった。

次に、*P. berghei* 感染後のマウスに 7 日間 MRP14 を静脈内投与し、肝障害への影響を PBS 投与のコントロール群と比較した。末梢血中感染赤血球率およびヘマトクリット値に関して、MRP14 投与による影響は見られなかった。一方、MRP14 投与群では血清中 AST・ALT 濃度のさらなる上昇及び巣状壊死レベルの悪化が認められた。また、MRP14 投与による MRP14 陽性および MRP8 陽性マクロファージ集簇の増強も確認された。さらに、MRP14 投与は非感染マウスにおいても同様に MRP 陽性マクロファージの集簇を誘導し、IL-1 $\beta$ ・IL-12・TNF- $\alpha$ ・iNOS といった炎症性因子、および CCL2・CCR2 といった走化性因子の発現を誘導した。以上の結果から、*P. berghei* 感染において分泌される MRP14 は肝臓における MRP 陽性マクロファージ集簇及び炎症性サイトカイン・NO 産生を促進し肝障害を悪化させることが明らかになった。

## 【第 2 章】

C57BL/6 マウスにおける様々な炎症性疾患モデルの先行研究において、MRP14-KO マウスでは炎症反応が抑制され病態改善が認められることが報告されている。従って、第 1 章の結果から BALB/c マウスでも MRP14 を欠損させることで炎症反応が減弱し肝障害が改善されると仮説をたて、第 2 章では、MRP14-knockout (KO) BALB/c マウスを作製し、*P. berghei* 感染 MRP14-KO BALB/c マウスにおける肝障害を解析した。しかしながら仮説に反して、MRP14-KO マウスの血清中 AST・ALT 上昇及び巣状壊死レベルに wild-type (WT) マウスとの差は認められず、MRP14-KO マウスでも WT マウスと同様な肝障害が生じていた。また、肝臓における MRP8 陽性マクロファージ集簇数にも MRP14-KO マウスと WT マウスの間に有意差は認められなかった。肝臓におけるサイトカイン等の炎症性因子及び走化性因子の発現においても、MRP14-KO マウスと WT マウスの間にほとんど差は認められなかった。以上の結果から、MRP14-KO マウスにおいても *P. berghei* 感染における肝障害は引き起こされることが明らかになった。

## 【第 3 章】

第 1 章では細胞外 MRP14 による肝障害の悪化が見られた一方、第 2 章においては MRP14-KO BALB/c マウスも WT マウスと同等の肝障害を呈した。これらの結果は、

C57BL/6 マウスを用いた先行研究により確立されてきた、「MRP14-KO マウスでは extracellular MRP14 及び MRP8 が抑制されるために炎症反応が抑制される」という仮説自体がそもそも BALB/c マウスに適用できないことを示唆していた。以上のことから、同じ MRP14-KO マウスでも BALB/c マウスと報告のある C57BL/6 マウスの 2 系統間に免疫学的性状の違いがあることが予想された。そこで第 3 章では、作製した MRP14-KO BALB/c マウスの免疫学的性状を解析するために、ナイーブマウスにおける免疫細胞の動態を解析するとともに、LPS 誘導性ショックモデルを用いて、報告されている MRP14-KO C57BL/6 マウスの結果との比較を行った。MRP14-KO C57BL/6 マウスでは骨髄細胞における LPS 刺激時の TNF- $\alpha$  分泌が抑制されており、また LPS 誘導性ショックに抵抗性を示すという報告があったことから (Vogl *et al.*, 2007, *Nat. Med.*,13(9):1042)、MRP14-KO BALB/c マウスでも同様であるか検証した。その結果、今回作製した MRP14-KO BALB/c マウスと WT マウスの間に LPS 誘導性ショックによる生存率の差は認められず、LPS 刺激時の MRP14-KO 骨髄細胞からの TNF- $\alpha$  産生量はむしろ WT より有意に高い値を示した。一方で、LPS 刺激後の肝臓における MRP8 陽性細胞集簇数は MRP14-KO BALB/c マウスで有意に少なく、数時間という急性炎症における MRP8 陽性細胞の集簇に MRP14 が関与することが示唆された。以上の結果から、C57BL/6 マウスと異なり、BALB/c マウスにおける細胞内 MRP14 欠損は骨髄細胞の応答性に影響を与え、TLR4 シグナルを増強することが明らかになった。

#### 【結論】

本研究により、ローデントマラリアにおいて、細胞外 MRP14 は炎症性サイトカイン産生及び MRP14 陽性マクロファージ集簇を促進することで炎症反応カスケードを増幅し、肝障害を悪化させる重要な因子であることが明らかになった。一方で、MRP14-KO BALB/c マウスでも肝障害が認められたが、この背景には、先行研究の MRP14-KO C57BL/6 マウスと本研究で作製した MRP14-KO BALB/c マウスの免疫学的性状が大きく異なり、細胞内 MRP14 の欠損によって骨髄細胞がより炎症反応に応答性を増したことが考えられる。実際、MRP14-KO BALB/c マウスでは骨髄細胞の TLR4 シグナルの過反応性が認められ、これが LPS 刺激時に MRP14-KO BALB/c マウスでも WT と同程度の炎症性サイトカイン発現が維持されていた一因と考えられた。以上のことから、BALB/c マウスにおいて MRP14 の欠損は単純に細胞外 MRP14 の炎症促進作用という機能欠損だけではなく、細胞内 MRP14 欠損による TLR4 シグナルの過反応をもたらすことが明らかとなった。本研究は今まで注目されていなかった細胞内 MRP14 の機能という新たな視座を据えたという点でも有意義な研究であり、多面的な MRP14 の機能を解明する嚆矢となると期待される。本研究を通して明らかとなった MRP14 の免疫病理学的な機能をさらに詳細に解析することは、MRP14 コントロールによるマラリア肝障害の治療につながると考えられる。